

Bangor University

DOCTOR OF PHILOSOPHY

Development of alginate hydrogels for the treatment of diabetic foot ulcers

Chan, Kenny

Award date:
2022

Awarding institution:
Bangor University

[Link to publication](#)

General rights

Copyright and moral rights for the publications made accessible in the public portal are retained by the authors and/or other copyright owners and it is a condition of accessing publications that users recognise and abide by the legal requirements associated with these rights.

- Users may download and print one copy of any publication from the public portal for the purpose of private study or research.
- You may not further distribute the material or use it for any profit-making activity or commercial gain
- You may freely distribute the URL identifying the publication in the public portal ?

Take down policy

If you believe that this document breaches copyright please contact us providing details, and we will remove access to the work immediately and investigate your claim.

Download date: 11. Apr. 2024

Bangor University

DOCTOR OF PHILOSOPHY

Development of alginate hydrogels for the treatment of diabetic foot ulcers

Chan, Kenny

Award date:
2022

[Link to publication](#)

General rights

Copyright and moral rights for the publications made accessible in the public portal are retained by the authors and/or other copyright owners and it is a condition of accessing publications that users recognise and abide by the legal requirements associated with these rights.

- Users may download and print one copy of any publication from the public portal for the purpose of private study or research.
- You may not further distribute the material or use it for any profit-making activity or commercial gain
- You may freely distribute the URL identifying the publication in the public portal ?

Take down policy

If you believe that this document breaches copyright please contact us providing details, and we will remove access to the work immediately and investigate your claim.

Download date: 01. Jun. 2022

Development of alginate hydrogels for the treatment of diabetic foot ulcers

Thesis submitted to School of Natural Sciences, Bangor University

in partial fulfilment for the degree of Doctor of Philosophy

by

Kai Yu Chan



PRIFYSGOL
BANGOR
UNIVERSITY

Prifysgol Bangor • Bangor University

© Dec 2021

Declaration to include in your thesis

I hereby declare that this thesis is the results of my own investigations, except where otherwise stated. All other sources are acknowledged by bibliographic references. This work has not previously been accepted in substance for any degree and is not being concurrently submitted in candidature for any degree unless, as agreed by the University, for approved dual awards.

Yr wyf drwy hyn yn datgan mai canlyniad fy ymchwil fy hun yw'r thesis hwn, ac eithrio lle nodir yn wahanol. Caiff ffynonellau eraill eu cydnabod gan droednodiadau yn rhoi cyfeiriadau eglur. Nid yw sylwedd y gwaith hwn wedi cael ei dderbyn o'r blaen ar gyfer unrhyw radd, ac nid yw'n cael ei gyflwyno ar yr un pryd mewn ymgeisiaeth am unrhyw radd oni bai ei fod, fel y cytunwyd gan y Brifysgol, am gymwysterau deuol cymeradwy.

Acknowledgments

This research would not have been possible without the support and encouragement from so many individuals. Firstly, I would like to acknowledge the support of the Knowledge Economy Skills Scholarship (KESS II) Fund through Bangor University and the contribution of ConvaTec Ltd for funding this project and providing me with this opportunity.

Secondly, I would like to express my gratitude towards Dr Hongyun Tai for her supervision and guidance during the planning and development of this project at Bangor University. Her advice and passion to bring out the best in me are deeply appreciated. I am thankful for what I have learnt from her and to have been under her supervision.

Thirdly, I would like to thank Phil Bowler, Dave Parsons and Rocio Burgos-Amador of ConvaTec GDC Deeside. Phil has always been a role model with his passion and dedication to his work, and his patience and kindness has been felt whenever we meet. Thank you to Dave and Rocio for being so kind and accommodating during my trips to the GDC, and for your help with arranging training and help from other staff members amidst your busy schedules.

I would like to give my sincere thanks to my family for their continuous support and contribution. Your kindness and guidance will never be forgotten, and the lockdown in 2020 helped me recognise the true meaning of family, to appreciate and be thankful for them. Thank you for never giving up on me.

On the subject of family, my Bangor family definitely deserves my thanks and it wouldn't be right for me not to acknowledge them. Thank you for being by my side as I grow and mature into who I am and sticking with me through thick and thin. My deepest thanks to the 501 society: Chester, David, James, Tom, Sohad, Richard, and its honorary members Jamie, Charlotte and Alice. Thank you to Mohammed and Shayma for your guidance and kindness and being my parental figures in the department. Thank you to Dr Paddy Murphy and Dr Andrew Davies for your company during lunch hours and always providing me with motivation for work.

Thank you to Dr Marc Bouillon for helping me discover my passion in chemistry, which was a key factor in me undertaking a PhD. Thank you to Nick, Enlli, Glynne and Gwynfor for their excellent technical support since my first year as an undergraduate student. Thank you to the chemistry tower itself and to Mr Gwynfor Davies, who is an integral part of the chemistry family and whose warmness was always felt.

Thank you to my TrioSciCymru and outreach family: Delwen, Benji, Shiv, Emma, Jack and Lorrie, for always being there to support me no matter what and helping me discover my passion for and the significance of outreach programmes. Thank you for your support and camaraderie when the department faced its darkest hours amidst fear of department closure. Special thank you to Rebecca for your company during this long and arduous journey. The lessons you have taught me will be remembered for always. Thank you to Andrew, Sarah and Mikaela for your continuous company and positive energies throughout and beyond lockdown.

Lastly, my sincerest thanks are saved for Dr Lorrie Murphy, Dr Paddy Murphy and Ori Springer. Without you, I would not be here today. Thank you for always providing motivation, encouragement and feedback on my work, and thank you for always keeping me in check. Thank you Ori for keeping me grounded and always putting a smile on my face.

I would like to dedicate my accomplishments to my late grandfather, who was my best friend and the kindest man I've known.

Diolch yn fawr i chi gyd / 感謝你們一直以來的支持,

Kenny K Y Chan

Abstract

The focus of this thesis was to develop a novel hydrogel wound dressing from alginate, a biocompatible naturally occurring polysaccharide found primarily in green algae, to be administered through injection, gelling *in-situ* and removed as one entity for the treatment of chronic diabetic foot wounds. This thesis comprises of four chapters as described below:

Chapter one offers an insight into the project through a systematic review from a medical and biological, and from a chemical perspective. *Diabetes Mellitus*, its complications and the onset of diabetic foot ulcers and the medical 'TIME' protocol of wound care and management are discussed which encompasses the precautions and challenges in wound healing. Diabetic foot ulcer wound therapeutics are reviewed. Dressing format and dressing materials are discussed with a short discussion of their advantages and disadvantages. This chapter leads onto general fundamentals and basic concepts of alginate polymer chemistry. Literature review of polymerisation techniques involving alginates related to this project are presented and hydrogels and its inclusion in diabetic wound therapy are also included herein.

Chapter two describes the methodologies and equipment used as part of this project. In this chapter, the fundamentals of analytical techniques used for the presentation of data in this thesis will be presented and discussed. In this chapter, the scientific background to aid interpretation and comprehension of scientific data are included. This chapter concludes with details of full experimental procedures for the synthesis of hydrogel precursors, the preparation of alginate hydrogel via multi-modal crosslinks, and the characterisation of alginate gelation and post-gelation, including the *in-situ* rheological study of the gelation mechanism.

Chapter three contains five subsections and focuses on the data obtained as part of this work. Discussions and arguments pertaining to the scientific findings are presented. An overview of the chapter is presented in section 1, along with the GPC profiles of the alginate raw materials.

Section 2 details the synthesis of glycidyl acrylate from glycidol and acryloyl chloride, where yields upwards to 78 % and product purity of 88 % were obtained. Section 3 describes the acrylate modification of sodium alginate using glycidyl acrylate to synthesise the precursor for hydrogel preparation. The resultant material was characterised using ^1H NMR to estimate the degree of substitution using anomeric proton signals where a maximum of 30 % substitution was recorded for mannuronate-rich alginates and the same reaction using guluronate-rich alginates afforded a maximum substitution of 33 %. In addition, the effects of time and temperature on the reaction step were studied.

Section 4 describes the thiolate modification of sodium alginate using cysteine hydrochloride and cysteamine hydrochloride as the thiolation agent. ^1H -NMR analyses using anomeric proton signals estimated a peak thiolation substitution of 12 %, with mass yields upwards to 78 % obtained. The thiol content of prepared alginate samples were quantified using Ellman's Assay and converted to present thiol density, where a theoretical maximum of $743 \frac{\mu\text{g thiol}}{\text{g alginate}}$ thiol density was calculated. The effects of pH on the thiolation step was investigated, and pH 4.0 was found to be the optimum pH during the chemical work-up.

In section 5, an *in-situ* one-pot technique of hydrogel preparation via Michael-type addition is developed. Herein, alginate moieties underwent multiple techniques to form hydrogels, but with an emphasis on covalent crosslinking via Michael-type addition reaction. Ionotropic gelation using calcium chloride produced a stiff hydrogel instantaneously, and photo-gelation using Irgacure 2959 photoinitiator produced a robust hydrogel after 7 minutes of curing under a UV- β lamp.

Covalent crosslinking was achieved between acrylate and thiol functional groups using acrylate modified alginate as the acrylate moiety and pentaerythritol tetrakis(3-mercaptopropionate) thiol crosslinker or thiol modified alginate as the thiol moiety. The observations and results from laboratory testing were compared with *in-situ* rheological experiment data, where the gelation times recorded were 1 hour for laboratory gelation and 50 minutes on the rheometer.

Within this section, the results from materials testing would be included such as release studies, gelation studies, including *in-situ* rheological study of alginate

gelation, and microscopy tests on dried alginate fibres and alginate hydrogels. A mini conclusion may be found at the end of each chapter sections.

Chapter four summarises the research presented in this thesis and draws general conclusions. Herein, the reader will also see comments made by the author with regards to the research direction and future modifications to the project to retain its novelty for successive researchers.

List of abbreviations

°C – Degrees Celsius

< – Less than

≤ – Less than or equal to

μg – Microgram

μm – Micrometre

> – More than

≥ – More than or equal to

δ – Phase angle

2D – Two-dimensional

% w/v – Weight/volume percentage

% w/w – Weight/weight percentage

Ca. – circa

CaCl₂ – Calcium chloride

CMC – Carboxymethylated cellulose

d – Doublet

dd – Doublet of doublets

DE/Et₂O – Diethyl ether

DFU – Diabetic foot ulcer

DKA – Diabetic ketoacidosis

DLS – Dynamic light scattering

DoS % - degree of substitution (%)

DPN – Diabetic peripheral neuropathy

DTNB - 5,5'-Dithiobis(2-nitrobenzoic acid) (Ellman's Reagent)

DTT – Dithiothreitol

ECMs – Extracellular matrices

EDCI - 1-Ethyl-3-(3-dimethylaminopropyl)carbodiimide

ESEM – Environmental scanning electron microscopy

FT-IR – Fourier-transform infrared spectroscopy

g – Gram

G^* - Complex modulus

G'' – Loss modulus

G' – Storage modulus

GDM – Gestational *Diabetes Mellitus*

G-G – Guluronate-guluronate di-axial glycosidic linkage

G-M – Guluronate-mannuronate glycosidic linkage

GMA – Glycidyl methacrylate

GPC – Gel permeation chromatography

h – Hour

High M – Alginate sample procured from Sigma-Aldrich; richer in mannuronate residues

High G – Alginate sample provided by ConvaTec Rhymney; richer in guluronate residues

Hz - Hertz

IDDM – Insulin dependent *Diabetes Mellitus*

IMS – Industrial methylated spirits

K – Kelvin

LVE region – Linear viscoelastic region

m – Multiplet

M – Molar concentration

mM – Millimolar concentration

mg – Milligram

M-G – Mannuronate-guluronate glycosidic linkage

mL – Millilitre

mm - Millimetre

M-M – Mannuronate-mannuronate di-equatorial glycosidic linkage

mmol – Millimoles

M_n – Number average molecular weight

M_p – Peak average molecular weight

M_w – Weight average molecular weight

MWCO – Molecular weight cut-off

NIDDM – Non-insulin dependent *Diabetes Mellitus*

nm - Nanometre

NMR – Nuclear magnetic resonance spectroscopy

Pa - Pascal

PAD – Peripheral arterial disease

PBS – Phosphate buffered saline

PDI – Polydispersity index

PEG – Poly(ethylene glycol)

PEGDA – Poly(ethylene glycol)diacrylate

PLA – Poly(lactic acid)

Pmu – Per mass unit

POC – Protocol of Care

PVA – Poly(vinyl alcohol)

QT – Pentaerythritol Tetrakis(3-mercaptopropionate)

RI – Refractive index

r.t. – Room temperature

s – Second or Singlet

SA – Sodium alginate

SA-GA/Acr-Alg – Glycidyl acrylate-modified sodium alginate

SEC – Size exclusion chromatography

SEM – Scanning electron microscopy

T – Time

TEA/NEt₃ – Triethylamine

Thio-Alg – Thiolate-modified sodium alginate

TIME – Tissue debridement, Infection control, Moisture maintenance, Epidermal advancement

UT – University of Texas

UV – Ultraviolet

UV-vis – Ultraviolet-visible spectroscopy

List of Figures

Figure 1.1. The four successive stages of wound healing.....	6
Figure 1.2. The T.I.M.E protocol of wound management.....	7
Figure 1.3. 1C_4 and 4C_1 configurations of sodium alginate in chair conformation.....	16
Figure 1.4. The anatomy of brown sea algae.....	17
Figure 1.5. Anomeric region of 1H -NMR spectrum of an alginate polysaccharide indicating combinations of oligomeric block sequences. Copyright © 2011 John Wiley & Sons, Ltd.....	18
Figure 1.6. Diagram depicting areas of topological entanglement (left) and cohesional entanglement (right) on polymeric strands.....	19
Figure 2.1. The acrylating agent used in this thesis, glycidyl acrylate.....	27
Figure 2.2. The thiolating agents used in this thesis, L-cysteine hydrochloride and Cysteamine hydrochloride.....	28
Figure 2.3. 1H -NMR spectra of alginic acid performed at 50 °C, 60 °C, 70 °C and 80 °C. Figure used with authorisation.....	29
Figure 2.4. Illustration of analyte separation and elution in a GPC column and chromatograph prediction.....	33
Figure 2.5. Flow and deformation properties for solid and liquid state materials.....	34
Figure 2.6. Material shear thickening and thinning with force application.....	34
Figure 2.7. Time-dependent viscoelastic fluids.....	35
Figure 2.8. Diagram of material shear and mathematical calculations to calculate shear rate.....	36
Figure 2.9. Mathematical relationship between G' , G'' and G^*	37
Figure 2.10. Simplified schematic of a scanning electron microscope.....	39
Figure 2.11. Simplified schematic of a confocal microscope.....	40

Figure 2.12. Annotated photograph of a rheometer.....	50
Figure 2.13. Diagram of a rheometer platform.....	51
Figure 3.1. GPC chromatograph of High M alginate procured from Sigma-Aldrich. The diagonal red line corresponds to the calibration curve.....	54
Figure 3.2. GPC chromatograph of High G alginate procured from ConvaTec Rhymney. The diagonal red line corresponds to the calibration curve.....	54
Figure 3.3. A stacked ^1H NMR spectrum of glycidol (top), acryloyl chloride (middle) and synthesised glycidyl acrylate (bottom)... ..	58
Figure 3.4. Annotated ^1H NMR spectrum of glycidyl acrylate.....	59
Figure 3.5. ^1H NMR spectrum of an acrylate-substituted High-M alginate. NMR conducted at 70 °C, D_2O , 500 MHz with 256 scans.....	61
Figure 3.6. ^1H NMR spectrum of an acrylate-substituted High-G alginate. NMR conducted at 70 °C, D_2O , 500 MHz with 256 scans.....	61
Figure 3.7. Difference in appearance in the colour of alginate solution after a 4 h acrylation reaction. Left – an acrylated alginate solution prepared at 60 °C. Right – an acrylated alginate solution prepared at r.t. (25 °C).....	65
Figure 3.8. Acrylated alginate dried via lyophilisation (left) and dried <i>in vacuo</i> at room temperature (right).....	68
Figure 3.9. Dried High-M (left) and High-G (right) acrylated alginate.....	69
Figure 3.10. Dried High-M (left) thiolated alginate and High-G (right) thiolated alginate.....	71
Figure 3.11. ^1H -NMR spectrum of thiolate-substituted High-M alginate. NMR conducted at 25 °C, D_2O , 500 MHz with 256 scans.....	72
Figure 3.12. ^1H -NMR spectrum of thiolate-substituted High-G alginate. NMR conducted at 25 °C, D_2O , 500 MHz with 256 scans.....	73
Figure 3.13. Calibration curve of thiol concentration in HPLC water.....	76
Figure 3.14. Stacked ^1H -NMR spectrum of thiolate-substituted High-G alginates performed under pH 6.0 (top), pH 5.0 (middle) and pH 4.0 (bottom).....	79

Figure 3.15. Stacked ^1H -NMR spectrum of thiolate-substituted High-G alginates performed under 40 °C (top) and at 25 °C (bottom).....	81
Figure 3.16. Thiolated alginate in solution after reacting against cysteine for 3 hrs in r.t. (25 °C K). Gel aggregation is visible in solution (1 % w/w G-Alg in DI- H_2O).....	82
Figure 3.17. Left – Cysteine dissolved in aqueous alkaline media (Dil. NaOH; pH 8.0). Middle – pH-adjusted cysteine solution added to sodium alginate solution (1 % w/w G-alg in DI- H_2O). Right – Following addition of cysteine in powder form to sodium alginate solution (1 % w/w G-alg in DI- H_2O).....	82
Figure 3.18. Left – High-G Thiolated alginate in solution following reaction and awaiting purification. A visible gel lump can be seen in solution. Right – Two samples of thiolated alginate (Left – M, Right- G) in solution after purification awaiting drying. Wisps of milky white can be seen in the alginate solution on the right.....	83
Figure 3.19. Photographs of gels formed from photogelation. Left to right: 2.5 % w/v acrylated alginate with photoinitiator, 3.5 % w/v acrylated alginate with photoinitiator, covalent-crosslinked 3.5 % w/v alginate gel with photoinitiator, covalent-crosslinked 3.5 % w/v alginate gel with photoinitiator.....	86
Figure 3.20. Oxidation of dithiothreitol into disulphide.....	88
Figure 3.21. Photograph depicting no gelation (left), gel particulate formation (middle) and bulk gel formation (right).....	89
Figure 3.22. Photograph of gelation study between acrylated alginate, thiolated alginate and QT crosslinker.....	91
Figure 3.23. Prepared alginate gels being loaded with carmoisine solution.....	92
Figure 3.24. Carmoisine calibration curve in HPLC water at 412 nm.....	93
Figure 3.25. Graph showing release profiles of different alginate gels.....	94
Figure 3.26. Rheological data from time test experiment using acrylated alginate with QT crosslinker.....	95
Figure 3.27. Rheological data from time test experiment using acrylated alginate with thiolated alginate. Sample dehydration is apparent from $T = 25000 \text{ s}$	96

Figure 3.28. Photographs of hydrogels formed during rheological testing. Left – acrylated alginate with QT crosslinker. Right – acrylated alginate with thiolated alginate.....	97
Figure 3.29. Rheological data of oscillatory frequency sweep between 0.1 and 100.0 Hz. A shear thinning behaviour was observed.....	97
Figure 3.30. Data from time test rheological experiments. Left – 50 mm parallel plate. Right – 20 mm parallel plate.....	98
Figure 3.31. Overlay of storage modulus values obtained from rheological experiment. Alginate samples were High-G and all exhibited DoS% between 25-30 % with varying concentration in solution. Loss moduli and phase angle values omitted for simplicity.....	100
Figure 3.32. Overlay of storage modulus values obtained from rheological experiment. Alginate samples were High-G, dissolved at 5.8 % w/v and exhibited varying DoS%. Loss moduli and phase angle values omitted for simplicity.....	100
Figure 3.33. Rheological data from oscillatory time test on a High-M alginate sample, low DoS%, dissolved at low concentration.....	101
Figure 3.34. Rheological data from oscillatory time test on a High-G alginate sample, low DoS%, dissolved at medium concentration.....	102
Figure 3.35. Creep test data of formed alginate gel.....	103
Figure 3.36. SEM images of acrylated (left) and thiolated (right) alginate.....	104
Figure 3.37. Confocal image of alginate hydrogel. A: Focal plane image of hydrogel. B: Dimension measurement from its highest point. C: Visualisation of the cross section. D: Microscopic image.....	104
Figure 3.38. Microscopic image of an alginate gel. Droplets of QT crosslinker can be seen embedded under the gel surface.....	105
Figure A.1. GPC trace of High-M alginate.....	121
Figure A.2. GPC trace of High-G alginate.....	122
Figure A.3. ¹ H NMR spectrum of GA1.....	123

Figure A.4. ^1H NMR spectrum of GA2.....	124
Figure A.5. ^1H NMR spectrum of GA3.....	125
Figure A.6. ^1H NMR spectrum of GA4.....	126
Figure A.7. ^1H NMR spectrum of High-M acrylated alginate.....	127
Figure A.8. ^1H NMR spectrum of High-G acrylated alginate.....	128
Figure A.9. ^1H NMR spectrum of acrylated alginate reaction conducted at room temperature for 4 hours.....	129
Figure A.10. ^1H NMR spectrum of acrylated alginate reaction conducted at room temperature for 12 hours.....	130
Figure A.11. ^1H NMR spectrum of acrylated alginate reaction conducted at room temperature for 24 hours.....	131
Figure A.12. ^1H NMR spectrum of TA2.....	132
Figure A.13. ^1H NMR spectrum of TA5.....	133
Figure A.14. ^1H NMR spectrum of TA6.....	134
Figure A.15. ^1H NMR spectrum of TA7.....	135
Figure A.16. ^1H NMR spectrum of TA8.....	136
Figure A.17. ^1H NMR spectrum of TA9.....	137
Figure A.18. ^1H NMR spectrum of TA10.....	138

List of Tables

Table 1.1. Classification of DFU based on its characteristics.....	5
Table 1.2. Advantages and disadvantages of different types of dressings used in DFU treatment.....	8
Table 1.3. Materials commonly researched for DFU wound dressings, their advantages and their disadvantages.....	12
Table 3.1. Tabulated information of alginate samples obtained from GPC analyses.....	54
Table 3.2. Simplified table of some acrylate syntheses performed. Refer to thesis Chapter Section (2.2.3.1) for quantities used at different reaction scales.....	55
Table 3.3. Simplified table of reaction parameters trialled and trialled conditions with the alginate acrylation step.....	63
Table 3.4. Expected range of degree of substitution in alginate acrylation reactions performed at 60 °C.....	64
Table 3.5. Tabulated view of experimental maximum DoS% values obtained from acrylation reaction kinetic studies. Results for reaction time of 48 h were omitted due to lack of data. *Estimated DoS% too low to report with confidence.....	66
Table 3.6. Expected range of degree of substitution in alginate thiolation reactions.....	71
Table 3.7. Tabulated information of alginate thiolation experiments performed, with estimated M/G ratio and DoS%.....	74
Table 3.8. Tabulated data from UV-vis spectroscopy trials of thiolated alginate samples.....	77
Table 3.9. Tabulated results of thiol density of various synthesised thiolated alginate samples along with their respective DoS%.....	77

Table 3.10. Simplified view of reaction parameters trialled and trialled conditions with the alginate thiolation step.....	78
Table 3.11. Conditions used for ionotropic gelation trials.....	85
Table 3.12. Information of volumes used for photogelation trials.....	85
Table 3.13. Conditions used for photogelation experiments.....	86
Table 3.14. Simplified overview of laboratory gelation study conditions using acrylated alginate and thiolated alginate.....	90
Table 3.15. Simplified overview of laboratory gelation study conditions using acrylated alginate and QT crosslinker.....	90
Table 3.16. Tabulated view of volumes handled for rheological experiments using acrylate-modified alginate and QT crosslinker.....	99
Table 3.17. Tabulated view of volumes handled for rheological experiments using acrylate-modified alginate and thiolate-modified alginate.....	99

List of Schemes

Scheme 1.1. Photoinitiation of Irgacure 2959®.....	20
Scheme 1.2. Preparation of methacrylatedalginate by alkylation of hydroxyl functional group.....	21
Scheme 1.3. i) Thiolation of sodium alginate. ii) Formation of disulphide linkage to form gel and basic hydrolysis leading to gel dissolution.....	22
Scheme 3.1. Poly-acrylation of glycidyl acrylate.....	56
Scheme 3.2. Mechanism of synthesis of glycidyl acrylate from glycidol.....	57
Scheme 3.3. Alkylation of sodium alginate to introduce acrylate functionality.....	60
Scheme 3.4. Two potential pathways for acrylate substitution on alginate.	63
Scheme 3.5. Reduction of Ellman's Reagent (DTNB) with 2-mercaptoethanol into TNB.....	75
Scheme 3.6. Removal of EDCI activating group by acid-catalysed amide formation.....	80
Scheme 3.7. Simplified depiction of crosslink mechanism between acrylated alginate and different thiol moieties to form hydrogel.....	88

Table of Contents

Chapter One: Introduction

1.1 Context.....	1
1.2 Diabetes: onset, complications, surgical procedures, and wound management.....	1
1.2.1 <i>Diabetes Mellitus</i>	2
1.2.1.1 Classifications of <i>Diabetes Mellitus</i>	2
1.2.1.2 Onset symptoms.....	3
1.2.2 Complications of <i>Diabetes Mellitus</i>	3
1.2.3 Diabetic foot ulcers.....	4
1.2.3.1 Ulcer classification.....	4
1.2.3.2 Medical procedures.....	5
1.2.3.3 Wound care and management.....	6
1.2.3.4 Wound dressings.....	8
1.2.3.4.1 Wound dressing materials.....	10
1.3 Chemistry of alginates and its use in biomedical applications.....	16
1.3.1 Natural occurrence and chemical composition.....	16
1.3.2 Molecular weight and polydispersity.....	17
1.3.3 Alginate-based systems in DFU treatment.....	19
1.3.4 Chemical behaviour.....	20
1.3.5 Alginate chemical modifications.....	20
1.3.5.1 Methacrylated and acrylated alginates.....	21

1.3.5.2 Thiolated alginates.....	22
1.3.6 Toxicological considerations.....	23
1.3.7 Alginate gelation and post-gelation tests.....	23
1.4 Project aims and rationale.....	24

Chapter Two: Analytical techniques, Experimental and Characterisation

2.1 Fundamentals of analytical methodologies.....	26
2.1.1 Nuclear Magnetic Resonance (NMR) spectroscopy.....	26
2.1.2 UV-visible (UV-vis) spectroscopy.....	29
2.1.2.1 Conversion of UV readings into thiol density.....	30
2.1.3 Gel Permeation Chromatography (GPC)	31
2.1.4 Rheology.....	33
2.1.5 Scanning Electron Microscopy (SEM) and confocal microscopy.....	38
2.2 Experimental Procedures.....	40
2.2.1 Materials.....	40
2.2.2 Synthesis of hydrogel precursors.....	41
2.2.2.1 Glycidyl acrylate.....	41
2.2.2.2 Acrylation of sodium alginate.....	43
2.2.2.3 Thiolation of sodium alginate.....	43
2.2.3 Preparation of alginate hydrogels.....	45
2.2.3.1 Ionotropic gelation.....	46
2.2.3.2 Covalent gelation via <i>in-situ</i> Michael-type addition.....	46
2.2.3.3 Photogelation.....	47
2.2.4 Analytical characterisation procedures.....	48

2.2.4.1 Nuclear Magnetic Resonance (NMR) spectroscopy characterisation.....	48
2.2.4.2 Thiol content determination using Ellman's Reagent.....	48
2.2.4.3 Gel Permeation Chromatography (GPC) analysis.....	49
2.2.4.4 Hydrogel gelation characterisation.....	49
2.2.4.4.1 Release studies.....	49
2.2.4.4.2 Rheological studies.....	50
2.2.4.4.3 Scanning Electron Microscopy (SEM) and confocal microscopy tests.....	52

Chapter Three: Results and Discussion

3.1 Overview.....	53
3.1.1 GPC analysis of sodium alginates.....	53
3.2 Synthesis of Glycidyl Acrylate.....	55
3.2.1 Factors affecting yields and purity of synthesised acrylate.....	56
3.2.2 NMR Characterisation of glycidyl acrylate.....	57
3.3 Acrylation of Sodium Alginate.....	59
3.3.1 Characterisation of acrylated alginate.....	60
3.3.1.1 NMR characterisation of acrylated alginate.....	60
3.3.2 Factors affecting the degree of substitution (DoS%) and yield.....	62
3.3.3 Comparison of High-M vs High-G alginate.....	69
3.3.4 Conclusion.....	70

3.4 Thiolation of Sodium Alginate.....	70
3.4.1 Thiolated alginate.....	70
3.4.1.1 NMR characterisation of thiolated alginate.....	72
3.4.1.2 UV-vis spectroscopic analysis of thiolated alginate.....	75
3.4.2 Factors affecting the degree of substitution (DoS%) and yield.....	78
3.4.3 Setbacks.....	82
3.4.4 Conclusion.....	83
3.5 Alginate hydrogels: preparation, characterisation and tests.....	84
3.5.1 Preparation of alginate hydrogels.....	84
3.5.1.1 Preparation by ionotropic crosslinking.....	84
3.5.1.2 Preparation by photogelation crosslinking.....	85
3.5.1.3 Preparation by covalent crosslinking.....	87
3.5.1.3.1 Thiol moieties.....	87
3.5.1.3.2 Preparation of alginate hydrogels.....	89
3.5.2 Characterisation of prepared hydrogels.....	92
3.5.2.1 Release studies of alginate gels.....	92
3.5.3 <i>In-situ</i> hydrogel characterisation.....	94
3.5.3.1 Rheological test data.....	94
3.5.3.2 Microscopy tests.....	103
3.5.4 Conclusion.....	105

Chapter Four: Conclusions, project direction and future work

4.1 Introduction.....	107
4.2 General discussion.....	107

4.3 Future work.....	108
-----------------------------	------------

References.....	110
------------------------	------------

Appendix

A,1 GPC data.....	121
--------------------------	------------

A.2 NMR data.....	123
--------------------------	------------

Chapter 1: Introduction

1.1 Context

Diabetic foot ulceration (DFU) is a frequent and chronic complication amongst diabetic patients, with patients undergoing scalpel debridement or limb amputation. There is a demand from physicians for wound dressings to address a multitude of clinical issues, in addition to being highly cost-effective. Alginates are generally regarded as biocompatible and expresses strong mucoadhesive properties and light-haemostatic effects as well as high moisture retention. Its attractive mechanical properties and high chemical versatility makes it a sought-after material for wound therapeutic development.

1.2 Diabetes: onset, complications, surgical procedures, and wound management

This section aims to give a brief overview into diabetes with the inclusion of some current knowledge and literature. Diabetes research is a broad area and this section does not aim to provide a definite and thorough view into the disorder. However, to set the scope of this project, it is important to provide to the readers some context regarding its causation, diagnosis, and methods of treatment to justify the project aims. This section will cover how diabetes is classed as a chronic medical disorder, and how genetic and environmental factors play a role in its onset. The diagnosis and clinical procedures will be discussed in brief, and options regarding post-operative wound therapy will be detailed. The clinical challenges faced by clinicians along with clinical demands will be presented, which sets the landscape for this work.

1.2.1 Diabetes Mellitus

Diabetes Mellitus, commonly known as diabetes, is a well-known medical disorder affecting the lives of over 460 million individuals worldwide. The number of diabetic patients is estimated to surpass 700 million by 2045.^{1,2} The way of life for many individuals has become convenient due to global urbanisation. This has paved the way for, and promoted, a lifestyle more sedentary particularly for those living in more developed countries. These transitions have contributed to the prevalence of diabetes.^{3,4}

Diabetes is a metabolic disorder and is described as metabolic change brought on by blood glucose levels being in a state of constant elevation, resulting in alterations in lipid, protein and carbohydrate metabolism due to changes in insulin production, insulin secretion, insulin action or a combination of the three processes.⁵ Diabetes is generally classified as type 1, referred to as congenital *diabetes mellitus*, or type 2 which is developed at later stages in life as a result of lifestyle consequences.⁶ However, other classifications of diabetes do exist, albeit lesser known, such as type 3 Alzheimer-onset diabetes and gestational diabetes which affects expectant mothers in the third trimester of pregnancy as a result of glucose intolerance.⁷

1.2.1.1 Classifications of Diabetes Mellitus

Type 1 diabetes, or insulin-dependent *diabetes mellitus* (IDDM), is the aftermath of pancreatic β -cells destruction resulting in insulin insufficiency and consequential total dependence on exogenous insulin via intravenous administration.⁸ Diagnosis for IDDM patients is usually made during early stages in life, hence the coining of the term neonatal diabetes, or juvenile-onset diabetes.⁹ Type 2 diabetes, or non-insulin-dependent *diabetes mellitus* (NIDDM), is usually diagnosed in later stages in life. Type 2 diabetes accounts for over 90 % of all diabetic diagnosis and is defined by a consistent high level of blood sugar present.¹⁰ Alzheimer onset diabetes is understood to be a sub-classification of the Type 2 diabetes and is more common amongst patients above age 65.¹¹ Patients usually suffer from high blood pressure and high cholesterol which could be the result of dysregulated glucose metabolism,

in addition to oxidative stress, reduced insulin signalling efficiency and production of advanced glycans which are characteristics common for both diseases.^{12,13}

Gestational *diabetes mellitus* (GDM) is caused by an impairment in glucose tolerance during gestation and poses as a further risk factor for the onset of type 2 diabetes in women.^{14,15} NIDDM and GDM, unlike IDDM, may be reversed through balanced dieting or lifestyle changes.

1.2.1.2 Onset symptoms

The symptoms of diabetes are often overlooked or dismissed in confusion with other bodily ailments as the chronic progression is slow and may not become noticeable to be of attention until long-term damage is being sustained. Onset symptoms may include frequent urination, excessive thirst and hunger, inexplicable weight loss, increased or constant fatigue, irritability, blurry vision and dry skin as a result of poor blood flow.¹⁶ If left undiagnosed and untreated, diabetes can inflict long-term damage, including life threatening complications, which severely impacts the body's function and compromises the patient's quality of life.

1.2.2 Complications of Diabetes Mellitus

Diabetic ketoacidosis (DKA) is a grievous diabetes-related complication brought on by a lack of insulin in the body which consequently breaks down lipids as a source of energy, releasing ketones. The build-up of ketones in the body poisons the blood, rendering blood serum more acidic which can pose serious threats. DKA affects IDDM patients predominantly but can also manifest in NIDDM patients.^{17,18} Diabetic peripheral neuropathy (DPN) is a common complication amongst diabetic patients due to poor blood flow and consistently high glycaemic levels. Peripheral nerve fibres are progressively damaged with distal extremities made more susceptible.^{19,20} Another common complication is peripheral arterial disease (PAD), caused primarily by atherosclerosis, which results in poor blood flow and a more complicated wound

recovery process.^{21,22} The combination of DPN and PAD results in a reduced response to pain detection and wounds more susceptible to infections and further complications, which makes any trauma difficult to detect and challenging to heal.^{23,24}

1.2.3 Diabetic foot ulcers

Diabetic foot ulceration (DFU), linked closely to DPN and PAD, is a frequent and serious complication amongst diabetic patients. Ulcerations are classed as neuropathic and neuroischaemic depending on factors of causation and patient prognoses with different classification systems.^{25,26} However, two systems that are most commonly used for diabetic foot ulcer grading are the University of Texas (UT) classification system and the Meggitt-Wagner classification system.^{27,28} Table 1.1 shows a modernised DFU classification system based on the information obtained from the UT and Meggitt-Wagner classification systems.^{29,30}

1.2.3.1 Ulcer classification

Neuropathic foot ulcers represent the majority of DFU cases, although both neuropathic and neuroischaemic foot ulceration can occur simultaneously.³¹ The wound condition varies widely depending on the patient, but wounds are generally classed as dry or wet wounds, with wet wounds being further classified as bleeding, low-exudate or exudate-heavy wounds. Slough or eschar may also be present which are complexes of fibrins, extracellular matrix (ECM) proteins, exudates and microorganisms in its wet or dry form. Wound tissues may also experience tissue necrosis due to poor blood flow, which leads to gangrenous tissue formation. Some wounds may heal unevenly and at different rates at different parts of the wound site, which is called a complex wound.^{29,32,33}

Table 1.1. Classification of DFU based on its characteristics.²⁹

Characteristics	Neuropathic ulcer	Neuroischaemic ulcer
<i>Patient demographic</i>	Any	Strong history with ailments brought on by unhealthy lifestyle
<i>Causation</i>	Minor trauma	May occur spontaneously
<i>Mode of occurrence</i>	Patient may be unaware of onset	Sudden in onset with pain and foot discoloration
<i>Foot temperature</i>	Normal or warm	Cold
<i>Ulcer site</i>	Predominantly at pressure areas	Edges of feet, tips of toes or backs of heels.
<i>Ulcer appearance</i>	With border indentation	Border indent with some degree of tissue necrosis
<i>Pain during debridement</i>	Very little to none; dependent on neuropathy	Moderate

1.2.3.2 Medical procedures

Acute ulcers typically require sharp debridement to promote wound healing and epithelization. However, in more severe cases where necrotic tissue has begun to form, limb amputation becomes necessary to prevent further harm to the patient.^{34,35} Regardless of the clinical procedure performed, patients are left with an open wound whereby the wound site is often rugged and irregular with the potential to be cavernous (tunnelling wound) which requires varying degrees of wound care and dressing applications.^{36,37} Given the nature of the wound and factors which negatively impact the wound healing process, the wound should be assessed regularly as it heals.^{36,37} DFU wounds are highly susceptible to further infection as a result of high glycaemic levels which translates to dysregulated wound healing where the four recovery stages may reverse in progression or uneven wound healing

(Figure 1.1), resulting in a complex wound whereby the same wound site undergoing multiple stages of recovery which requires further debridement to re-initiate the healing process.³⁶

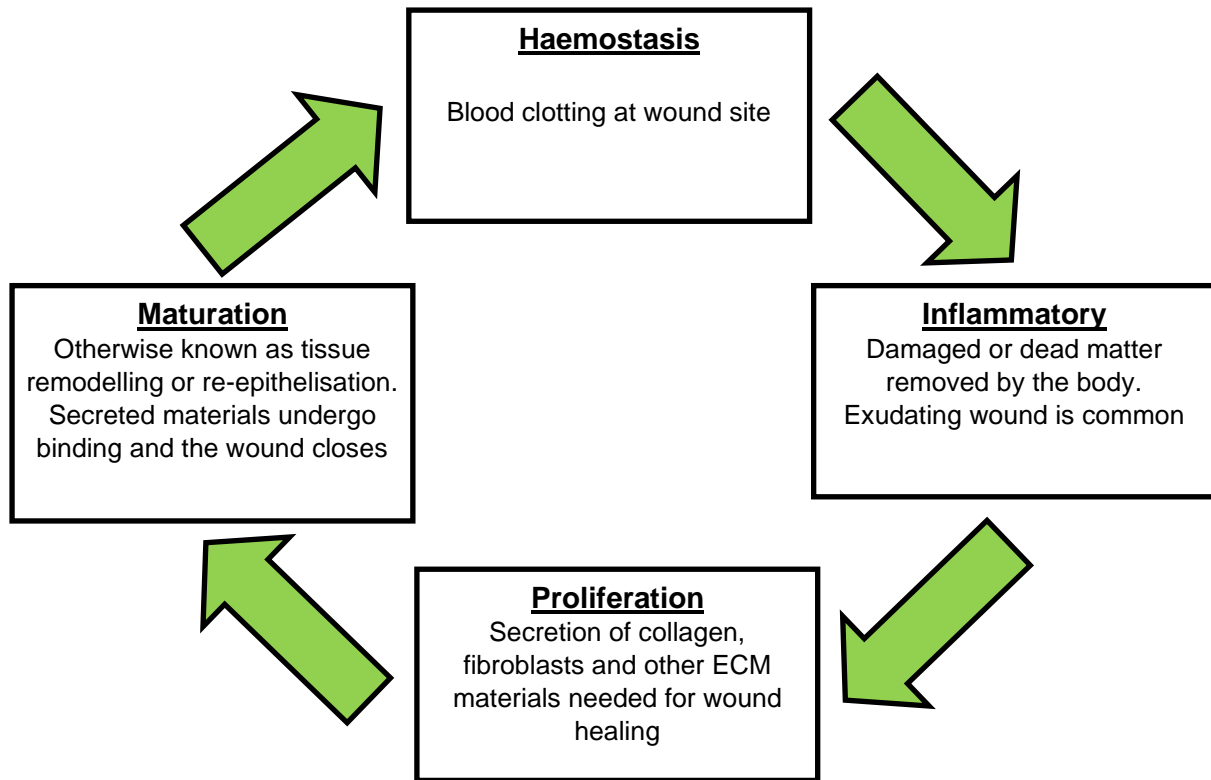


Figure 1.1. The four successive stages of wound healing.³⁸

1.2.3.3. Wound care and management

The management of ulcer wounds becomes a shared responsibility between physicians, nurses, carers and the patients themselves. Generally, medical personnel refer and adhere to the **T.I.M.E** (**T**issue debridement, **I**nfection control, **M**oisture maintenance of wound site, **E**pidermal advancement) concept and Protocol of Care (POC) in wound care in order to promote better wound management and better wound healing (Figure 1.2).³⁹ The protocols include selecting the optimal method of tissue removal based on patient prognosis and wound assessments, wound cleansing, timely dressing changes, selecting the most appropriate wound dressing material depending on wound environment and the usage of antibiotics or

antimicrobials to hinder the growth of microorganisms at the wound site. Wound care and management are often overlooked by carers and patients, and in turn poses a challenge on clinicians to source remedies and dressings which are easy to use and highly effective even in the hands of a non-professional.^{40,41} There is a demand for wound dressings which are suitable for application on different types of wounds, address clinical needs, are cheap to procure and are cost-effective.

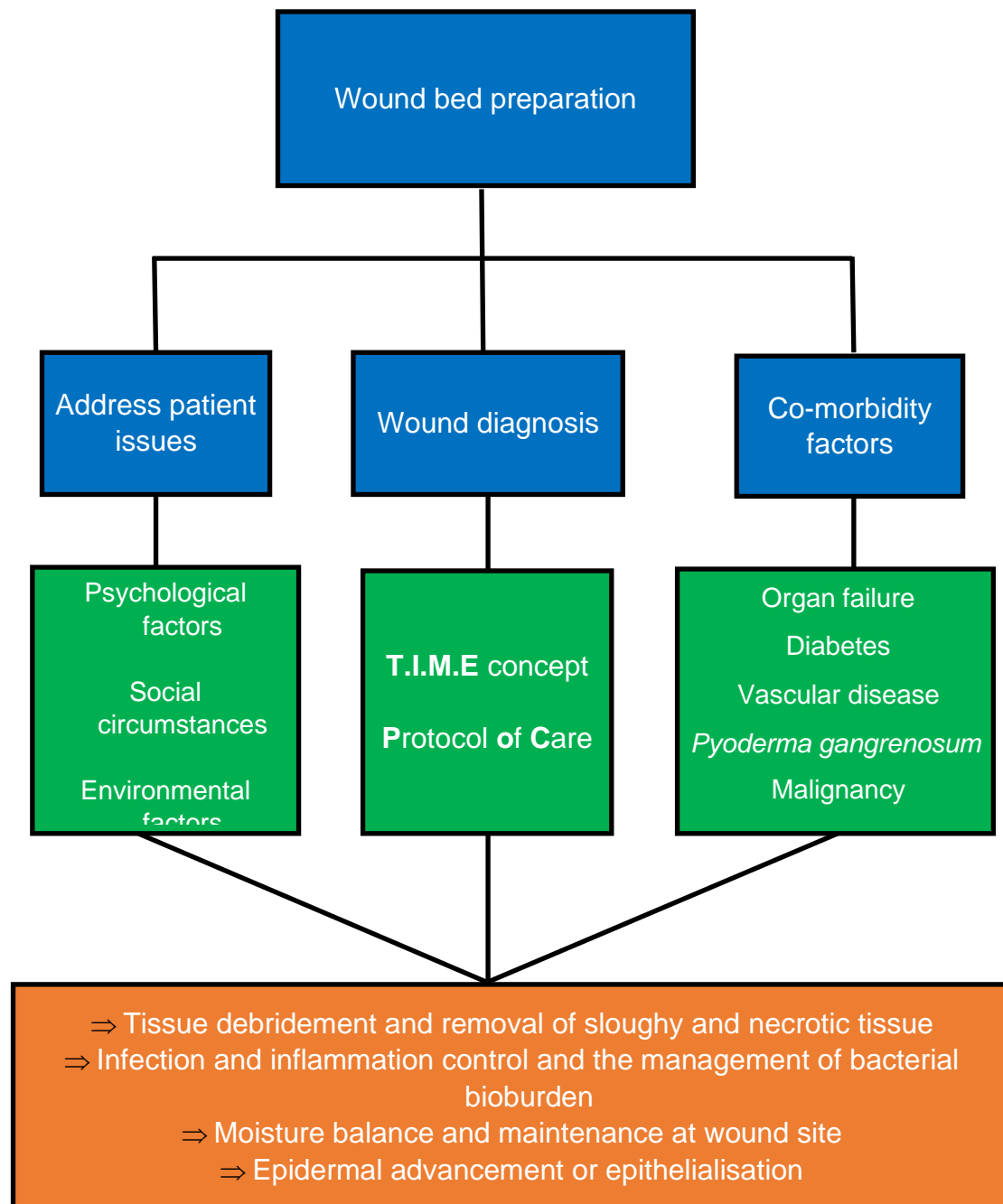


Figure 1.2. The T.I.M.E protocol of wound management.^{39,41,42}

1.2.3.4 Wound dressings

Historically, gauze wound dressings served as a protective barrier between the wound site and the atmosphere, preventing microorganisms from entering the wound.⁴³ Modern day dressings have been innovated to facilitate wound healing by providing a number of beneficial properties such as moisture donation and wicking, exudate and autolytic debris removal, enabling gas exchange, infection prevention and promote wound healing with the inclusion of growth factors.⁴⁴ Human skin is widely considered as a superb dressing due to its cellular compatibility and thus modern wound dressings try to mimic its natural properties.⁴⁵ Numerous commercial wound dressings were made available to address different clinical needs, many of which were fabricated from different types of materials and in different formats (Table 1.2).¹⁶ It is important to note that there is no single perfect wound dressing as wound sites may vary from patient to patient and the wound condition may drastically change at different stages of wound healing. The wound site dimensions and its environment should be taken into consideration when selecting the most appropriate wound dressing.^{38,44,46,47}

Table 1.2. Advantages and disadvantages of different types of dressings used in DFU treatment^{37,48–50}

Type of dressing	Advantages	Disadvantage
Film	Good longevity	
	Facilitates autolytic debridement	
	Easy to fit around the exterior of the wound	Limited absorption capacity
	Can be applied and removed without great disturbance	May cause wound maceration in exudate-heavy wounds
	Semi occlusive	
	Good visualisation of wound site	
Hydrocolloid		Not optimal for infected wounds
	Exudate wicking	
	Facilitates autolytic debridement	Suspected to cause maceration
	Occlusive	
	Good longevity	Stains wound site Wounds become malodorous

Table 1.2 continued. Advantages and disadvantages of different types of dressings used in DFU treatment^{37,48–50}

Type of dressing	Advantages	Disadvantage
Hydrogel	Exudate wicking and moisture donation	
	Non-antigenic	
	Very high wound site conformity	Suboptimal for infected wounds
	Harm free application and removal	May be unsuitable for neuroischaemic ulcers
	Induces cooling effect	May cause wound maceration
	Can incorporate bioactive reagents	in exudate-heavy wounds
	Allows gas and metabolite exchanges	
Fibre	<i>Highly absorbent</i>	
	<i>High wound site conformity</i>	
	<i>Can be applied and removed without great disturbance</i>	<i>Residual fibres may remain in wound site on removal</i>
	<i>Can be doped with bioactive reagents</i>	<i>May not fill the entirety of the cavity efficiently</i>
	<i>Good longevity</i>	
Foam	Highly absorbent	Not suitable for low exudate or dry wounds
	Good thermal insulation	
	Easy to fit around the exterior of the wound	Can adhere to wound and potentially cause dermatitis
	Allows gas and water vapour exchange	Malodorous wound

Among the different types of dressings, films, foams and fibre dressings are the most used in hospitals generally due to their low costs and high effectiveness.⁵¹ Films and foam dressings fit around the wound site's exterior with ease and offers comfort in the post-operative stage. The swelling properties of fibre dressings are useful with tunnelling or cavernous wound sites where a tight wound packing is required to facilitate good healing.^{46,47} Despite their advantages, all three dressing types require dressing adhesive to secure the dressing in place which, upon removal, will induce pain and potentially aggravate the wound site.^{52,53}

Hydrocolloid dressings are used to facilitate wound debridement and promotes granulation. The dressing is paired with a film, foam or fibre layer to suit different clinical needs and provide cushioning. However, this type of dressing requires frequent changes which increases cost of wound management. The inclusion of iodine will stain the wound site which can make wound inspections difficult.⁴⁷

Hydrogels are networks of polymeric crosslinks able to absorb and retain the majority of its mass as moisture. There is tremendous interest in using hydrogels for wound healing applications and are considered novel in chronic ulcer wound therapeutics. Its exudate wicking and moisture donation properties promotes healthy wound healing and its gas and metabolite permeability increases its non-antigenicity.^{54,55} It has structural recovery properties which minimises risks of gel particulates becoming dislodged in the wound site. Hydrogels have the added benefit of antimicrobial agent and growth factor incorporation to facilitate autolytic debridement, combat infections and tissue granulation, making it suitable for most wound types. Its high moisture content may cause skin maturation on exudate-heavy wounds, so it has been typically favoured beyond the haemostatic stage of wound recovery.^{44,50} The usage of polymeric hydrogels as diabetic wound therapeutics will be further discussed in Section 1.3.5.

1.2.3.4.1 Wound dressing materials

Wound dressings are produced from materials from natural and synthetic origins to express different desirable properties to address clinical needs but composite material dressings are also common.

Natural materials such as collagen, chitosan, carboxymethylated cellulose (CMC) and alginate are often used as their nature assumes their biocompatibility (Table 1.3). Whereas poly(ethylene glycol) (PEG), poly(lactic acid) (PLA) and poly(vinyl alcohol) (PVA) are popular synthetic materials for wound dressings as their synthetic nature ensures higher uniformity and minimises discrepancies in their properties, in addition to having great tensile strength and strong resistance against *in vivo*

degradation.⁵⁶ However, in some rare cases, patients may express symptoms of dressing rejection due to its synthetic origin and lower biocompatibility.⁵⁷

Table 1.3. Materials commonly researched for DFU wound dressings, their advantages and their disadvantages. Polysaccharide chemical structures are presented in their protonated form.^{58–64}

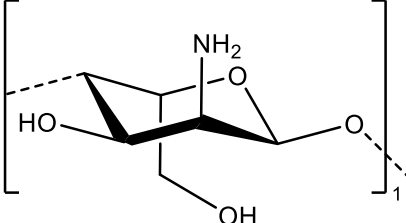
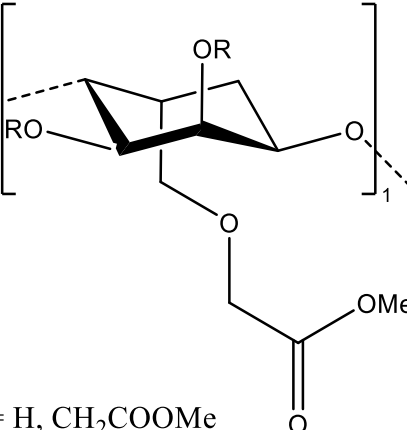
Material	Chemical structure	Advantages	Disadvantages
Collagen	$(X-Y-Gly)_n$ Two amino acid residues with glycine being the third in sequence	Optimal simulant for human skin Excellent tensile strength Moisture retention Highly resistant to <i>in vivo</i> degradation	Sourced from animals Scarce and high cost Risk of transmitting infectious disease from the source
Chitosan		Biocompatible Bio-adhesive Non-antigenic Antimicrobial High chemical versatility	Sourced primarily from animals Problems with solubility Risk of transmitting infectious disease from the source
CMC	 $R = H, CH_2COOMe$	Naturally abundant Biocompatible Highly resistant to degradation High rigidity Regulates growth factors in wound site	Lack of flexibility Lowly soluble Can undergo biodegradation

Table 1.3 continued. Materials commonly researched for DFU wound dressings, their advantages and their disadvantages. Polysaccharide chemical structures are presented in their protonated form.^{58–64}

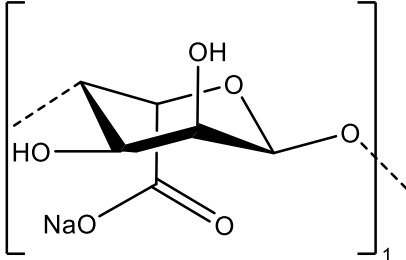
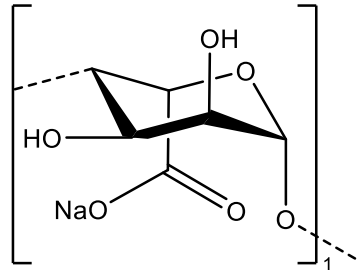
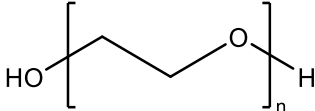
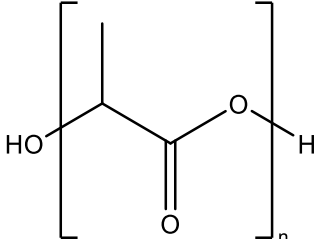
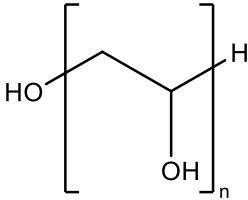
Material	Chemical structure	Advantages	Disadvantages
Sodium alginate <i>(mixture of β-D-mannuronate and α-D-guluronate)</i>	 <p>β-D-mannuronate</p>	Naturally abundant Highly biocompatible Low toxicity Mucoadhesive High chemical versatility pH sensitivity can be used for drug release models	Reliant on cationic interactions to remain stable and rigid over time
	 <p>α-D-guluronate</p>		

Table 1.3 continued. Materials commonly researched for DFU wound dressings, their advantages and their disadvantages. Polysaccharide chemical structures are presented in their protonated form.^{58–64}

Material	Chemical structure	Advantages	Disadvantages
PEG		Biocompatible Non-immunogenic Low toxicity Lightly lubricative Degradable on demand	Can undergo hydrophilic dissolution Reliant on other materials to achieve desired stability
PLA		Biocompatible Non-toxic High tensile strength Degradable on demand	Hydrophobic nature makes it difficult to handle Reliant on other materials to enhance performance
PVA		Biocompatible Non-toxic Non-carcinogenic High enzymatic and chemical degradation resistance Mucoadhesive Degradable on demand	Can undergo hydrophilic dissolution

Collagen is the most abundant protein to exist in human extracellular matrices (ECMs) and facilitates cell anchorage, migration and proliferation.⁶⁵ It expresses good tensile strength, provides resistance against degradation and is known to be the optimal material to simulate skin. However, its scarcity and cytocompatibility gives rise to its high price tag.^{66–69} Chitosan, the thermochemical deacetylated product of chitin, was the most researched material in the previous decade.⁷⁰ Its non-antigenicity, antimicrobial and bio-adhesive properties attracted the attention of many to harness those properties into wound therapeutic development. Its amino groups render it insoluble below pH 5.0, which can be circumvented by derivatising the amino and hydroxyl functional groups.

Cellulose is commonly used due to their high natural abundance and its highly porous structure translates to its high absorbency.^{71,72} A high degree of intra and inter-molecular hydrogen bonding lends itself to its high stability, tensile strength and, adversely, poor solubility in water. As such, cellulose is functionalised to afford its carboxymethylated derivative to express better bioresorbable and biodegradable behaviour.⁷³

Alginates are generally regarded as biocompatible, low in toxicity and expresses excellent mucoadhesive properties which excels in managing exudate-heavy wounds. Its high abundance, coupled with its multimodal chemical reactivity makes it the novel material in wound therapeutics^{44, 44,55,74} The chemistry of alginates as wound therapeutics will be discussed further in Section 1.3.

PEG expresses low toxicity and is lightly lubricative. Its hydrophilicity can be controlled by including a more relatively hydrophobic copolymer such as PLA, which possesses high tensile strength and is biodegradable.⁵⁵ Its biodegradability has become an attractive property in recent dressing development as it lends itself to its ability to dissolve on demand for easy dressing removal.^{62,63} PVA suffers from a lack of rigidity and thermal stability but is mitigated through crosslinking with another polymer to compensate for its lack of mechanical and tensile strength. In recent years, the degradability properties of synthetic polymers have been investigated to produce materials which degrade on demand through enzymatic or stimuli degradation with the aim of *in vivo* degradation in mind to address the issue of dressing residues remaining within the wound site following dressing removal.^{63,75}

1.3 Chemistry of alginates and its use in biomedical applications

This section provides literature and scientific research pertaining to alginates and alginate modifications, with an emphasis on alginate hydrogels for wound healing applications. Literature relevant to this project and similar research conducted by other researchers will also be presented. Lastly, the tests available to be conducted on hydrogels are briefly mentioned. Information and background of analytical tests conducted as part of this work can be found in the next thesis chapter.

This work uses alginate for hydrogel dressing development due to its high natural abundance, low-toxicity, high chemical versatility and multi-modal crosslinking mechanism (*vide infra*).

1.3.1 Natural occurrence and chemical composition

Alginates, found primarily within the cell walls and cell membranes of algae, are a family of linear polysaccharides which consists of a racemic mixture of (1→4) β -D-mannuronate and α -L-gulonate (Figure 1.3). The name of its uronic monosaccharide give rise to the denotation M- and G-residues.

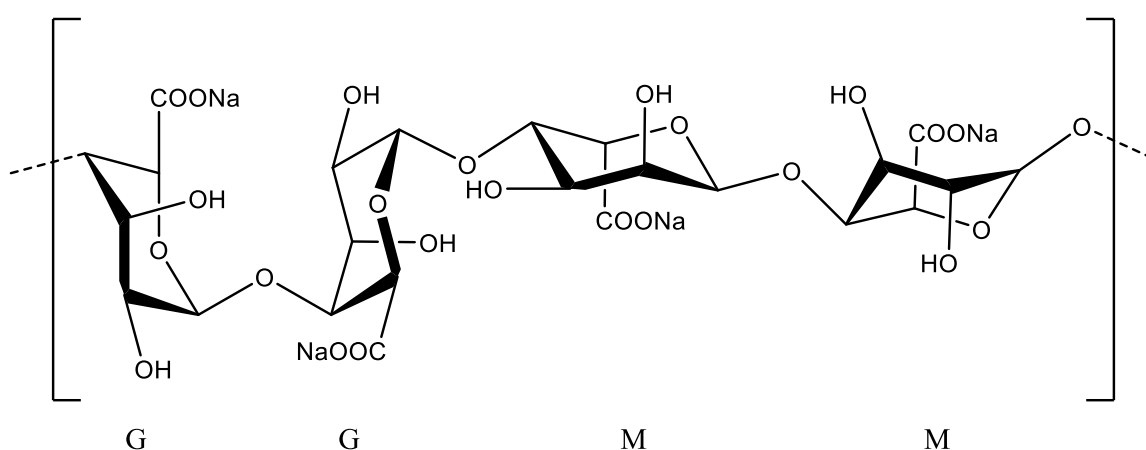


Figure 1.3. 1C_4 and 4C_1 configurations of sodium alginate in chair conformation.

Mannuronates can be found concentrated at the sporophylls and guluronates are found primarily in the blades and stipes of the macroalgae (Figure 1.4). Alginate

contains a mixture of di-equatorial (M-M), di-axial (G-G), equatorial-axial (M-G) and axial-equatorial (G-M) glycosidic linkages. The equatorial arrangement of M-block alginates allows high degree of flexibility. The enantiomer therefore expresses higher malleability compared to its G-counterpart. G-residues have higher structural rigidity due to the 'egg-box effect', first reported by Grant in 1973.⁷⁶ The spatial configuration of G-residues forms a cavity in which a divalent cation can sit and establish strong ionic links which is sterically protected by polymeric strands.

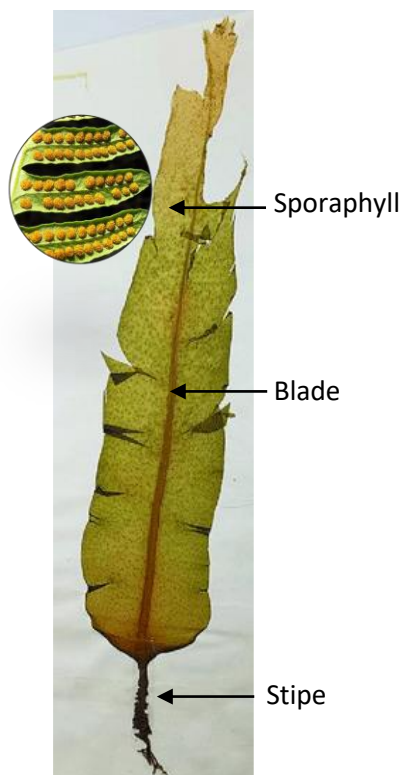


Figure 1.4. Anatomy of brown sea macroalgae.

1.3.2 Molecular weight and polydispersity

Alginate is commercially available with molecular weights averaging between 10^3 and 10^5 kDa. Oligomeric and monomeric alginate is prepared via partial or full depolymerisation of the polysaccharide chain.^{77,78} The length of the polysaccharide chain may be estimated using mass spectrometry or size exclusion chromatographic data and establishing a mass ratio between a monosaccharide unit and the polymer.

The chain length may also be calculated by dividing the total molecular weight with respect to the molecular weight of a singular monomeric unit (Equation 1).^{77,78}

$$\text{Number of repeating units} = \frac{\Sigma \text{ Molecular weight}}{\text{Molecular weight (monomeric unit; 208.06)}} \quad \text{Eqn. 1}$$

The molecular weight of the polymer is deduced using gel permeation chromatography (GPC), and three parameters that define their physical properties are obtained which are the peak molecular weight (M_p), the number-average molecular weight (M_n) and the weight-average molecular weight (M_w). For more information on GPC please refer to Section 2.1.3.

Alginate's PDI ranges from 0.3 to 3.0 depending on algae species, enantiomeric excesses, environmental factors and source location.⁷⁹ The relationship between the block length of alginate enantiomers and the enantiomeric excess was first reported by Grasdalen⁸⁰ using NMR resonance peaks integrations to estimate the ratio of mannuronate to guluronate present in alginate (Figure 1.5), coined the M/G ratio (Equations 2 and 3).^{81,82}

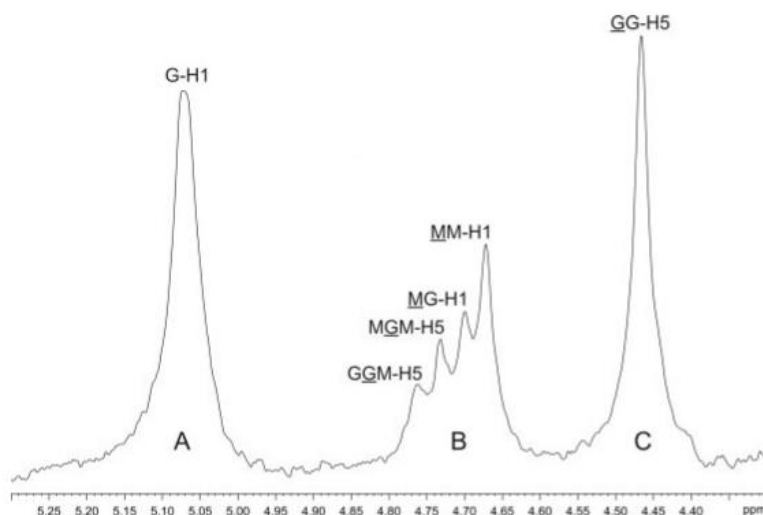


Figure 1.5. Anomeric region of ^1H -NMR spectrum of an alginate polysaccharide indicating combinations of oligomeric block sequences. Copyright © 2011 John Wiley & Sons, Ltd.⁸³

$$Fraction_G = \frac{Integration_A}{Integration_B + Integration_C} \quad Eqn\ 2$$

$$Fraction_M = 1 - Fraction_G \quad Eqn\ 3$$

The viscosity of alginate solutions is related to the concentration, chain length and enantiomer of alginates used.⁸⁴ M-alginates were found to express higher viscosity than its G-counterpart when dissolved at similar concentrations. The reasoning for this observation may be attributed to topological chain entanglements of the polysaccharide backbone (Figure 1.6).

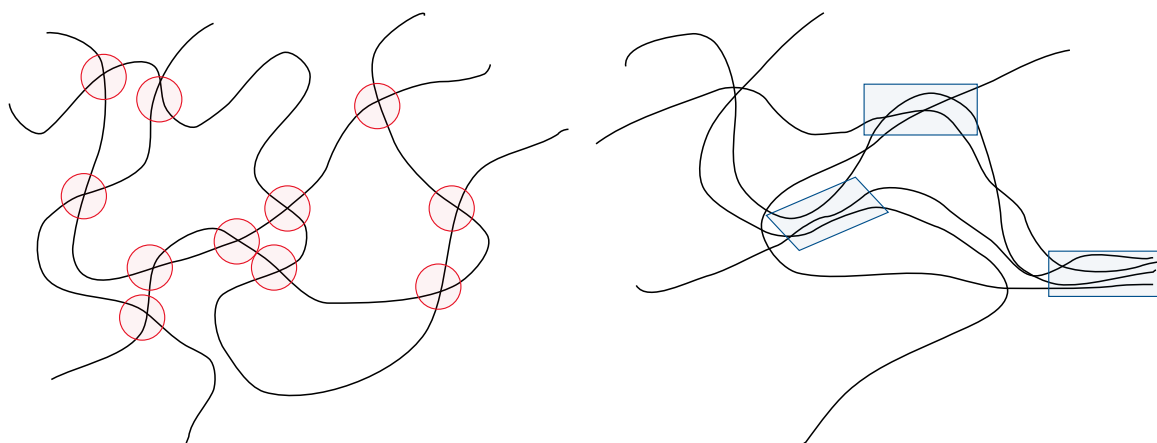


Figure 1.6. Diagram depicting areas of topological entanglement (left) and cohesion entanglement (right) on polymeric strands.⁸⁵

1.3.3 Alginate-based systems in DFU treatment

Alginate has been presented in the aforementioned dressing formats in ulcer wound therapeutics (Section 1.1.3.4). Alginate fibre dressings are commonly used due to its high absorbency and rigidity, such as the Aquacel®, Promogran® and MediHoney® dressings.^{47,86,87} Novel research into alginate include alginate hydrogels and the incorporation of coagulants, antimicrobial agents and growth factors to improve its wound healing efficacy. The addition of calcium is popular with alginate dressings as it facilitates haemostasis and bolster alginate's mechanical strength.^{88–90}

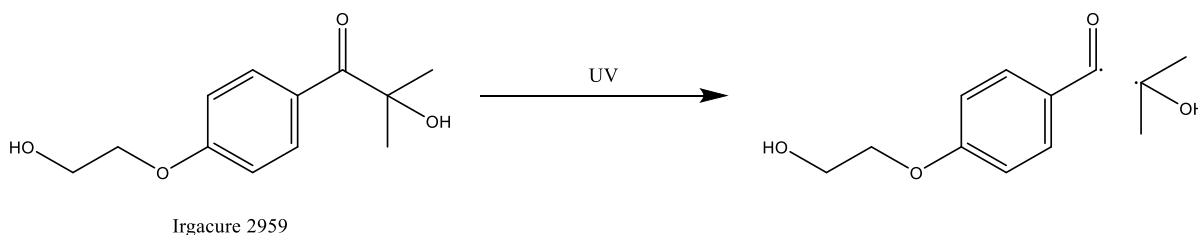
1.3.4 Chemical behaviour

Monovalent alginic salts, namely sodium, dissolve in water to afford alginic acid, with the pKa constant of guluronic acid and mannuronic acid at 3.65 and 3.38, respectively.⁹¹ Overall, there is negligible difference between the two enantiomers of alginate, but mannuronate dissolves more readily and undergoes functional group substitution more readily than guluronate as it experiences less steric hindrance from the polysaccharide backbone.⁹²

Water-dissolved sodium alginate undergo substitution with divalent cationic atoms and crosslink via ionotropic gelation to form a polymer network.⁹³ The resultant product is a stiff and brittle gel-like solid where, if sat in the same aqueous media, the kinetic equilibrium will shift towards the formation of sodium alginate, thus causing gel dissolution.

1.3.5 Alginate chemical modifications

Alginate has free carboxyl and hydroxyl functional groups distributed along the saccharide backbone. These can undergo chemical modification and gives rise to the potential of crosslinking via photo and covalent gelation to form hydrogels. The work published by Javvaji *et al.*⁹⁴ reported the photogelation of alginate using photo-protonation with calcium carbonate to form calcium alginate hydrogels intended for wound healing applications. The addition of calcium chelators induces dissolution over time, providing a degradation effect. Methacrylated alginate also undergoes photogelation through acrylic enolate linkage using photoinitiators such as Irgacure 2959[®] to form wound dressings for exudate-heavy wounds or for bone tissue engineering.^{95,96}



Scheme 1.1. Photoinitiation of Irgacure 2959[®]⁹⁷

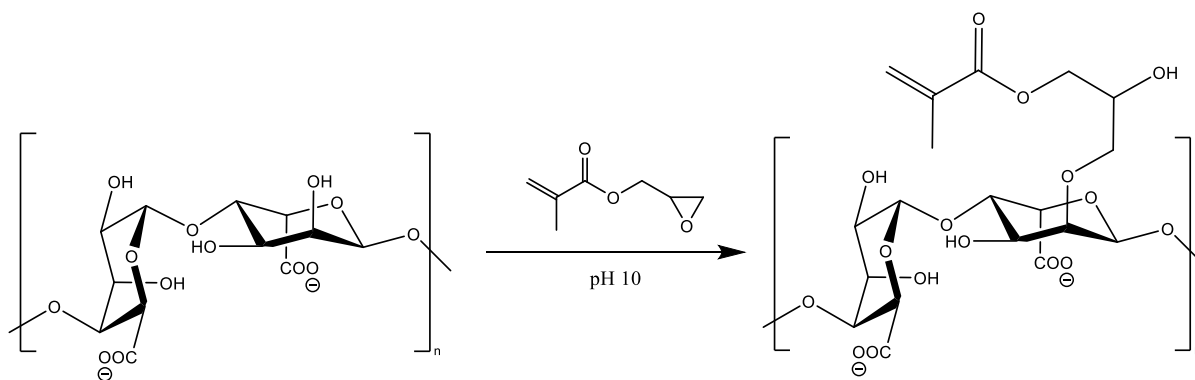
1.3.5.1 Methacrylated and acrylated alginate

Methacrylated alginate was extensively researched as a precursor material for photo-crosslinked hydrogels. The research published by Araiza-Verduzco⁹⁸ used photo-crosslinked methacrylated alginates as a material for load-bearing biomedical applications, and tailored the elasticity of the hydrogel by derivatising the alginate to induce steric effects and elongate chain lengths to tailor the strength of the enolate bond.

Photo-crosslinked methacrylated alginate-dextran composite hydrogels were also used as a vehicle for drug delivery, as published by Matricadi *et al.*⁹⁹ The gel porosity, and consequent drug delivery rate, is controlled by methacrylate substitution and polymeric chain length. The viscosity of the polymeric solution allows it to be administered via hypodermic needle, allowing it to be used in irregular wound sites.

Research published by Rubio-Elizalde *et al.*¹⁰⁰ saw methacrylated alginate used as a wound scaffold to increase wound recovery efficiency. The wound scaffold included PEG, increasing its resistance to biodegradation whilst maintaining its high biocompatibility, and included natural bioactive reagents to facilitate biofilm material and induce anti-inflammatory effects.

Wang *et al.*¹⁰¹ reported methacrylated alginate as a potential candidate for cell encapsulation in tissue engineering and myocardial repair (Scheme 1.2). Endothelial cells were encapsulated within the photo-crosslinked hydrogel which is injected *in vivo* and allowed to release *in-situ*.



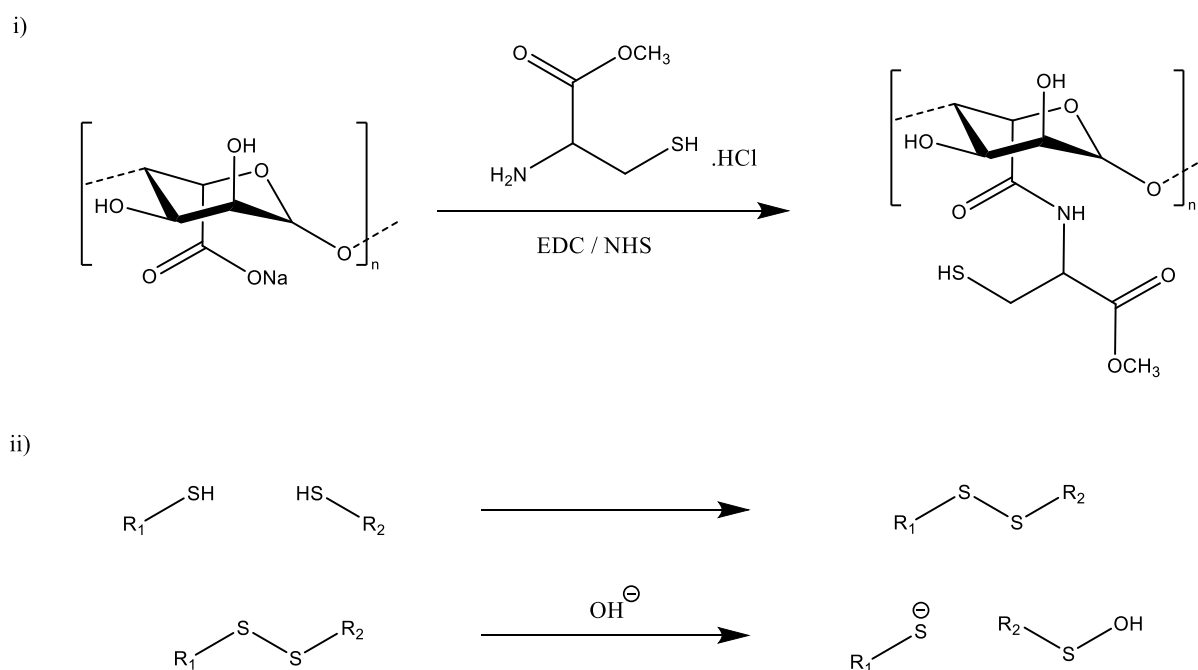
Scheme 1.2. Preparation of methacrylated alginate by alkylation of hydroxyl functional group.¹⁰¹

Non-methylated acrylate substituted alginates are less common as the acrylate functional group is less stable in air and light compared to its methylated counterpart. The absence of the methyl group encourages the material to gelate via covalent crosslinking. Alginate acrylation has been conducted previously for the bioapplications but as a superabsorbent hydrogel material¹⁰² and for keratinocyte inflammation alleviation.¹⁰³ There has been no acrylated alginates in chronic wound therapeutic development.

1.3.5.2 Thiolated alginates

Thiolate-functionalised alginate undergo gelation by forming covalent crosslinks with other functional groups, such as click thiol-ene/thiol-yne, Michael-type addition and thio-epoxy reactions for a wide variety of applications.¹⁰⁴

Xu *et al.*¹⁰⁵ reported an *in-situ*-formed thiolated alginate hydrogel for rapid haemostasis. Gel dissolution is induced with the use of reducing agents, such as dithiothreitol (DTT) to cleave the disulphide bond (Scheme 1.3).



Scheme 1.3. i) Thiolation of sodium alginate. ii) Formation of disulphide linkage to form gel and basic hydrolysis leading to gel dissolution.¹⁰⁵

Ooi *et al.*¹⁰⁶ presented thiol-ene alginate hydrogels as a bioink for 3D bioprinting of wound therapeutics. The usage of bioinks has increased in popularity for wound healing as the low extrusion volume allows rapid initial gelation of the material and allows high control over the shape of the construct for a variety of biomedical usages such as cardiovascular stents to 3D-printed wound dressings.^{107,108}

The thiolation of polymeric chitosan and dextran for diabetic wound healing has been previously published by Zhang *et al.*¹⁰⁹ The group mentioned the usage of oxidised dextran and thiolated chitosan crosslinked via base-catalysed disulphide formation.

1.3.6 Toxicological considerations

Keeping the end-application in mind, all chosen reagents and conducted reactions will need to be in compliance with toxicological limits to limit harm and improve biocompatibility whilst keeping cytotoxicity to a minimum. Strategies to reduce any reagents which exceed toxicological limits need to be employed, or its inclusion needs to be reconsidered in its entirety when designing experiments.¹¹⁰

1.3.7 Alginate gelation and post-gelation tests

The success of crosslinked alginates was determined according to an established system for hydrogel classification; failed gelation whereby solution remains in liquid form, gel particulate formation whereby some gelation has occurred but insufficient to form a bulk gel, and successful gelation where bulk hydrogel was obtained.^{93,111}

To establish hydrogel properties, crosslinked hydrogels undergo various tests depending on which information needed to be obtained. Swelling and release tests tell the extent of moisture absorption and moisture loss over time. Coupled with a model drug, this information can be used to simulate drug release profiles.

Mechanical and tensile strength tests are typically performed to establish the intrinsic strength. Creep, tack and structural recovery tests can be performed to simulate pulling, stretching and ripping which are processes where the hydrogel would

experience during application, removal and during usage.¹¹² The methodologies and tests performed in this thesis will be discussed in length in Chapter 2 under Section 2.1.

1.4 Project aims and rationale

The aim of this research is to develop an injectable hydrogel from functionalised alginates for primarily for diabetic foot ulcer treatment. The hydrogel will gelate *in-situ* and removable without breaking or causing harm to the patient. This product design is an upgrade to the sheet-based dressings which require the usage of adhesives which may cause harm on dressing removal, and the fibrous-type sheet dressings may leave debris or fibre strands on removal which increases the risk of further infection. This project is designed to allow the hydrogel's properties to be made tailorable, to suit a variety of wound types, by controlling the concentrations of moieties used in gelation to improve control over gelation time, moisture retention behaviour and structural integrity.

Sodium alginate will undergo acrylate modification using glycidyl acrylate via an alkylation process, herein referred to as acrylation, and thiol modification via an amide formation using L-cysteine and cysteamine hydrochloride, herein referred to as thiolation. Acrylated alginate is taken for crosslinking with thiolated alginate and pentaerythritol Tetrakis(3-mercaptopropionate) (QT), a tetra-thiolated crosslinker, to form a hydrogel *in-situ* via a Michael-type addition reaction. In this work, emphasis is placed on gelation via covalent crosslinking, but other forms of gelation including ionotropic and photogelation are also incorporated as a fail-safe measure in the event of covalent link cleavages and additionally as a method to form a gel more rapidly to reduce dressing application time. The novelty of this research lies with the usage of glycidyl acrylate as the acrylate moiety and the end-application. The usage of glycidyl methacrylate is common for wound therapeutics but are used almost exclusively for photogelation to form gel. The absence of the methyl functional group along the vinyl group will, in theory, increase its reactivity and allow it to readily

undergo Michael-type addition to form gel. The usage of glycidyl acrylate in wound therapeutic development is not yet widely documented.

Synthesised alginates will be characterised using NMR experiments, and thiol content of thiolated alginates will be quantified using Ellman's Assay. The gelation behaviour and its mechanical profile will be established using *in-situ* rheological testing and prepared gels to undergo microscopic imaging to investigate its porosity and moisture retention, which is supplemented with model drug release tests with aims to include antimicrobial agents or growth factors as post-modification.

Chapter 2: Analytical techniques, Experimental and Characterisation

This chapter contains two sections and it describes the materials, analytical techniques and experimental procedures used in this project. Section 1 entails the fundamental knowledge pertaining to the scientific methodologies used as part of the research work. The scientific background for interpretation and understanding of the data presented can be found in this section. Section 2 highlights the experimental and characterisation procedures conducted as part of this project. Generic materials and solvents used as part of the research work will be listed. Herein, the procedures for the synthesis and handling of alginate hydrogel precursors and the *in-situ* preparation and testing of alginate hydrogels are detailed

2.1 Fundamentals of analytical methodologies

This section provides a brief introduction into the analytical methods used to improve understanding to aid the interpretation of the data presented in this thesis. This section does not provide the full technical background into the analytical methods.

2.1.1 Nuclear Magnetic Resonance (NMR) spectroscopy

The first documentation of NMR spectroscopy was reported by Rabi in 1938.¹¹³ This analytical method would become integral for structural determination. NMR uses changes in chemical shifts in response to different magnetic strengths, which in turn gives information on the molecule's chemical, physical and structural data.¹¹⁴

Modern day NMR features the analysis of molecules with respect to ^1H , ^{13}C , ^{15}N , ^{19}F and ^{31}P nuclei.¹¹⁵ For in-depth background about this analytical method, please refer to the works published by Harris, Gruyter and Bharti and Roy.^{115–117}

For this project, the focus of spectral interpretation lies with the chemical shifts pertaining to acrylate, thiolate signals and, in the case where alginate was analysed, the anomeric proton signals and, to a lesser degree, the alginic backbone chemical shifts.

The acrylating reagent contains a sp^2 -hybridised carbon atom in the acrylate functional group as found in glycidyl acrylate (Figure 2.1). The arrangement of the carbon atoms give rise to a doublet (d), a doublet-of-doublets (dd) and a doublet (d) shift pattern in the range of δ 6.1 to 6.7 ppm in the starting material and δ 5.8 to 6.5 ppm in the synthesised product. The change in chemical shift value is clearly resolved and can be used to determine the extent of acrylation, and consequently how much unreacted acryloyl chloride exists in the product.

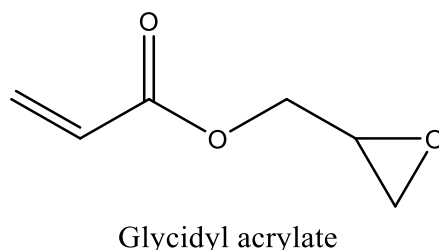


Figure 2.1. The acrylating reagent used in this thesis, glycidyl acrylate.

The intensity of the acrylate signal allows a good visualisation of the chemical shifts of the acrylate even after alginate acrylation, as the chemical signals are diluted by the polysaccharide signals.¹¹⁸

The thiolation reagents, L-cysteine hydrochloride and cysteamine hydrochloride (Figure 2.2), contain two sp^3 -hybridised carbon atoms bonded to one another. Consequently, two bands of peaks can be seen around δ 3.4 ppm and 3.7 ppm for L-cysteine with a mixture in multiplicity. For cysteamine these bands of peaks are less shifted due to the absence of a neighbouring carboxylic group and can be found around δ 3.1 ppm and 3.4 ppm instead.

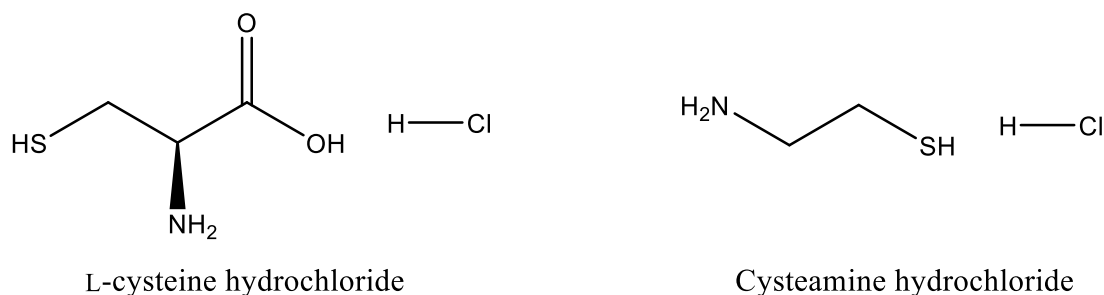


Figure 2.2. The thiolating agents used in this thesis, L-cysteine hydrochloride and Cysteamine hydrochloride.

The range of chemical shifts of polysaccharide is large when accounting for the anomeric and backbone signals.¹¹⁹ However, the ones of interest in this research are the anomeric proton signals as the backbone signals experience heavy interference with the deuterium oxide signal which appears at δ 4.8 ppm at 25 °C.

To mitigate this, water suppression is used in addition to increasing the experiment temperature. Increasing the experiment temperature lessens the effect of shielding by weakening the hydrogen bond interactions and lessens the effect of water molecule aggregation, which displaces the water signal upfield. Suppressing the solvent signals at a region where it is displaced from the anomeric signal region allows more precise analysis of spectral data and the estimation of M/G ratio and degree of substitution.¹²⁰ Figure 2.3 shows four NMR spectra of the same alginic acid sample performed at different temperatures.¹²¹

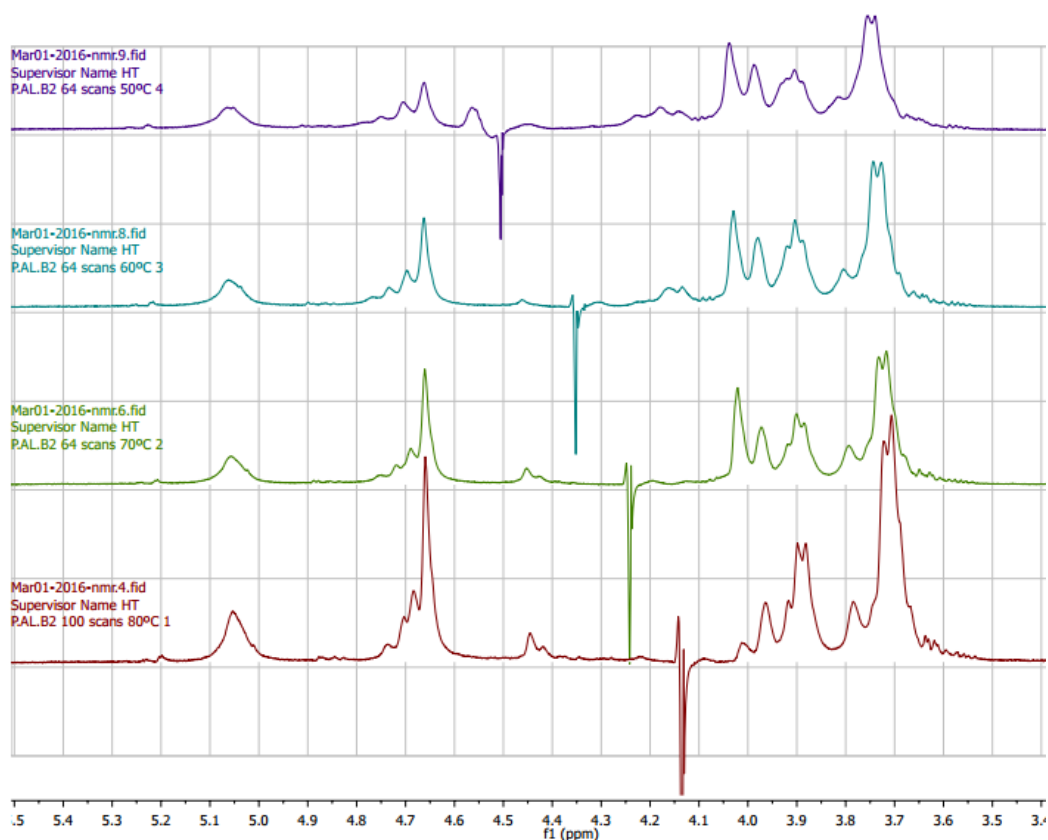


Figure 2.3. ^1H -NMR spectra of alginate acid performed at 50 °C, 60 °C, 70 °C and 80 °C. Figure used with authorisation.¹²²

2.1.2 UV-visible (UV-vis) spectroscopy

UV-vis spectroscopy uses the principles of the Beer-Lambert law to determine the concentration of analytes in solution. Please refer to the book published by Skoog, Holler and Crouch for the basic principles of UV-vis spectroscopy.¹²³

The Beer-Lambert equation (Equation 4) is expressed as:

$$A = \varepsilon c l \quad \text{Eqn. 4}$$

A = Absorbance value ε = Molar attenuation coefficient

c = Concentration of the sample l = Length of the light pathway

The equation of a straight line may be used to form a correlation between the Beer-Lambert law and the equation of a straight line.¹²⁴ The Beer-Lambert law assumes the line to be centred at the origin, but in practice an adjustment in absorption value is necessary to account for human and technical error. This can be represented by the subtraction of the background absorption value from the true absorbance value to obtain an adjusted absorption value.

2.1.2.1 Conversion of UV readings into thiol density

The conversion from UV absorbance values into thiol density is achieved using a series of calculations (Equations 5 to 11). Thiol content is reported as the density of thiol per mass unit (pmu) of alginate and is reported as $\frac{\mu\text{g thiol}}{\text{g alginate}}$. This requires the calculation of the sample concentration in relation to the sample mass and its thiol content, and consequently establish the mass of thiol present in one gram of thiolated alginate.

$$\text{As established : } A = \varepsilon c l \equiv y = mx \quad \text{Eqn. 5}$$

$$c \text{ (in moles)} = \frac{A}{\varepsilon l} \equiv \frac{y}{m} \quad \text{Eqn. 6}$$

$$\text{Mass unit (in mg)} = \text{Conc. of sample} \left(\text{in } \frac{\text{mg}}{\text{mL}} \right) \times \text{Vol. of sample (in mL)} \quad \text{Eqn. 7}$$

$$\text{Moles (thiol) p.m.u} = c \text{ (in moles)} \times \text{volume (in mL)} \quad \text{Eqn. 8}$$

$$\text{Grams (thiol) p.m.u} = \text{Moles (thiol) p.m.u} \times \text{Mr (thiol; 33)} \quad \text{Eqn. 9}$$

$$\text{Micrograms (thiol) p.m.u} = (\text{Grams (thiol) p.m.u}) \times 10^6 \quad \text{Eqn. 10}$$

$$\text{Thiol density} \left(\text{in } \frac{\mu\text{g thiol}}{\text{g alginate}} \right) = (\text{Micrograms (thiol) p.m.u}) \times \frac{1000 \text{ mg}}{\text{Mass unit}} \quad \text{Eqn. 11}$$

2.1.3 Gel Permeation Chromatography (GPC)

GPC was first reported by JC Moore in 1964 as a revolutionary method for polymer analysis.¹²⁵ GPC is a form of size exclusion chromatography (SEC) and relates to the Mark-Houwink-Sakurada equation where the relation between intrinsic viscosity of a polymer and its molecular weight is established (Equation 12).¹²⁶

$$[\eta] = K M^a \quad \text{Eqn. 12}$$

$[\eta]$ = Intrinsic viscosity M = Molecular weight

a and K = Mark – Houwink parameters (constants)

When the Mark-Houwink parameters are known, a plot of $\log[\eta]M$ versus volume or time can be made, which serves as a universal calibration curve for a particular solvent system to determine a material's molecular weight.¹²⁷

GPC is commonly used to characterise macromolecules such as oligomers and polymers as a polymer's physical and chemical properties undergo large changes depending on its molecular weight and chain length.¹²⁸ For example, polystyrene of different classifications may be found as a solid, viscous oil or as a liquid at room temperature.¹²⁹

Due to the magnitude and range of the molecular weight, the peak molecular weight (M_p), the number-average molecular weight (M_n) and the weight-average molecular weight (M_w) of macromolecules become of interest. The relationship between the two molecular weights calculates the polydispersity index (PDI), which provides the degree of chain length uniformity of polysaccharide chains (Equations 13 to 15).^{77,78} Monodispersed polymer chains by definition have a PDI value of 1.0.⁷⁴

$$M_n = \frac{\sum N M}{\sum N} \quad \text{Eqn. 13}$$

$$M_w = \frac{\sum w M}{\sum w} \quad \text{Eqn. 14}$$

$$PDI = \frac{M_w}{M_n} \quad \text{Eqn. 15}$$

N = number of molecules w = weight fraction of molecules

M = pre – determined mass

This method involves passing the sample through a gel column (stationary phase) using a solvent (mobile phase) at a constant flow rate where elution occurs, with larger macromolecules first eluted from the column due to its size and inability to penetrate gel pores, with smaller macromolecules being eluted last due to it being permeating and becoming trapped within the gel pores in the process (Figure 2.4).

Modern day GPC machines are connected to a variety of detectors including refractive index (RI), ultra-violet (UV), viscometer, dynamic light scattering (DLS), fluorescence and infra-red detectors. For more in-depth explanation on this analytical method, please refer to the book published by Gellerstedt.¹³⁰

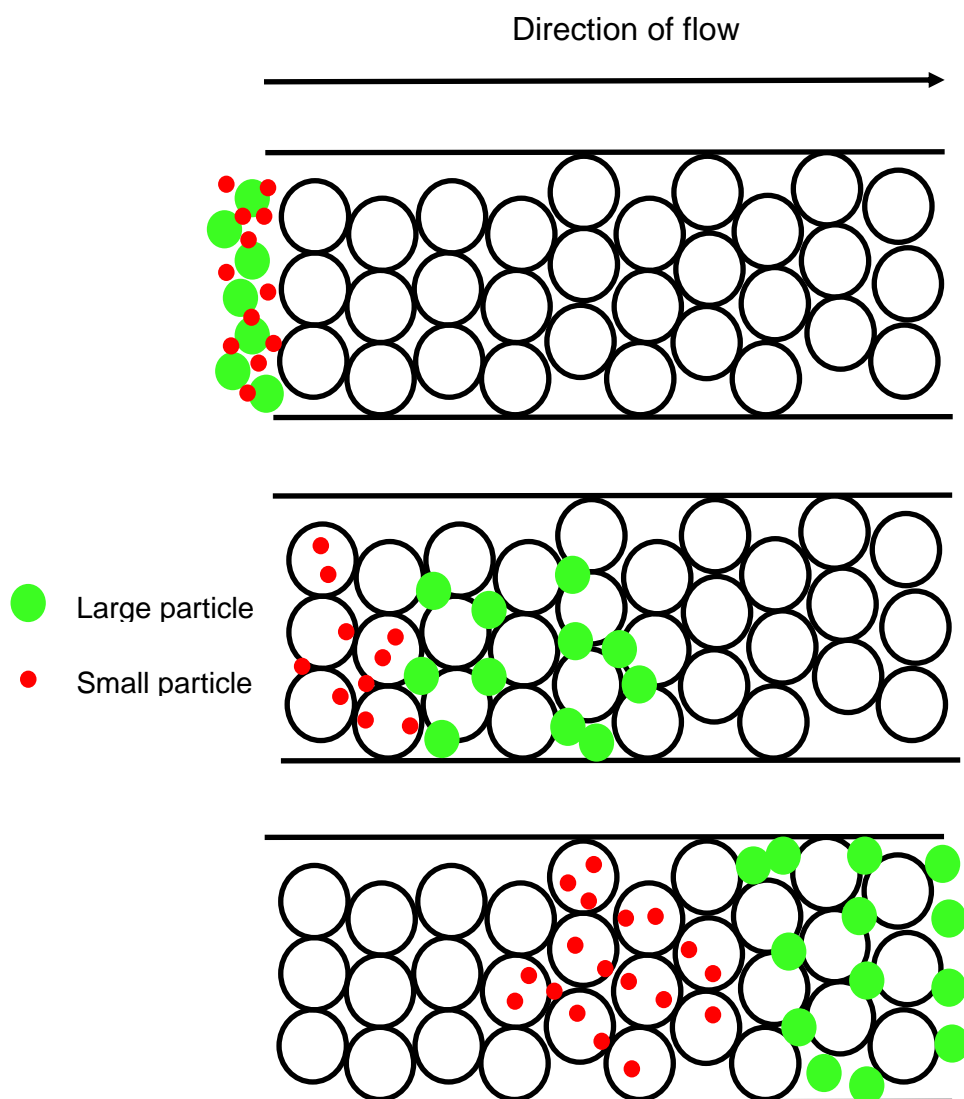


Figure 2.4. Illustration of analyte separation and elution in a GPC column and chromatograph prediction.¹³⁰

2.1.4 Rheology

Rheology is the study of flow behaviour and deformation of solid and liquid state matters under applications of stress. Its naming dates back to 1920 where the term was first coined by Bingham and Reiner.^{131,132} It assumes the majority of solid and liquid matters are classed as ideally solid, ideally liquid, viscoelastic solid or viscoelastic liquids (Figure 2.5). For more information about the technical background please see the publications by Malvern International and Anton Paar.^{133,134}

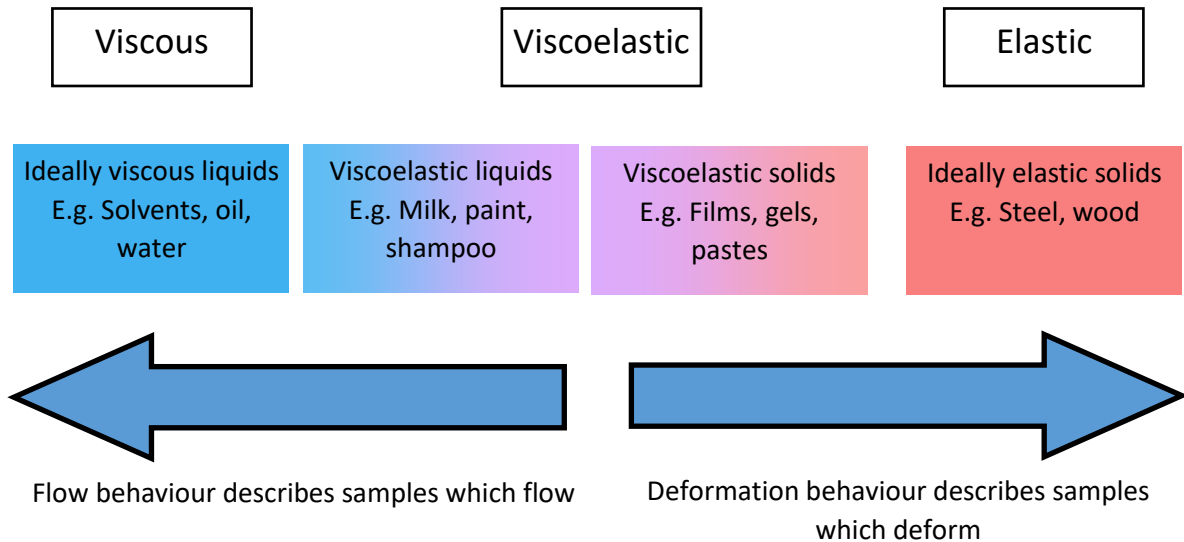


Figure 2.5. Flow and deformation properties for solid and liquid state materials.¹³⁴

As force is applied to the viscoelastic materials, shearing of the material occurs. Viscoelastic materials are classed as a dilatant fluid if their viscosity increases when force is applied or as a pseudoplastic fluid if the opposite behaviour is observed. In cases where viscosity is linearly proportional to stress applied, the viscoelastic material is said to express a Newtonian behaviour (Figure 2.6).¹³⁵

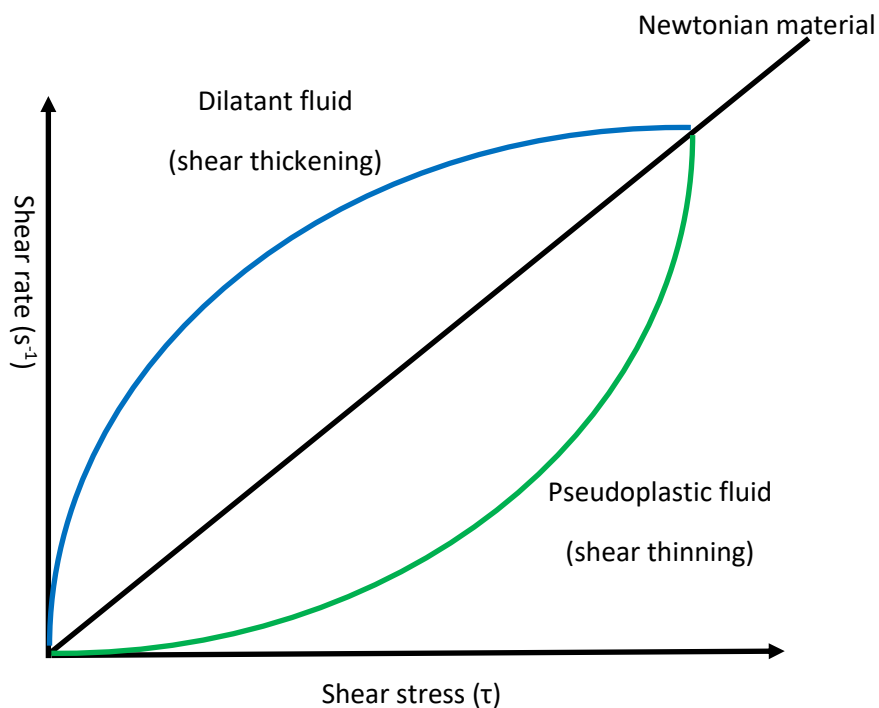


Figure 2.6. Material shear thickening and thinning with force application.¹³⁴

Over time, the structural integrity of some viscoelastic materials may undergo changes and can be further classed as a rheopectic or thixotropic material (Figure 2.7).¹³⁵

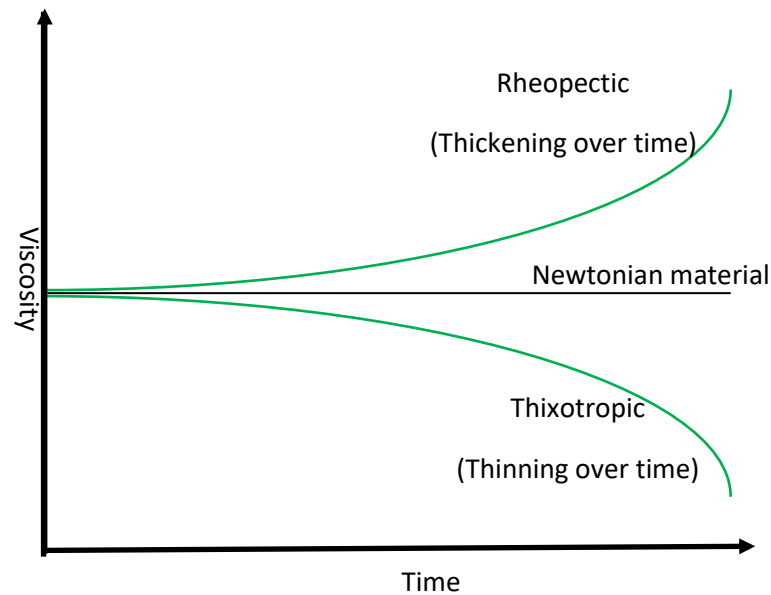
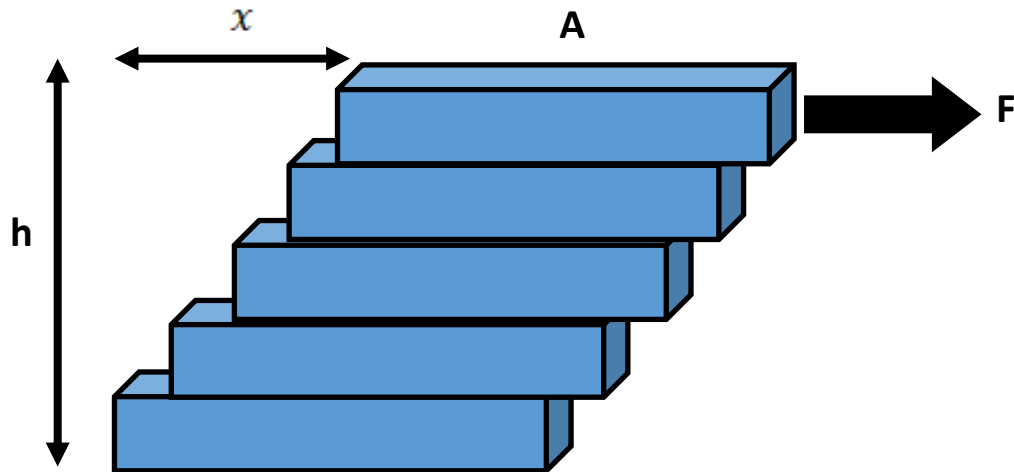


Figure 2.7. Time-dependent viscoelastic fluids.¹³⁴

The focus of the rheology experiments in this thesis is to determine the gelation timepoint of alginate solutions to form hydrogels *in-situ*. Alginate solutions are classed as a viscoelastic liquid and, upon gelation, will become a viscoelastic solid. As a result, the flow behaviour of the material is monitored for the gelation step, and the resultant material undergoes structural deformation tests to ascertain its rigidity.

Shear flow is measured by the magnitude of sample displacement, or shear stress, across an area upon force application. When displacement of the material has occurred, the shear strain can be calculated using the displacement distance in relation to the sample height. The shear rate can be described as the change in shear strain over time. Figure 2.8 and Equations 16 to 18 demonstrate the relationship between the different functions.



$$\sigma = F/A \quad \text{Eqn. 16}$$

$$\gamma = x/h \quad \text{Eqn. 17}$$

$$\dot{\gamma} = \delta\gamma/\delta t \quad \text{Eqn. 18}$$

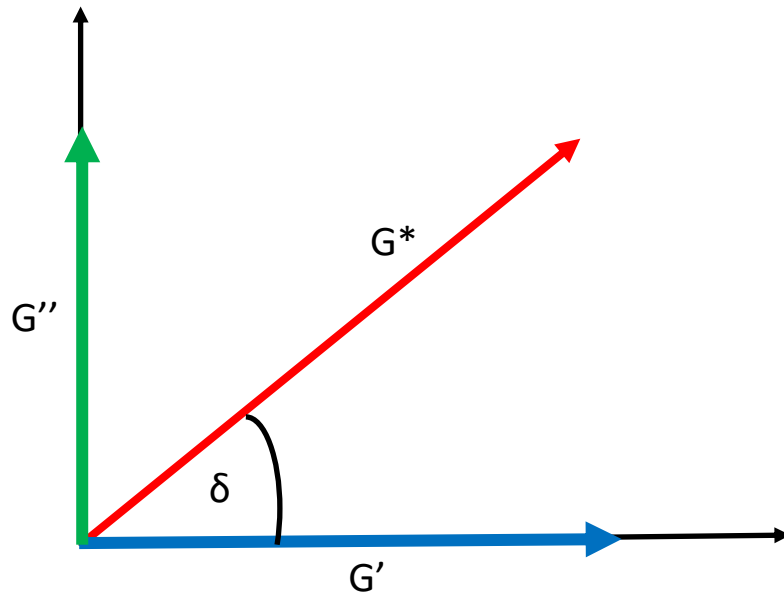
σ = Shear stress A = Area F = Force x = displacement distance

h = Sample height γ = Shear strain $\dot{\gamma}$ = Shear rate

Figure 2.8. Diagram of material shear and mathematical calculations to calculate shear rate.¹³⁶

The flow behaviour of a sample determines whether a material behaves more like a viscous (liquid) or elastic (solid) material. This also establishes the linear viscoelastic region (LVE), which indicates the range of frequency in which a test can be performed without causing structural destruction to the material.

To monitor the change in viscoelasticity, oscillatory or rotational frequency sweep tests are performed in order to obtain the storage modulus, which represents a sample's elastic behaviour, the loss modulus, which represents a sample's viscous behaviour and the complex modulus, which represents the relationship between a sample's elastic and viscous behaviour, is calculated using the phase angle between the geometry and the sample (Figure 2.9 and Equations 19 to 22).



$$G' = G^* \cos \delta \quad \text{Eqn. 19}$$

$$G'' = G^* \sin \delta \quad \text{Eqn. 20}$$

$$G^* = \sqrt{G'^2 + G''^2} \quad \text{Eqn. 21}$$

$$\tan \delta = G''/G' \quad \text{Eqn. 22}$$

$G' = \text{Storage modulus}$ $G'' = \text{Loss modulus}$ $G^* = \text{Complex modulus}$

$\delta = \text{Phase angle}$

Figure 2.9. Mathematical relationship between G' , G'' and G^* .¹³⁶

In the work presented in this thesis, gelation is said to have occurred when the alginate solution, a viscoelastic liquid, has gelled to become a viscoelastic solid. This can be determined by observing the storage and loss moduli. When the loss modulus is greater than the storage modulus, the sample is said to be a viscoelastic liquid. When the storage modulus is greater than the loss modulus, the sample is said to be a viscoelastic solid and has successfully crosslinked to form a hydrogel.

Dehydration of a sample can sometimes occur mid-experiment. Numerous environmental factors can contribute towards this phenomenon. In cases when sample dehydration has occurred, the sample often shrink in size, causing sample

slippage and resulting in a loss of contact between the geometry and sample. Data point fluctuations are often a good indicator of a loss of contact. A clear indication for sample dehydration is when a “ramping” behaviour is observed, where both storage and loss moduli values increase in a linear fashion with occasional plateaus.¹³⁷

2.1.5 Scanning Electron Microscopy (SEM) and confocal microscopy

Although the technology dates back further in the 20th century, the first high-resolution scanning electron microscope was invented by von Ardenne in 1937. This analytical technique relies on using a beam of primary electrons to excite a sample on a small area to produce secondary electrons. These electrons are picked up by a secondary electron detector to produce an image. The raster scan generator directs the electron beam to different areas of the sample to produce multiple pictures of the specimen, which are then stitched together to produce a full image of the specimen (Figure 2.10) Specimen are often sputter-coated with nanogold to improve image quality by reducing background glare.

Confocal microscopy uses the same principles as fluorescence microscope, but the clever incorporation of pinholes prevents light rays above and below the focal plane to reach the detector, thus increasing the image resolution. Images taken of numerous focal spots are stitched together to form a sharp image. As one specific focal plane of a specimen is inspected at a time, this enables the creation of a 3D image by imaging a specimen along the z-axis (Figure 2.11).

For more information about the technical background of these two analytical techniques, please refer to the publications by McMullan, Semwogerere and Weeks, and Nwaneshiudu *et al.*^{138–140}

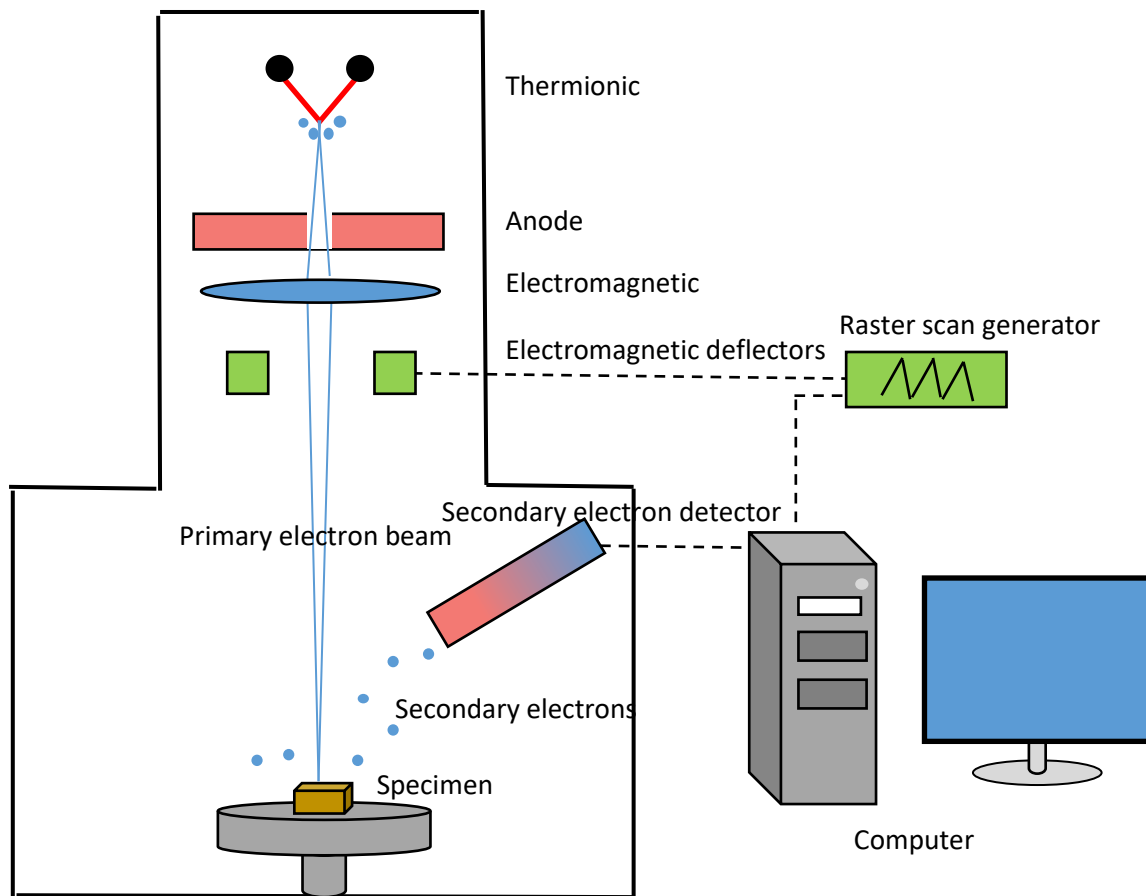


Figure 2.10. Simplified schematic of a scanning electron microscope.¹³⁸

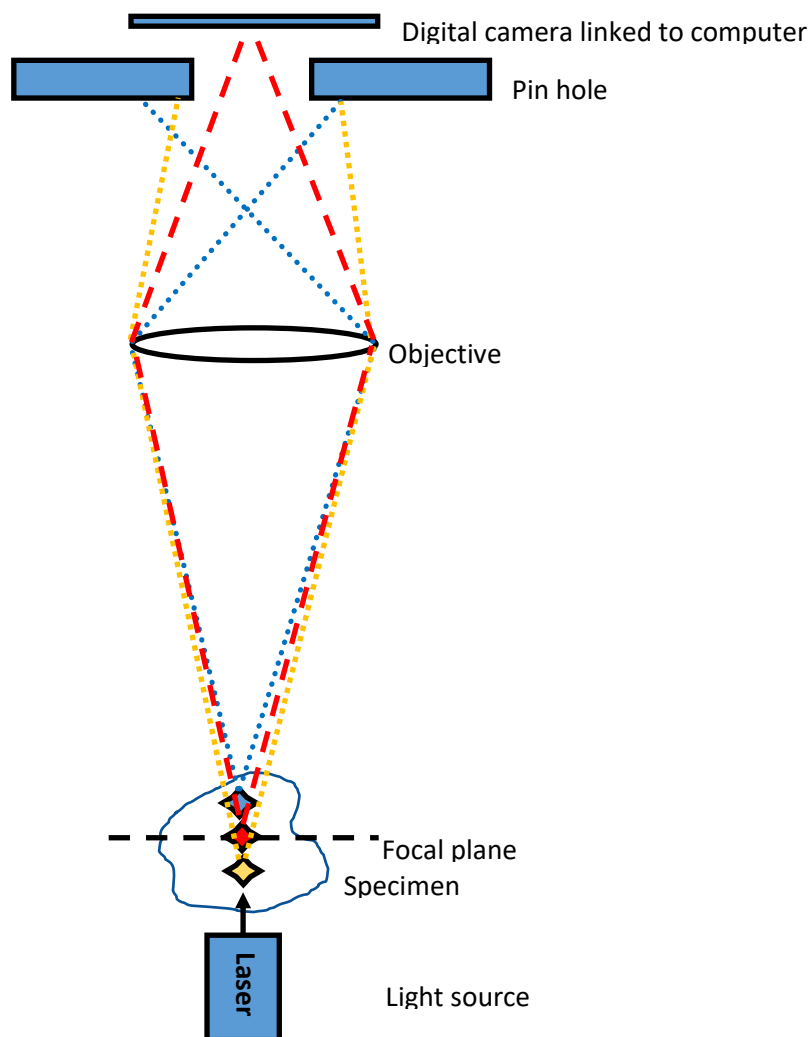


Figure 2.11. Simplified schematic of a confocal microscope.¹³⁹

2.2 Experimental Procedures

2.2.1 Materials

All solvents (hydrous and anhydrous) were purchased from Fisher Scientific at the highest possible grade unless stated otherwise. Deuterated solvents used for NMR analyses were procured from VWR and contain 99.6 % deuterium minimum. High-M sodium alginate (powder; purchased as alginic acid sodium salt) was purchased from Sigma-Aldrich and High-G alginate (powder) was gifted by ConvaTec Rhymney. Dialysis tubing (regenerated cellulose, MWCO 2kDA) was purchased from

Spectrum Labs and stored in water in the fridge before use. GPC calibration standards were purchased as a kit from VWR and stored in the fridge until used.

All procured reagents were used without further purification unless stated otherwise. Glycidol (96 %), triethylamine (TEA, ≥99 %) and cysteamine hydrochloride (98 %; purchased as 2-aminoethanethiol hydrochloride) were purchased from ACROS Organics. Hydroquinone (≥99.5 %), 1-Ethyl-3-(3-dimethylaminopropyl)carbodiimide (EDCI) hydrochloride, L-cysteine hydrochloride (anhydrous, ≥99 %), Ellman's reagent (DTNB, ≥98 %; purchased as 5,5'-Dithiobis(2-nitrobenzoic acid)), phosphate buffered saline (PBS, powder, pH 7.4 and pH 6.8), carmoisine (analytical standard), Irgacure 2959 (98 %; purchased as 2-Hydroxy-4'-(2-hydroxyethoxy)-2-methylpropiophenone) and QT(> 95%; purchased as Pentaerythritol tetrakis(3-mercaptopropionate)) were procured from Sigma-Aldrich. Acryloyl chloride (96 %, stabilised with 400 ppm phenothiazine), hydrochloric acid (HCl, 37 %), sodium hydroxide (NaOH, > 98%, pellets), magnesium sulphate (anhydrous, >95 %) and calcium chloride (CaCl₂, anhydrous, 93 %) were purchased from VWR. Dithiothreitol (≥99 %) was purchased from Fisher Scientific. All stock solutions were made up using HPLC-grade water unless stated otherwise. All applications and usages of PBS was performed using PBS (pH 7.4) unless stated otherwise.

2.2.2 Synthesis of hydrogel precursors

In this thesis, the experimental aim is to functionalise alginate with acrylate and thiol moieties. Glycidyl acrylate is synthesised as a precursor material for alginate acrylation reactions. All synthesised material were sealed and stored at low temperatures in purged brown glass vessels.

2.2.2.1. Glycidyl Acrylate

Glycidyl acrylate was synthesised via the method reported by Zhang *et al.*¹⁴¹ In a small scale experiment, glycidol (7.0 mL, 105 mmol), TEA (20.5 mL, 145 mmol) and

hydroquinone (23.4 mg, 0.2 mmol) were suspended in anhydrous diethyl ether (300 mL) in a N₂ purged flask and cooled to 0 °C. Acryloyl chloride (10.1 mL, 125 mmol) was added dropwise to the reaction over a period of 30 minutes. The reaction mixture was left to stir for 1 hour at 0 °C and then at ambient temperature overnight (14 – 16 h). The resultant mixture was filtered and the organic layer was washed thrice with water (3 x 75 mL), dried over magnesium sulphate before concentrating *in vacuo* on a IKA RV10 rotary evaporator to afford a pale-yellow oil. The oil was taken for ¹H-NMR characterisation using CDCl₃ at 10 mg/mL concentration and stored in the freezer in a purged light-sensitive container. For NMR analysis procedures please see Section 2.2.2.1.

GA1: 7.0 mL glycidol, 20.5 mL TEA, 22.7 mg hydroquinone, 300 mL anh. DE and 10.0 mL acryloyl chloride was used. No changes were made to the experimental procedure.

GA2: 14.0 mL glycidol, 40.6 mL TEA, 45.4 mg hydroquinone, 600 mL anh. DE and 20.2 mL acryloyl chloride was used. No changes were made to the experimental procedure.

GA3 and GA4: 35 mL glycidol, 100 mL TEA, 112.5 mg hydroquinone, 1.5 L anh. DE and 50.0 mL acryloyl chloride was used. No changes were made to the experimental procedure.

¹H NMR (400 MHz, CDCl₃) δ 6.44 (dd, J = 17.3, 1.1 Hz, 1H, CH₂=CH), 6.14 (dd, J = 17.3, 10.4 Hz, 1H), 5.86 (d, J = 10.5, 1.1 Hz, 1H, CH₂=CH), 4.47 (dd, J = 12.3, 3.0 Hz, 1H, CH₂-CH), 3.99 (dd, J = 12.3, 6.3 Hz, 1H, CH₂=CH), 3.23 (ddt, J = 3.6, 2.9 Hz, 1H, CH-CH₂), 2.84 (t, J = 4.5 Hz, 1H, CH₂-CH epoxide), 2.65 (dd, J = 4.8, 2.6 Hz, 1H, CH₂-CH epoxide).

Impurities: ¹H NMR (500 MHz, CDCl₃, 298 K): δ 3.48 (q, 3H Et₂O), 2.50 (q, 2H, TEA), 1.21 (t, 2H, Et₂O), 3.48 (q, 3H, Et₂O), 1.00 (t, 3H, TEA)

2.2.2.2. Acrylation of sodium alginate

The procedure for the acrylation of sodium alginate was taken and further adapted from the procedure reported by Wang *et al.*¹⁰¹ The volumes of glycidyl acrylate used was changed to tailor reactions and exert better control over the acrylation degree in syntheses.

Sodium alginate is dissolved in deionised water to 0.02 g/mL concentration (0.5 g, 25 mL). Glycidyl acrylate (High: 4.0 mL, 34.4 mmol, Med: 2.16 mL, 18.6 mmol, Low: 1.08 mL, 9.3 mmol) is added to the solution in a purged flask and stirred at room temperature. Sodium hydroxide (1 M) is added until pH 10.0 is reached. The reaction mixture is left to stir at 60 °C under N₂ atmosphere for 5 hours and precipitated in excess cold IMS to afford a white wispy polymer. Purification of the crude product is achieved by washing thrice with IMS (3 x 75 mL) and freeze-dried using a LTE mini lyotrap freeze dryer to afford the final product. The purified product is taken for ¹H-NMR experiments in D₂O at 7.5 mg/mL concentration and stored in a sealed, light-sensitive container in the freezer until used. For NMR analysis procedures please see Section 2.2.2.1.

¹H NMR (500 MHz, D₂O, 343 K) δ 7.01 (dd, J = 3.6 Hz, 1H, acrylate DB), 6.79 (dd, J = 10.7 Hz, 1H, CH-vinyl), 6.58 (d, J = 10.7 Hz, 1H, acrylate DB), 5.60 (s, 4H, alginate anomeric proton), 5.21 (m, 4H, alginate anomeric proton), 5.00 (s, 3H, alginate anomeric proton).

Impurities: (500 MHz, D₂O, 343 K) δ 4.26 (s, 1H, glycidyl acrylate), 3.65 (q, 3H, Et₂O), 1.17 (t, 2H, Et₂O).

2.2.2.3. Thiolation of sodium alginate

The thiolation of sodium alginate was taken and further adapted from the work published by Bernkop-Schnürch, Kast and Richter.¹⁴² In addition to the original protocol, a different thiol moiety was used. In order to tailor the thiolation degree, experiments with different mass ratios of thiol moiety to alginate were performed.

In a typical reaction, sodium alginate is dissolved in deionised water to 20 g/L concentration. EDCI solution (5 mL, 50 mM; deionised water) is added to the stirring alginate solution, adjusted to pH 6.0 and left to incubate for 45 minutes at 37 °C under inert atmosphere. The thiol moiety (cysteine hydrochloride or cysteamine hydrochloride), dissolved in solution (thiol:polymer mass ratio 1:1, 1:1.5, 1:2, 5 mL; deionised water), is added to the reaction vessel. The resultant mixture is left to react at room temperature under inert atmosphere for 3 hours whilst stirring. The crude product is purified in dialysis tubing against 1 mM HCl and adjusted to pH 4.0, with two further dialysis against 1 % w/w NaCl in 1 mM HCl for 24 hours per trial before being lyophilised using a LTE mini lyotrap freeze dryer to afford the white polymer. Synthesised thiolated alginates were taken for UV testing for thiol-content analysis. ¹H NMR characterisation of synthesised thiolated alginate was performed using D₂O at 7.5 mg/mL concentration and stored in a sealed, light-sensitive container in the freezer until used. Please refer to Section 2.2.2.1. for NMR analysis procedures and Section 2.2.2.2 for the procedures for UV determination of thiol-content. To investigate the effects of pH on the reaction, the pH during dialysis for some trial experiments was adjusted to pH 5.0 and 6.0.

TA1: High-M alginate used. 50 mL alginate solution (1 g alginate content) and 5 mL EDCI solution (47.9 mg EDCI) was used. 1 g cysteamine hydrochloride was added without modification. No changes were made to the synthesis procedure. The dialysis volume was 150 mL with each dialysis trial.

TA2: High-M alginate used. 50 mL alginate solution (1 g alginate content) and 5 mL EDCI solution (47.9 mg EDCI) was used. 1 g cysteine hydrochloride was added without modification. No changes were made to the synthesis procedure. The dialysis volume was 150 mL with each dialysis trial.

TA3: High-M alginate used. 50 mL alginate solution (1 g alginate content) and 5 mL EDCI solution (47.9 mg EDCI) was used. 1.5 g cysteamine hydrochloride was added without modification. No changes were made to the synthesis procedure. The dialysis volume was 150 mL with each dialysis trial.

TA4: High-M alginate used. 50 mL alginate solution (1 g alginate content) and 5 mL EDCI solution (47.9 mg EDCI) was used. 1.5 g cysteine hydrochloride was added

without modification. No changes were made to the synthesis procedure. The dialysis volume was 150 mL with each dialysis trial.

TA5: High-M alginate used. 50 mL alginate solution (1 g alginate content) and 5 mL EDCI solution (47.9 mg EDCI) was used. 2 g cysteine hydrochloride was added without modification. No changes were made to the synthesis procedure. The dialysis volume was 150 mL with each dialysis trial.

TA6: High-G alginate used. 50 mL alginate solution (1 g alginate content) and EDCI solution (47.9 mg EDCI) was used. 2 g cysteine hydrochloride was added without modification. No changes were made to the synthesis procedure. The dialysis volume was 150 mL with each dialysis trial.

TA7 and TA8: High-G alginate used. 50 mL alginate solution (1 g alginate content) and 5 mL EDCI solution (47.9 mg EDCI) was used. 2 g cysteamine hydrochloride dissolved in dil. NaOH (5 mL; pH 8.0) was added. No changes were made to the synthesis procedure. The dialysis volume was 5 L with each dialysis trial.

TA9 and TA10: High-G alginate used. 50 mL alginate solution (1 g alginate content) and 5 mL EDCI solution (47.9 mg EDCI) was used. 2 g cysteine hydrochloride dissolved in dil. NaOH (5 mL; pH 8.0) was added. No changes were made to the synthesis procedure. The dialysis volume was 5 L with each dialysis trial.

^1H NMR (500 MHz, D_2O , 343 K) δ 5.64 (s, 2H, alginate anomeric proton), 5.50 (s, 3H, alginate anomeric proton), 5.28 (s, 8H, alginate anomeric proton), 4.46 (m, 25H, alginic backbone), 4.0-3.3 (m, 3H, thiol moiety).

Impurities: (500 MHz, D_2O , 343 K) δ 2.75 (s, 1H, EDCI), 1.70 (s, 1H, EDCI).

2.2.3 Preparation of alginate hydrogels

In this research, alginate gelation tests were conducted in the laboratory and at a rheological testing facility belonging to the sponsoring company collaborator, ConvaTec GDC Deeside.

2.2.3.1 Ionotropic gelation

For ionotropic gelation of derivatised alginates in the laboratory, alginate solution (3.5 % w/v) or prepared alginate hydrogel was subjected to a CaCl_2 bath (1 % w/v) overnight. Depending on the desired gel morphology, alginate solution was either extruded out of a hypodermic needle or pipetted into a mould and the mould submerged into a calcium bath.

For ionotropic gelation for use in rheological studies, alginate solution (3.5 % w/v) was pipetted into a mould and the mould submerged into a bath containing CaCl_2 (0.1 % w/v and 1 % w/v) and left to sit for 10 seconds before being taken for rheological testing. Please refer to Section 2.2.2.4.2 for information on rheological testing parameters.

2.2.3.2 Covalent gelation via in-situ Michael-type addition

The procedure of covalent gelation of polymers using QT was inspired by the work of Dr Anna Tochwin¹¹¹ and the Tai research group.¹⁴³ Alginate hydrogels were produced in Eppendorf tubes for ease of inspection, manipulation, and transportation. For the work reported in this thesis, QT was dissolved in ethyl acetate at 5 % and 10 % w/v (weight/volume) with TEA added (0.1 % w/v). All alginate samples were dissolved at 3.5 % w/v using PBS solution. The total volume of solution handled amounted to 1.5 mL.

In a typical trial with QT in the laboratory, acrylated alginate solution was added to an Eppendorf tube along with QT solution in volume ratios of: 2.5:1 (1.07 mL:0.43 mL), 5:1 (1.25 mL: 0.25 mL) and 10:1 (1.36 mL: 0.14mL) and mixed with inversion of the tube. The mixed solution is left to incubate in an incubator at 37 °C and inspected at $T = 5, 10, 20, 30, 60, 120, 360$ and 1440 minutes. For some reactions, 20 % of the total volume was replaced with different aprotic solvents (dimethyl sulphoxide, tetrahydrofuran, ethyl acetate, acetone).

In a typical trial with thiolated alginate in the laboratory, acrylated alginate solution was added to an Eppendorf tube along with thiolated alginate solution in volume ratio of 1:1 (0.75 mL:0.75 mL) and mixed with inversion of the tube. The mixed solution is

left to incubate in an incubator at 37 °C and inspected at T = 5, 10, 20, 30, 60, 120, 360 and 1440 minutes.

The volume ratio and concentrations have been altered to for in-situ rheological testing experiments. The experimental work in this thesis uses alginate samples dissolved at three different concentration bands which were 5.8 % w/v, 2.8 % w/v and 1.39 % w/v, respectively and were referred to as high, medium and low concentration, respectively.

Acrylated alginate solution was mixed with QT solution (1.4 mL acrylate: 0.1 mL QT) or thiolated alginate solution (0.75 mL acrylate: 0.75 mL thiolate) and pipetted directly onto the Peltier plate after mixing until homogeneous without incubation. Please refer to Section 2.2.5 for procedures for loading sample onto the rheometer and Section 2.2.2.4.2 for rheological testing parameters.

2.2.3.3 Photogelation

Acrylated alginate was dissolved in PBS at 2.5 % w/v concentration overnight using a tube roller and 3.5 % w/v concentration using a Velp Scientifica OV5 Homogeniser in centrifugal tubes wrapped in foil to minimise light exposure. Irgacure 2959 was dissolved to 1 % w/v concentration (50 mg in 5 mL).

Acrylated alginate (250 µL) was mixed with a solution of Irgacure 2959 (15 µL) in a plastic mould before subjecting to a high intensity UV lamp (270-280 nm) in 12-minute intervals with 7-minute irradiation and 5-minute rest intervals. The obtained gels were stored under low light atmospheres until used.

2.2.4 Analytical characterisation procedures

2.2.4.1 Nuclear Magnetic Resonance (NMR) spectroscopy characterisation

^1H -NMR experiments were conducted at 400 MHz frequency (Bruker Ultrashield Plus 400 NMR spectrometer)) with 16 scans and at r.t. (25 °C).

^1H -NMR with water suppression experiments were carried out at 500 MHz (Bruker Avance 500 MHz NMR spectrometer). ^1H -NMR analysis of acrylated alginate samples was performed using 256 scans at 70 °C in D_2O . ^1H -NMR analysis of thiolated alginate samples was performed with 128 scans at 25 °C in D_2O .

2.2.4.2 Thiol content determination using Ellman's Reagent

The determination of thiol content by UV-vis was first reported in Ellman in 1959.¹⁴⁴ The procedure was taken and adapted for the experimental work. All thiol content determination work was performed using a PerkinElmer Lambda 35 UV-vis spectrometer. A 2-mercaptoethanol stock solution (1×10^{-3} M) was made up (7.04 μL in 100 mL). A DTNB stock solution (1×10^{-3} M) was made up (3.9634 mg in 10 mL) in PBS. Thiolated alginate was dissolved in HPLC-grade water (50 mg in 10 mL).

To establish a calibration curve, 2-mercaptoethanol stock solution was diluted to afford five solutions of different concentrations (3×10^{-4} M, 2×10^{-4} M, 1.5×10^{-4} M, 1×10^{-4} M and 5×10^{-5} M). In a separate vial, DTNB (203.8 μL) was made up to 1 mL with PBS (796.2 μL). These two solutions were mixed, transferred into quartz cuvettes and taken for UV analysis at 412 nm against a blank of PBS.

For sample analysis, thiolated alginate solution (0.5 mL) was mixed with DTNB solution (0.5 mL), transferred to quartz cuvettes and measured against a PBS blank at 412 nm.

2.2.4.3 Gel Permeation Chromatography (GPC) analysis

Alginate is dissolved at 1 mg/mL concentration in PBS buffer (pH 6.8), filtered through a 25 µm PTFE syringe filter into sample vials and left to stir overnight on a sample roller.

Experiments were performed on an Agilent PL-GPC 50 GPC/SEC machine fitted with a PLgel 20 µm Mixed-A column with an injection flow rate of 0.1 mL/min at 301 K. The column is flushed between experiments with PBS buffer (pH 6.8).

2.2.4.4 Hydrogel gelation characterisation

2.2.4.4.1 Release studies

Prepared alginate gels were dried *in vacuo*. The dried gels were loaded with a carmoisine solution (750 µL; 0.25 mg in 1 mL deionised H₂O) and left for 2 minutes to allow the gel to be permeated by the carmoisine prior to release. The release is simulated with the injection of HPLC-grade water (1 mL) into the sample well, with the release media drawn and replaced at set time intervals (T = 0, 30 60, 90 ,120, 180 and 240 minutes). The drawn solution was taken for UV-analysis in quartz cuvettes against a blank of HPLC-grade water at 515 nm using a PerkinElmer Lambda 35 UV-vis spectrometer.

A release study experiment included 8 trials. Trials 1-4 were the same as trials 5-8. Each trial included a control of acrylated alginate, which was the same alginate sample used to produce the hydrogels, and a blank gel with made from unmodified alginate.

Trial 1: Hydrogels were crosslinked via covalent and ionotropic crosslinking.

Trials 2: Hydrogels were crosslinked via photo and ionotropic crosslinking.

Trials 3 and 4: Hydrogels were crosslinked via covalent, photo and ionotropic crosslinking.

2.2.4.4.2 Rheological studies

All rheology-related work in this research was conducted using a Discovery HR-2 rheometer. For rheological measurements, a 50 mm parallel plate geometry and a 20 mm parallel plate geometry were used. A humidity cover was incorporated which was lubricated with silicone grease to provide a sealing effect. The water reservoir of the geometry was filled with deionised water for shorter experiments (>4 h) and silicone grease for overnight experiments (Figures 2.12 and 2.13).



Figure 2.12. Annotated photograph of a rheometer.

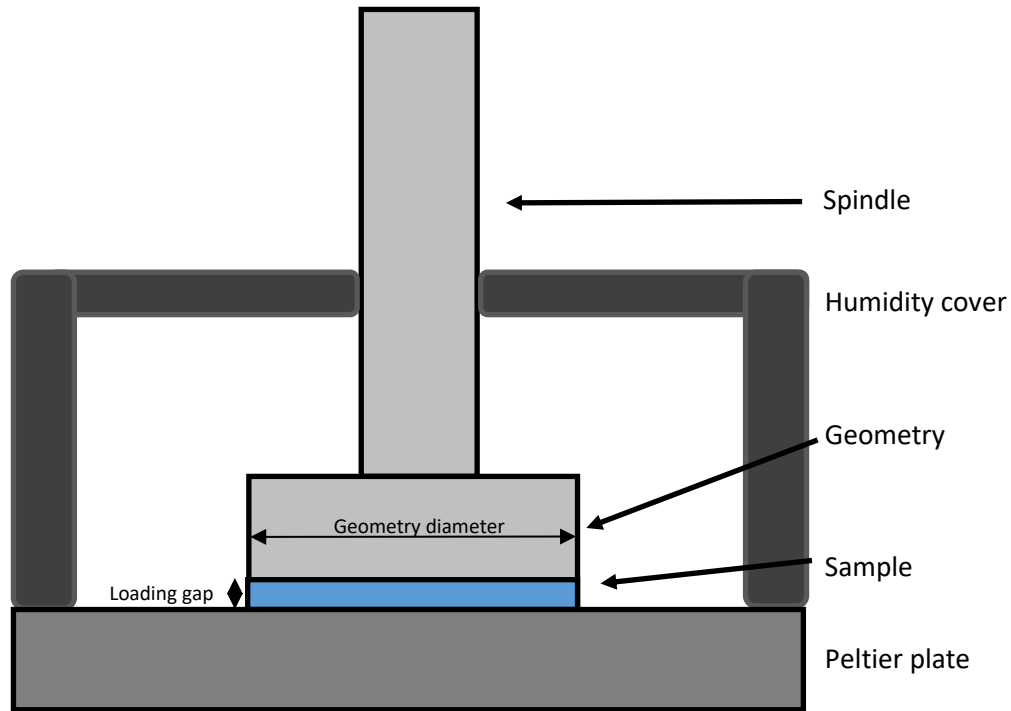


Figure 2.13. Diagram of a rheometer platform.

In this research, four different tests were conducted to establish a gel's rheological profile. These were temperature ramp tests, time sweep, oscillatory frequency sweep tests and creep tests. The test parameters and conditions for respective experiments were as follows.

Temperature ramp: Sample was loaded onto the Peltier plate set at 25 °C and trimmed. The temperature increase was set to 1 K/min until 37 °C was reached. The loading gap was set to 500 μm , trim gap offset 0 μm .

Time sweep: Sample was loaded onto the Peltier plate set at 37 °C. The experiment duration was set to be 10 minutes, 20 minutes, 30 minutes 150 minutes or, for overnight experiments, 1080 minutes. A 5.0×10^{-5} rad displacement was chosen.

Oscillatory frequency sweep: Sample was loaded onto the Peltier plate set at 25 °C or 37 °C and trimmed. The loading gap was set to 500 μm , trim gap offset 0 μm , strain at 0.5 % and angular frequency range from 0.1 Hz to 10.0 Hz.

Creep test: Crosslinked alginate hydrogel was loaded onto the Peltier plate set at 37 °C. The shear frequency was set to 0.1 Hz to 10.0 Hz for the initial creep. The material was allowed to structurally recover for 10 seconds and sheared for two

further cycles at 1.0 Hz to 10.0 Hz with 10 seconds recovery period in between each cycle.

In a typical trial, alginate solution was added to a mixing vessel followed by the addition of QT or thiolated alginate solution. The resultant solution was gently mixed to aid incorporation and to eliminate any trapped air bubbles. The solution was pipetted onto the Peltier plate, with the geometry lowered to the trim gap, and any excess sample was trimmed using a trimming tool. Please refer to Section 2.2.2.4.2 for information of rheological experiment conditions and protocols.

2.2.4.4.3 Scanning Electron Microscopy (SEM) and confocal microscopy tests

Scanning Electron Microscopy (SEM) was performed on dried derivatised alginates. Alginate samples were mounted onto a sputter and coated with nanogold before taken for SEM imaging on a JEOL JSM-7900F scanning electron microscope. Imaging of the sample was performed at 100x, 1000x and 10000x magnifications.

Microscopy tests of prepared alginate gels were conducted using a VHX High-Res digital confocal microscope. Samples were locked onto a platform using glass microscopic slides and the zoom adjusted to produce a clear image. A 3-D cross-section image of the sample was also taken.

Chapter 3: Results and Discussion

3.1 Overview

This chapter is further divided into five sections. Section 1 includes spectroscopic data of the alginate samples used and provides a brief insight into different alginic polysaccharide configurations and specifications. Section 2 details the synthesis of glycidyl acrylate, the precursor material of the alginic acrylate modification step, with spectral analyses and scientific explanations. Sections 3 and 4 of this chapter details the acrylate-functionalisation of alginate by alkylation, referred in this work as acrylation, and the thiol-functionalisation of alginate by amide bond formation, referred in this work as thiolation, respectively. Within, the reader should expect to see NMR characterisations of the synthesised materials, with factors impacting the reaction efficacy and yield being discussed, in addition to data comparison of the different specifications of alginates used in this project. Section 5 marks the end of this chapter with results and discussions of alginate hydrogel preparations using different chemical processes as well as the characterisation of prepared gels using analytical techniques including *in-situ* rheological experiments and SEM tests. Raw data of data presented can be found in the appendices.

3.1.1 GPC analysis of sodium alginates

GPC analyses of alginate samples accrued from Sigma-Aldrich (High M) and ConvaTec Rhymney (High G) indicated a Mp value of 106 kDa and 418 kDa, respectively, as shown by the peak annotated as '2' in Figures 3.1 and 3.2. The respective PDI values were 6.60 and 4.56, which suggest High G alginates being more uniform in chain lengths compared to High M alginates. Information pertaining to chromatograph data can be found under Table 3.1. Alginate solutions for GPC testing were left stirring overnight to observe any precipitation behaviour that may occur over time, which may block the gel column and cause damage to the machine.

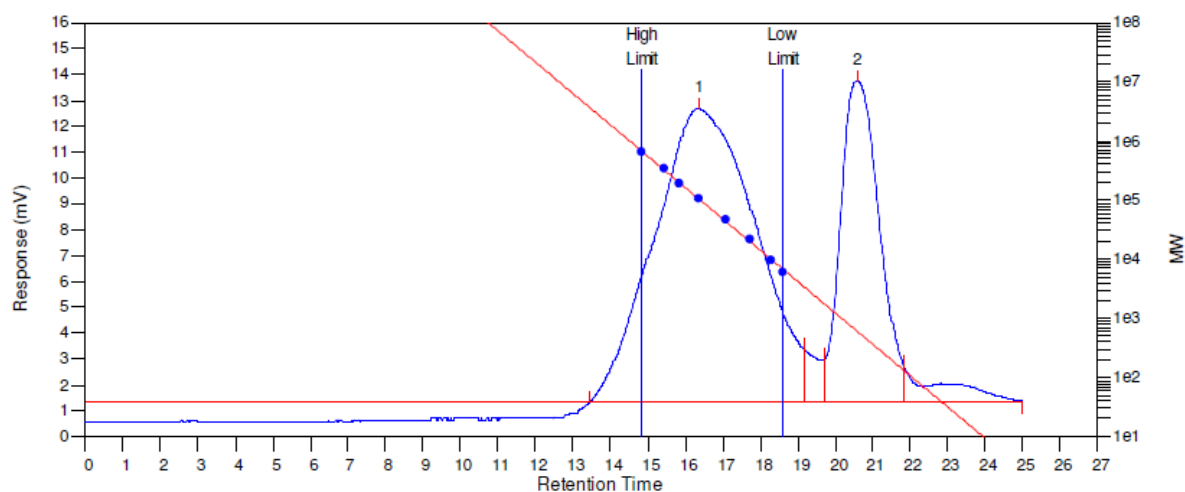


Figure 3.1. GPC chromatograph of High M alginate procured from Sigma-Aldrich. The diagonal red line corresponds to the calibration curve.

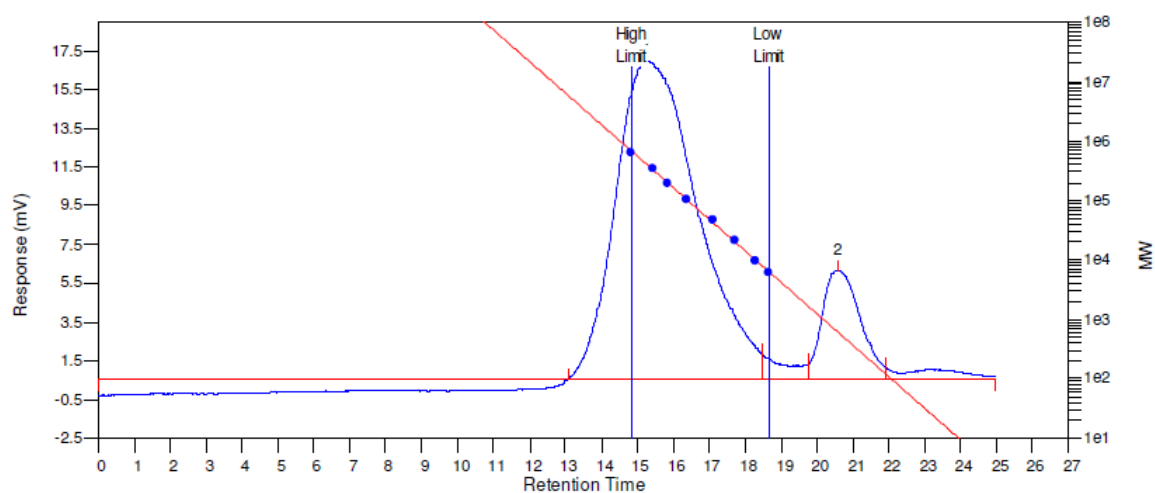


Figure 3.2. GPC chromatograph of High G alginate procured from ConvaTec Rhymney. The diagonal red line corresponds to the calibration curve.

Table 3.1. Tabulated information of alginate samples obtained from GPC analyses.

Sample	Notation	Mp (kDa)	Mn (kDa)	Mw (kDa)	PDI
Sigma-Aldrich	High M	106.9	32.2	215.6	6.60
ConvaTec Rhymney	High G	418.1	103.8	473.6	4.56

The ratio of mannuronates to guluronates present in the sample, M/G ratio, is calculated to be 2.0 (High-M alginate) and 0.5 (High-G alginate), hence its name, using $^1\text{H-NMR}$ analytical data (Equations 2 and 3 in Chapter 1 Section 1.3.2) reported by Grasdalen in 1983.⁸⁰ The appearance of two peaks in the chromatograph suggests the existence of two sample mass distribution, and could be attributed to the presence of oligomeric alginate in addition to polymeric alginate.

3.2 Synthesis of Glycidyl Acrylate

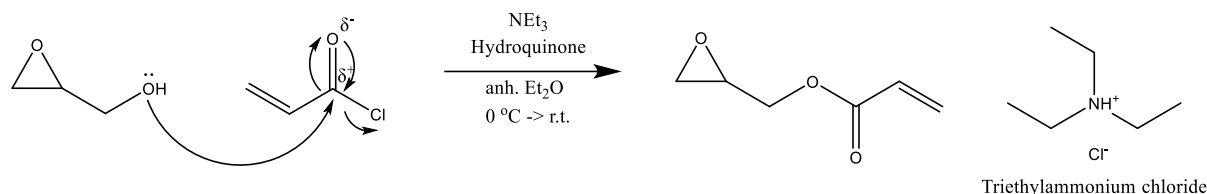
Despite further purification steps, traces of impurities remain inside the purified product, namely unreacted starting materials, and solvents. The impurity content is estimated to be between 12 and 28 % of total mass, as determined by the product purity equation (Equation 21).¹⁴⁵ Table 3.2 offers a tabulated view into the scales of syntheses performed as well as resultant yields and relative purities, all confirmed by $^1\text{H-NMR}$ characterisations.

$$\text{Product purity} = \left(\frac{\Sigma \text{ integration value of product signals}}{\Sigma \text{ integration value}} \right) \times 100 \% \quad \text{Eqn. 21}$$

Table 3.2. Simplified table of some acrylate syntheses performed. Refer to thesis Chapter Section (2.2.3.1) for quantities used at different reaction scales.

Experiment number	Reaction scale	Σ reaction volume (mL)	Yield (%)	Purity (%)
GA1	Small	170	49.9	90
GA2	Medium	675	77.8	91
GA3	Large	1685	67.0	95
GA4	Large	1685	71.0	95

reaction and reducing reaction yields. It was discovered that although the chloride salt slowly disintegrates over the course of reaction at room temperature, the reaction yield saw a reduction from ca. 70 % to between 55 and 65 % afforded thus it was beneficial to manually break apart the salt as it forms in order to ensure a higher yield.



Scheme 3.2. Mechanism of synthesis of glycidyl acrylate from glycidol.

3.2.2 NMR Characterisation of glycidyl acrylate

Spectral analytical data (Figure 3.3) show conclusive proof that the hydroxyl functional group on the glycidol has been successfully substituted with the acrylate moiety as indicated by the appearance of two sets of dd signals around δ 4.00 ppm and 4.5 ppm, as annotated on the spectrum. A fully peak-picked and integrated spectrum of glycidyl acrylate can be found under Figure 3.4. The sample purity was determined to be upwards to 88 % with impurities determined to be reaction solvent, unreacted organic material and triethylammonium chloride salt. The product was subsequently taken for further syntheses without additional purification as the concentration of impurities present in the synthesised acrylate should not have an adverse effect on the acrylation process.

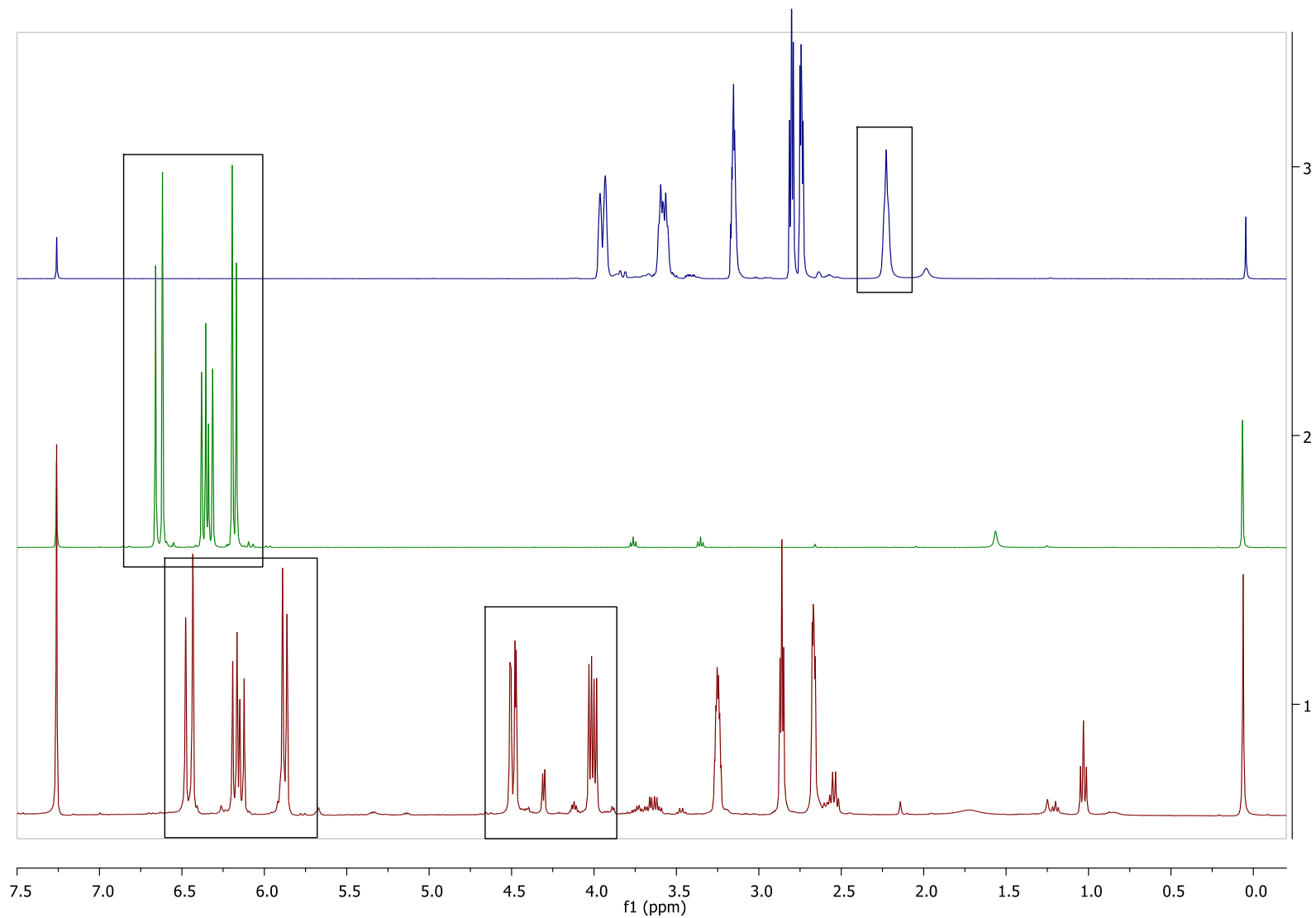


Figure 3.3. A stacked ^1H NMR spectrum of glycidol (top), acryloyl chloride (middle) and synthesised glycidyl acrylate (bottom).

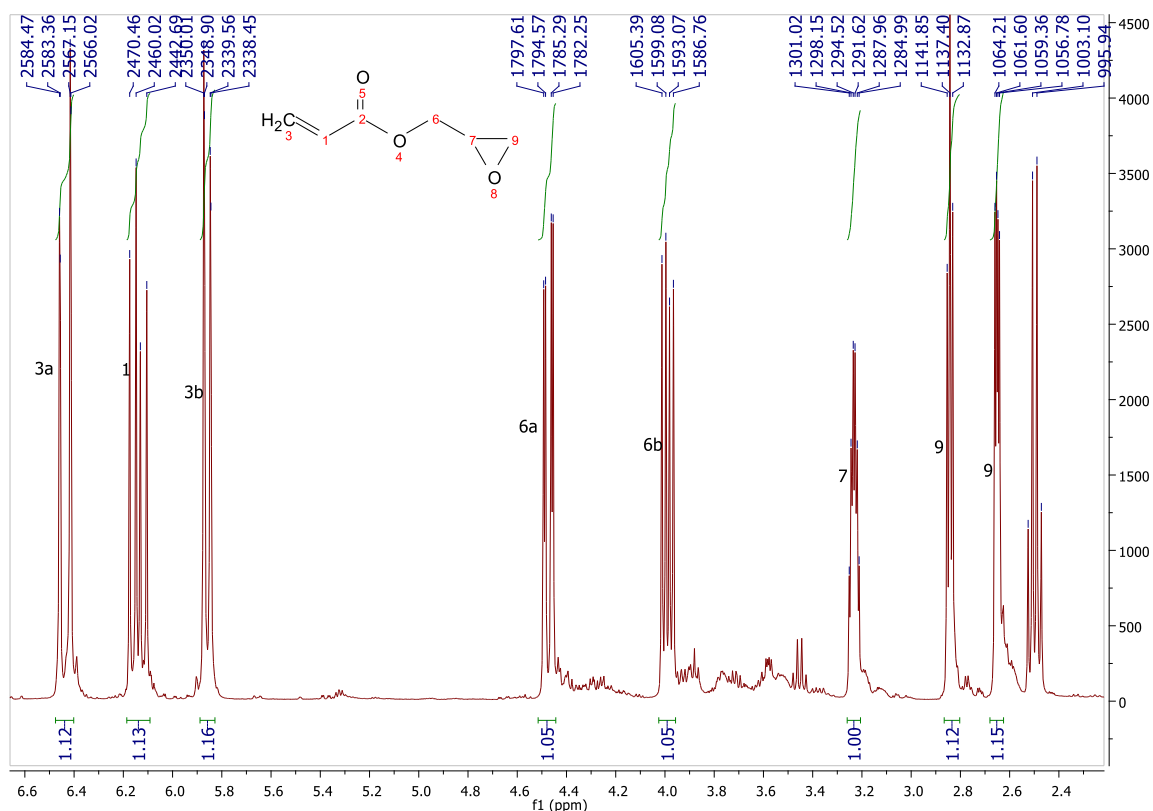
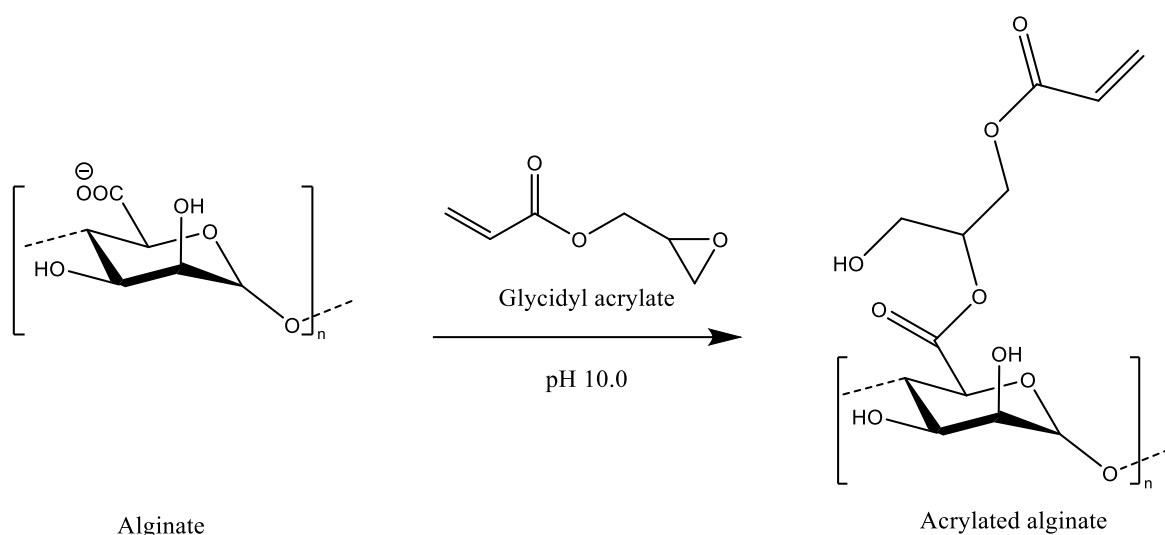


Figure 3.4. Annotated ¹H NMR spectrum of glycidyl acrylate.

3.3 Acrylation of Sodium Alginate

The tailorable parameters investigated as part of this research included the concentration of alginate solution, the alginate specification, the volume ratios of alginate solution and glycidyl acrylate, reaction temperature, pH, reaction time and alginate drying method and duration. Scheme 3.3 shows the acrylation of sodium alginate using glycidyl acrylate.



Scheme 3.3. Alkylation of sodium alginate to introduce acrylate functionality.

3.3.1 Characterisation of acrylated alginate

Water suppression NMR experiments were conducted to amplify the anomeric signals, found between δ 5.1 and 5.7 ppm, and minimise interference to signal integrations to improve the precision of the degree of substitution (DoS%) estimation to determine reaction efficiency and monitor the M/G ratio. The elevation of test temperature shifts the solvent signal upfield to alleviate interferences.¹²²

3.3.1.1 NMR characterisation of acrylated alginate

¹H-NMR spectroscopy was used to estimate the DoS% and the M/G values. Figures 3.5 and 3.6 show NMR spectra of acrylated alginate samples.

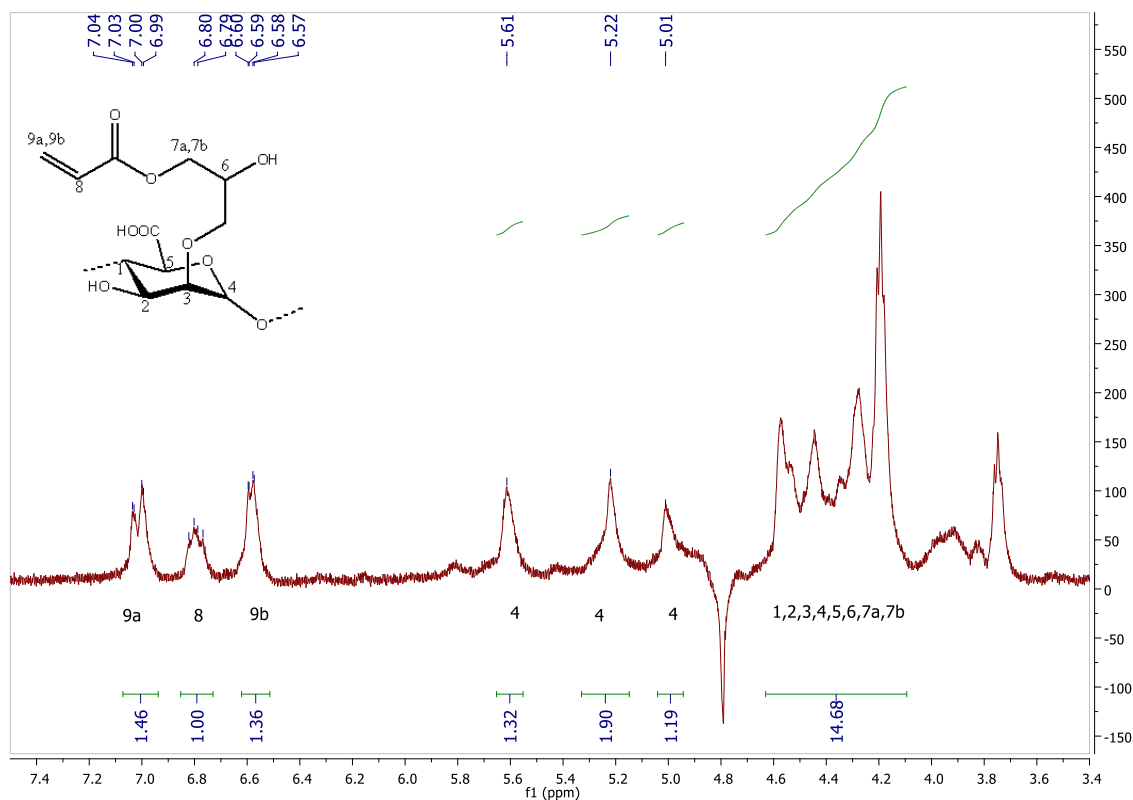


Figure 3.5. ^1H NMR spectrum of an acrylate-substituted High-M alginate. NMR conducted at 70 °C, D_2O , 500 MHz with 256 scans.

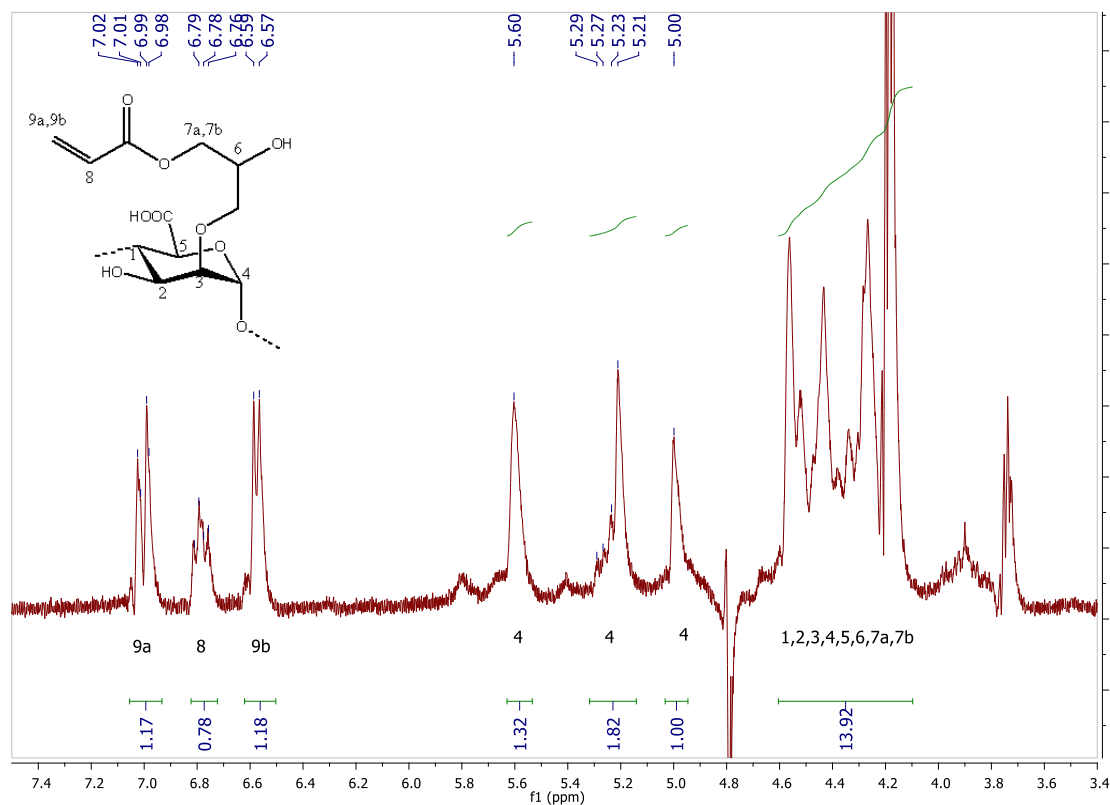


Figure 3.6. ^1H NMR spectrum of an acrylate-substituted High-G alginate. NMR conducted at 70 °C, D_2O , 500 MHz with 256 scans.

The characterisation was performed using five integration values with one belonging to acrylate, three pertaining to the anomeric protons and one for the alginic backbone. Theoretically there would be six different anomeric proton signals; three for a dimeric configuration (MM, GG, MG/GM) and three for a trimeric configuration (MMM, GGG, MGM/GMG). Though the trimeric signals were present between 4.6 and 4.8 ppm, it was decided to exclude the integration values in calculations as the NMR experiment temperature (70 °C) was too low to shift the solvent signal upfield, as observed at δ 4.8 ppm.⁸³ The scan numbers were insufficient to produce a clear signal to eliminate margins of error and for the anomeric peaks to show with sufficient clarity.

Based on the experimental results from acrylation reactions performed, a trend was established that the M/G values had the tendency to converge towards 1.0. High-G alginate consistently saw an increase in M/G value from 0.5 to between 1.2 and 1.3, and that High-M alginate saw a decrease in M/G value from 2.0 to between 1.4 and 1.5. This suggests the shift and conversion in spatial configuration of the mannuronates to the guluronates, and vice versa. It was hypothesised that the introduction of the acrylate functional group at the C-6 carbon atom caused misalignment and disruption to its uniform configuration due to steric forces, which contributed to the change in M/G values in the resultant product. It was discovered that the change in M/G value is more significant with increased DoS%, further reinforcing the hypothesis.

GPC and FT-IR experiments of synthesised alginates were not performed due to instrument failure and data export problem, respectively thus characteristics pertaining to its polymeric behaviour were not available.

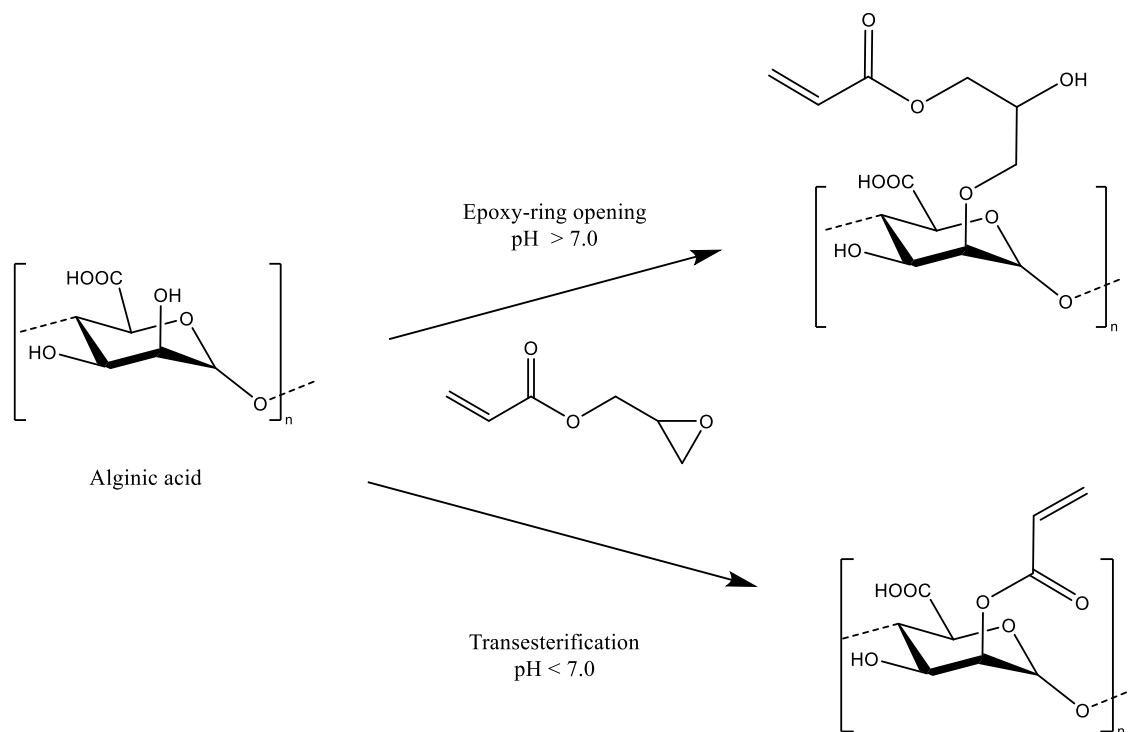
3.3.2 Factors affecting the degree of substitution (DoS%) and yield

As part of the project, various reaction parameters were trialled with and altered to optimise the synthetic process. Table 3.3 offers a tabulated view of reaction conditions altered and trialled as part of this work. Please refer to Chapter 2 Section 2.2.3.2 for further information pertaining to the experimental procedures performed.

Table 3.3. Simplified table of reaction parameters trialled and trialled conditions with the alginate acrylation step.

Parameters	Parameter variations		
Alginate concentration	2 % w/v (De-ionised water)		
pH	10.0		
Acr:Alg ratio (eq.)	3.9 “Low”	5.5 “Med”	7.8 “High”
Temperature	R.t. (25 °C)		60 °C
Reaction time	4 h	24 h	48 h
Precipitation medium	IMS		IMS:Acetone (2:1 v/v)
Drying method	Pump-assisted lyophilisation		R.t. (25 °C) drying <i>in vacuo</i>

The reaction was selected to proceed under a moderately alkaline condition (pH 10.0) to deprotonate the carboxylic functional group to increase substitution along the hydroxyl terminal (Scheme 3.4).¹⁴⁸

**Scheme 3.4.** Two potential pathways for acrylate substitution on alginate.¹⁴⁸

There was no detection of basic hydrolytic processes and was thus concluded to not be a deciding factor affecting the reaction outcome. The equivalent between alginate and acrylate moiety, unsurprisingly, played a large role in the resultant alginate afforded. The degree of substitution, as estimated by NMR analysis, showed that High-M alginate saw a conversion ratio of upwards to 30 % whereas its High-G counterpart yielded a higher conversion ratio with a peak substitution degree of 33 %. The similarity of substitution values indicated the spatial configuration of the polysaccharide had negligible obstructive effect on the accessibility of carboxyl functional groups by the acrylate needed to initiate the electrophilic substitutive process. The reaction procedure, adapted from the work of X. Wang *et al.*¹⁰¹, saw the usage of 3.9 equivalents of acrylate. Over the course of this research, equivalents of 5.5 and 7.8 were used to synthesise alginates with three different ranges of degrees of substitution referred to as “High”, “Med” and “Low” degree of substitution. Table 3.4. shows the range of afforded DoS% values from a series of acrylation reactions conducted at 60 °C, as calculated by NMR analyses. The optimal reaction time was trialled with kinetic study at set time intervals of T = 2 h, 4 h, 8 h, 24 h and 48 h to investigate its effects on DoS%. Conclusive data showing the extent of substitution was not available due to instrument failure.

Table 3.4. Expected range of degree of substitution in alginate acrylation reactions performed at 60 °C.

Equivalents	DoS% Denotation	Actual DoS% (High-M)	Actual DoS% (High-G)
4	Low	5 – 10	5 – 15
8	Med	15 – 20	15 – 25
15	High	25 – 30	25 – 35

Reaction temperature was found to have played a significant role in the conversion ratio of the acrylation process as theorised (Figure 3.7). With the reaction conducted at 60 °C, a maximum potential DoS% of 30 % was achieved after 4 hours with 35 % obtained following a 24-hour reaction. It was established that it was unfeasible to

conduct the reaction for less than 4 hours as the resultant product showed insufficient substitution. The decision to not conduct the reaction for 48 hours was to prevent the risk of thermodegradation of grafted acrylate functional groups, which were used to facilitate the covalent gelation process.



Figure 3.7. Difference in appearance in the colour of alginate solution after a 4 h acrylation reaction. Left – an acrylated alginate solution prepared at 60 °C. Right – an acrylated alginate solution prepared at r.t. (25 °C).

The same reaction, performed at room temperature, yielded a maximum DoS% of 5 % after 4 hours, with 12 % after 12 hours and 15 % after 24 hours (data not shown). It was concordant for reactions conducted at both temperatures that a reaction period of less than 4 hours resulted in poor product conversion and that a large proportion of acrylate used would be wasted as unreacted material. Table 3.5 offers a tabulated view of different DoS% values obtained for different alginate specifications under different trialled reaction conditions.

Table 3.5. Tabulated view of experimental maximum DoS% values obtained from acrylation reaction kinetic studies. Results for reaction time of 48 h were omitted due to lack of data. *Estimated DoS% too low to report with confidence.

Alginate specification	Equivalents	Temperature (°C)	Reaction time (h)	Max DoS% (%)
High-M	3.9	25	4	*
High-M	3.9	25	24	*
High-M	3.9	60	4	5
High-M	3.9	60	24	12
High-M	5.5	25	4	6
High-M	5.5	25	24	11
High-M	5.5	60	4	15
High-M	5.5	60	24	20
High-M	7.8	25	4	10
High-M	7.8	25	24	18
High-M	7.8	60	4	30
High-M	7.8	60	24	35
High-G	3.9	25	4	*
High-G	3.9	25	24	*
High-G	3.9	60	4	*
High-G	3.9	60	24	10
High-G	5.5	25	4	6

Table 3.5 continued. Tabulated view of experimental maximum DoS% values obtained from acrylation reaction kinetic studies. Results for reaction time of 48 h were omitted due to lack of data. *Estimated DoS% too low to report with confidence.

Alginate specification	Equivalents	Temperature (°C)	Reaction time (h)	Max DoS% (%)
High-G	5.5	25	24	12
High-G	5.5	60	4	15
High-G	5.5	60	24	25
High-G	7.8	25	4	5
High-G	7.8	25	24	12
High-G	7.8	60	4	18
High-G	7.8	60	24	22

Experimental data shows a trend in increased substitution with prolonged reaction time, increased reaction temperature and higher equivalents of acrylate used.

Other reaction parameters such as precipitation medium and drying method were trialled and investigated with the post-acrylation storage and handling in mind. The original reaction procedure utilised IMS as the precipitation medium to purify the modified alginate from unreacted acrylates.

A co-solvent system of IMS:Acetone (2:1) was used to increase the solvent volatility in order to ease the process of alginate drying. ^1H -NMR was used to detect traces of solvent, namely acetone and ethanol. All spectral data with the same drying times indicate the performance difference between the two precipitation media was considered negligible after lyophilisation (data not shown).

For drying *in vacuo* vacuum pump-assisted lyophilisation offered a rapid approach to dry the sample thoroughly and efficiently, but the resultant material was a sample with a compact, brittle and nest-like structure whereas drying at room temperature *in vacuo* on a Büchner funnel afforded a more open structure which is more pliable when handling (Figure 3.8). The two samples have no difference in its chemical composition but the different morphologies may contribute to its solubilities.

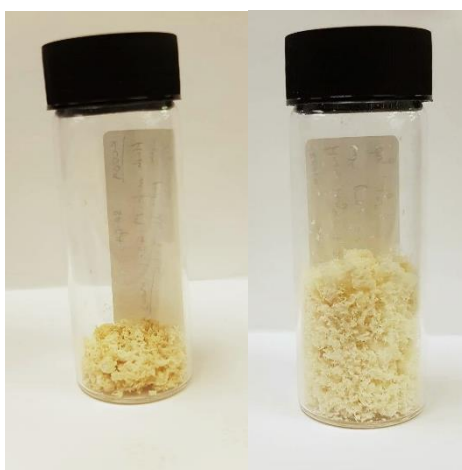


Figure 3.8. Acrylated alginate dried via lyophilisation (left) and dried *in vacuo* at room temperature (right).

Water solubility tests conducted on the same alginate sample dried using the two different drying methods showed that the solubility of the modified alginate has decreased after being subjected to extreme low pressures such as pump-assisted lyophilisation. This may be attributed to the low pressure environment causing the internal structure of the alginate to close in on itself, causing higher degree of topological polymeric chain entanglement which translated to increased time taken for polymeric chains to untangle in solvent for hydrogen bonds to form.

3.3.3 Comparison of High-M vs High-G alginate

Synthesised High-M alginates appeared more soft and less compact in appearance compared to its High-G counterpart, which resembled flakes of alginates and were more brittle and harder (Figure 3.9). There were negligible differences between their chemical profiles. The High-G modified alginates express lower water solubility as the polysaccharide backbone has more uniform arrangement which reduces hydrogen bond interactions, and higher viscosity in water due to the alginate having a longer chain length which translates to a higher molecular weight.

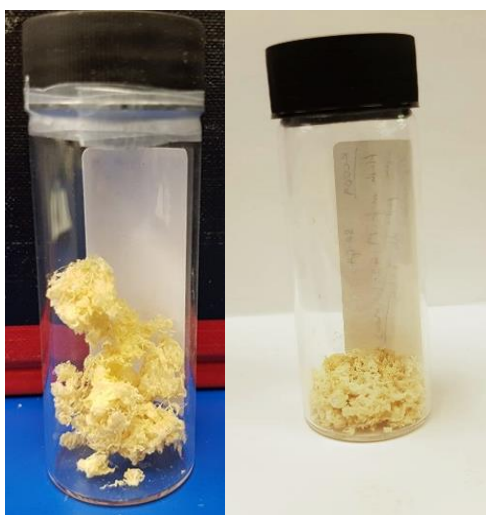


Figure 3.9. Dried High-M (left) and High-G (right) acrylated alginate.

3.3.4 Conclusion

In this work, alginate undergoes acrylation by substitution of the hydroxyl group with GA to allow an *in-situ* Michael-type addition reaction to proceed to form the covalent crosslinks necessary to produce hydrogel. The synthesis protocol was adapted from the work published by Wang *et al.*¹⁰¹ GA was chosen over glycidyl methacrylate (GMA) as the absence of the electron-donating methyl functional group decreases its stability, allowing the Michael-type addition reaction to occur more rapidly at the expense of decreased chemical stability. In addition, to retain the novelty of this research, the emphasis of the alginate gelation pathway lies heavily with gelation via covalent crosslinking as opposed to photogelation, wherein GMA undergoes rapid gelation to form a stiff hydrogel.^{101,149,150}

The acrylation step was performed at pH 10.0 to increase substitution at the carboxylic terminals instead of the hydroxylic terminals. The reaction can be reproduced with high confidence and for the acrylate substitution degree to be controllable to within $\pm 5\%$ of expected value. Various reaction parameters were altered and trialled to optimise the synthetic procedure, post-synthesis storage, and handling processes. Numeral factors contributing to the success of the reaction and controllability of substitution ratio were established, as confirmed by analytical characterisations. The acrylating reagent was used in large excess so further work is necessary to tailor the reaction procedures to minimise waste. IR experiments should be performed to establish a full spectrum of the substituted alginate and more comprehensive NMR tests such as ¹³C COSY and DEPTQ experiments are necessary to improve the precision of M/G ratio determination.

3.4 Thiolation of Sodium Alginate

3.4.1 Thiolated alginate

Purified thiolated alginate was white in colour with a wispy, open nest-like structure (Figure 3.10).



Figure 3.10. Dried High-M (left) thiolated alginate and High-G (right) thiolated alginate.

A faint sulphurous smell was detected when handling. The sulphurous smell intensified over time if left exposed to light, temperature or air. It was hypothesised this might be a product of photodegradation of thiol and the consequent release of mercaptans, such as methanethiol. The solute's aqueous solubility decreases after suspected oxidation as indicated by the presence of precipitate formation and sulphurous odour. Table 3.6 shows obtained range of DoS% values from a series of alginate thiolation reactions conducted at 40 °C.

Table 3.6. Expected range of degree of substitution in alginate thiolation reactions.

Alginate: Thiol moiety mass ratio	DoS% Denotation	Actual DoS% (High-M)	Actual DoS% (High-G)
1:1	Low	2 – 5	2 – 5
1:1.5	Med	5 – 10	5 – 10
1:2	High	10 – 13	10 – 13

3.4.1.1 NMR characterisation of thiolated alginate

Integration values from trimeric configurations (MMM, GGG, MGM/GMG), found between 4.8 and 5.0 ppm for thiolated alginate, were not taken for calculations as there was a large interference from the solvent signal observed at δ 4.8 ppm.⁸³ ^1H -NMR spectra of High-M and High-G thiolated alginate is presented under figures 3.11 and 3.12, respectively.

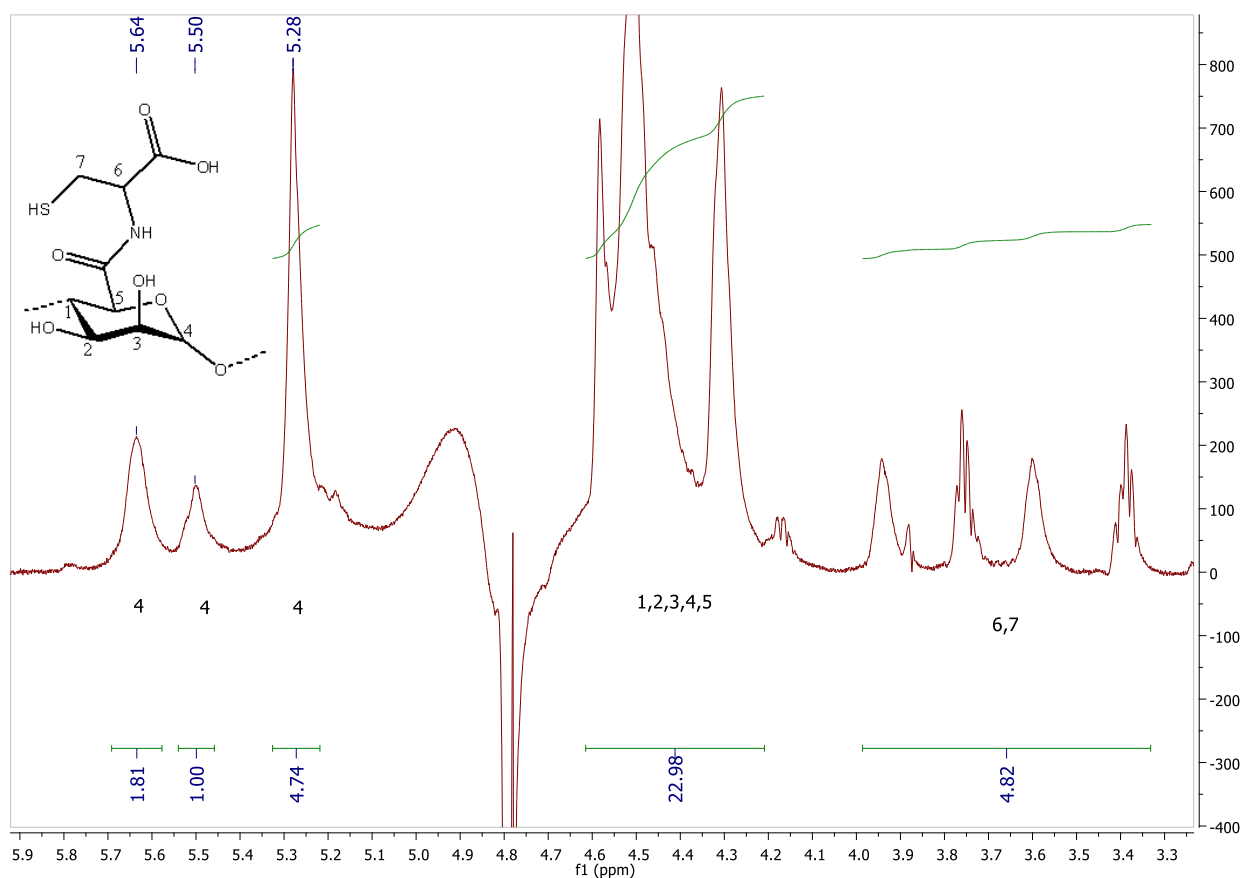


Figure 3.11. ^1H -NMR spectrum of thiolate-substituted High-M alginate. NMR conducted at 25 °C, D_2O , 500 MHz with 256 scans.

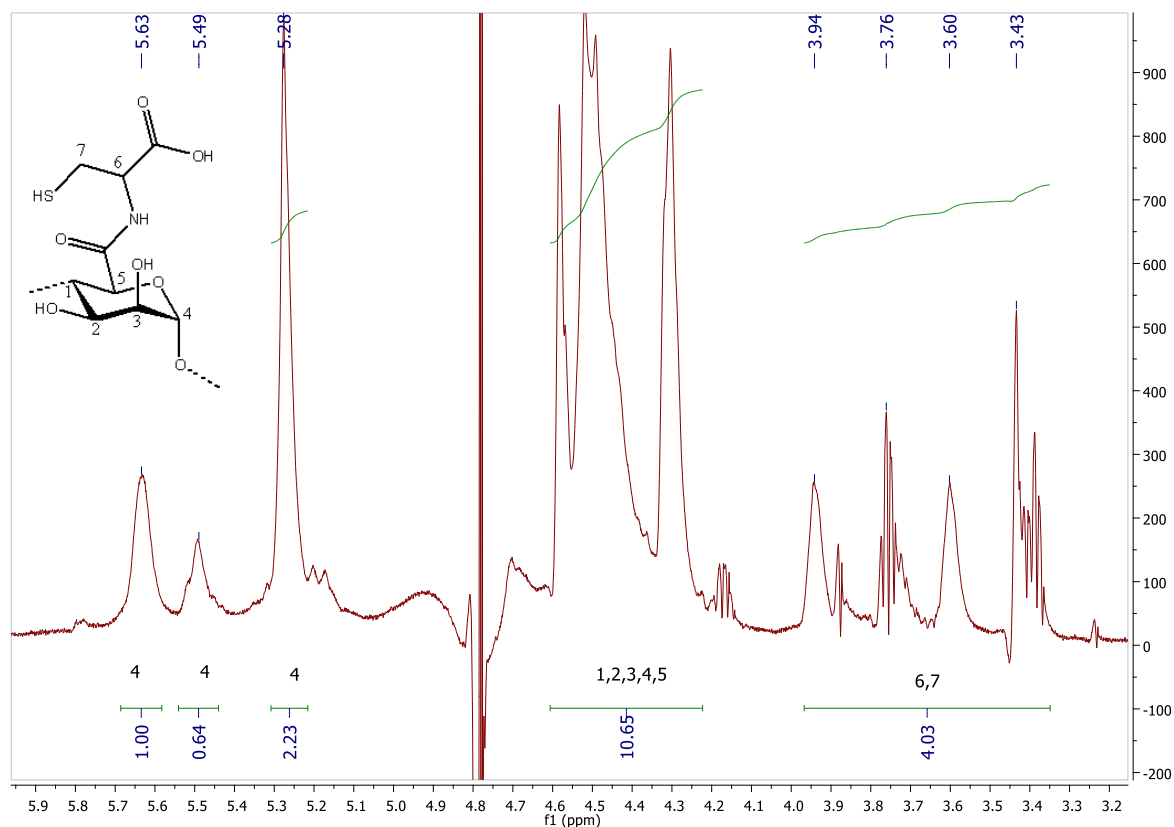


Figure 3.12. ^1H -NMR spectrum of thiolate-substituted High-G alginate. NMR conducted at 25 °C, D_2O , 500 MHz with 256 scans.

It was not feasible to conduct the NMR experiments at high temperatures due to the thiol moiety's sensitivity to heat. 2D NMR analyses were performed on synthesised alginate samples but yielded inconclusive data as the inability to suppress the water signal prevented accurate interpretation of afforded spectra. Table 3.7 shows a summary of estimated DoS% calculated through ^1H -NMR experiments.

Table 3.7. Tabulated information of alginate thiolation experiments performed, with estimated M/G ratio and DoS%.

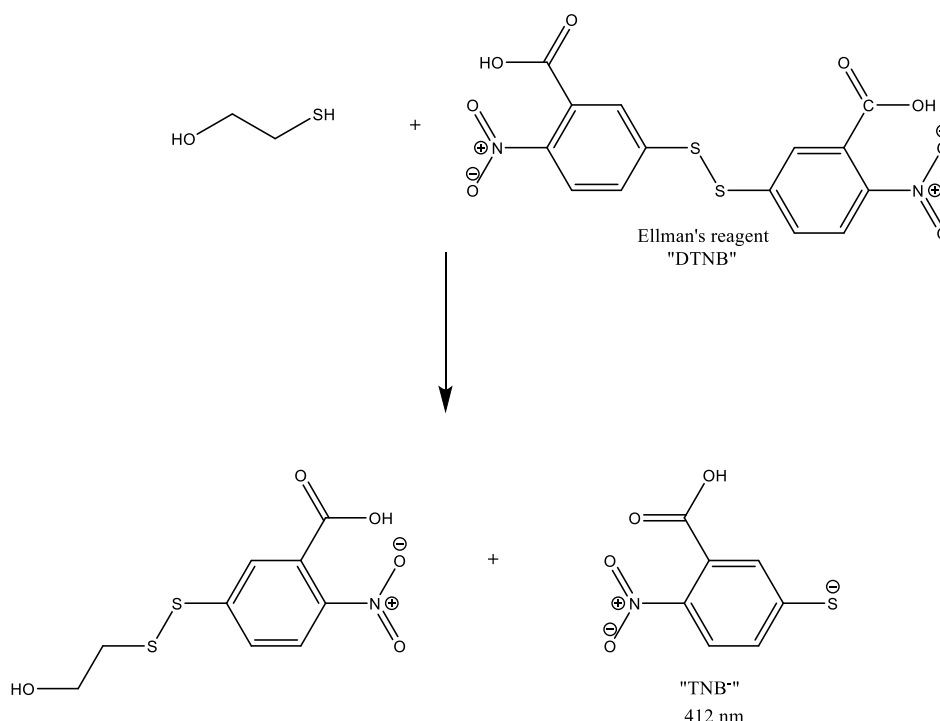
Experiment number	Mass obtained (g)	Yield (%)	Est.M/G ratio	Est. DoS% (%)
TA2	0.85	59.8	1.8	9
TA5	0.99	72.0	1.8	9
TA6	0.86	73.2	0.7	11
TA7	0.93	78.9	0.8	12
TA8	0.88	75.4	0.8	12
TA9	0.90	76.8	0.7	10
TA10	0.90	76.4	0.7	10

Thiolation trials conducted using High-M alginate saw its M/G ratio remain close to 2.0 even after reaction. The M/G ratio of thiolated alginate synthesised using High-G alginate suggest that a loss of linearity in the alginic spatial arrangement was observed. This was attributed to the steric effect induced by the introduction of cysteinium and cysteaminium cation onto the C-6 terminal.

The extent of substitution was poor (≥ 12 % DoS%) despite every attempt was made to minimise contact with light and air. The crude product was not taken for analyses as any unreacted thiol moieties present in the solution would cause the experiment results to become skewed from the actual value of degree of substitution.

3.4.1.2 UV-vis spectroscopic analysis of thiolated alginate

The thiol content was determined using UV-vis spectroscopic measurements by using Ellman's reagent reduced by thiol moieties. The concentration of the TNB⁻ anion is proportional to the concentration of thiol present in solution (Scheme 3.5).



Scheme 3.5. Reduction of Ellman's Reagent (DTNB) with 2-mercaptoethanol into TNB⁻.¹⁵¹

Three sets of standard calibrations were established using replicates of concentration standards between 5.11×10^{-5} and $2.56 \times 10^{-4} \text{ mol dm}^{-3}$ of 2-mercaptoethanol with Ellman's reagent in HPLC-grade deionised water. The calculated R^2 values were 0.9978, 0.9943 and 0.9595, respectively. The calibration curve which produced the highest R^2 value was reported and used for subsequent thiol content calculations (Figure 3.13). Each set of measurements were conducted in triplicates to minimise the margin of error.

The margin of error was suspected to be largely technical from the photodegradation of Ellman's reagent, impurities present in buffer solution, impurities present in handled glassware or scratches on the quartz cuvette surfaces.

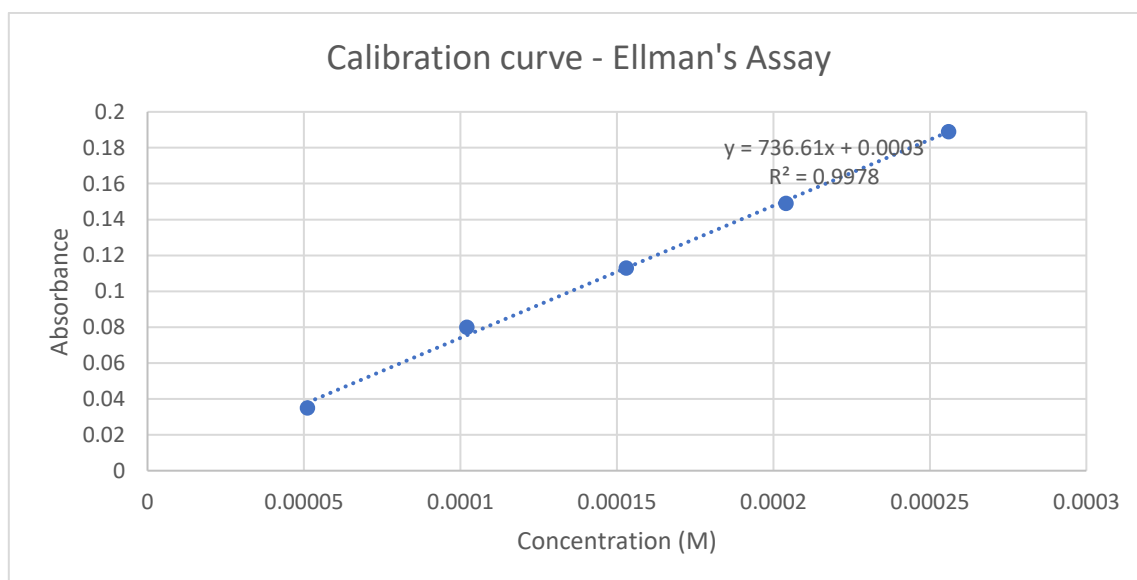


Figure 3.13. Calibration curve of thiol concentration in HPLC water.

During thiol quantification of thiolated alginate the background absorbance value from the TNB^- was subtracted from the total absorbance value to obtain the adjusted value which was used to determine the thiol density within the sample (Table 3.8).

Table 3.8. Tabulated data from UV-vis spectroscopy trials of thiolated alginate samples.

Experiment number	Total absorbance	TNB ⁻ background	Adjusted value
TA1	0.171	0.088	0.083
TA2	0.166	0.088	0.078
TA3	0.156	0.088	0.068
TA4	0.135	0.088	0.047
TA5	0.166	0.088	0.078

The UV-readings were converted to thiol density for ease of reading (Equations 5 to 11 in Chapter 2 Section 2.1.2.1). The thiol density was further converted to obtain an estimated DoS% value (Table 3.9).

Table 3.9. Tabulated results of thiol density of various synthesised thiolated alginate samples along with their respective DoS%.

Experiment number	Thiol density ($\frac{\mu\text{g thiol}}{\text{g alginate}}$)	Est. DoS(%)	Est. DoS from ¹ H-NMR (%)
TA1	743.7	0.9	9
TA2	698.9	0.9	9
TA3	609.3	0.7	7
TA4	421.1	0.5	6
TA5	698.9	0.9	9

The estimated DoS% from UV data analyses were not concordant with the estimated DoS% values calculated from NMR data. The calculated theoretical value from UV results were found to be out by a factor of 10. The reasoning for this phenomenon was unknown as the experiments were performed in triplicate and the mathematical approach and calculations reviewed multiple times. However, it may be hypothesised that due to the reductive process of mercaptans by the Ellman's reagent not having a 100 % efficiency, this has a knock-on effect on the quantification of free thiols by UV-vis spectroscopy which caused the discrepancies in estimated substitution values.

3.4.2 Factors affecting the degree of substitution (DoS%) and yield

Various reaction parameters were trialled and investigated in order to optimise the reaction process and yield obtained. Table 3.10 offers a tabulated view of reaction conditions altered and trialled as part of this work. Please refer to Chapter 2 Section 2.2.3.3 for further information pertaining to the experimental procedures performed.

Table 3.10. Simplified view of reaction parameters trialled and trialled conditions with the alginate thiolation step.

Parameters	Parameter variations		
Alginate	High-M	High-G	
Alginate concentration	2 % w/w (De-ionised water)		
Thiolating agent	Cysteamine hydrochloride		L-Cysteine hydrochloride
Wt. ratio (alginate:thiol agent)	1:1	1:1.5	1:2
Adjusted pH value	4.0	5.0	6.0
Temperature	25 °C		40 °C
Reaction time	4 h 16 h (overnight)		
Post-reaction adjusted pH value	4.0		6.0
Dialysis medium change frequency	0.5 day	1 day	2 days

NMR results showed that the effects of pH played a role in the outcome of the reaction as the estimated thiolation degree increased with lower reaction pH (Figure 3.14). This was achieved by comparing the integration values between the anomeric signals (δ 5.2 to 5.75 ppm) and thiol moiety signals (δ 3.4 to 3.9 ppm).

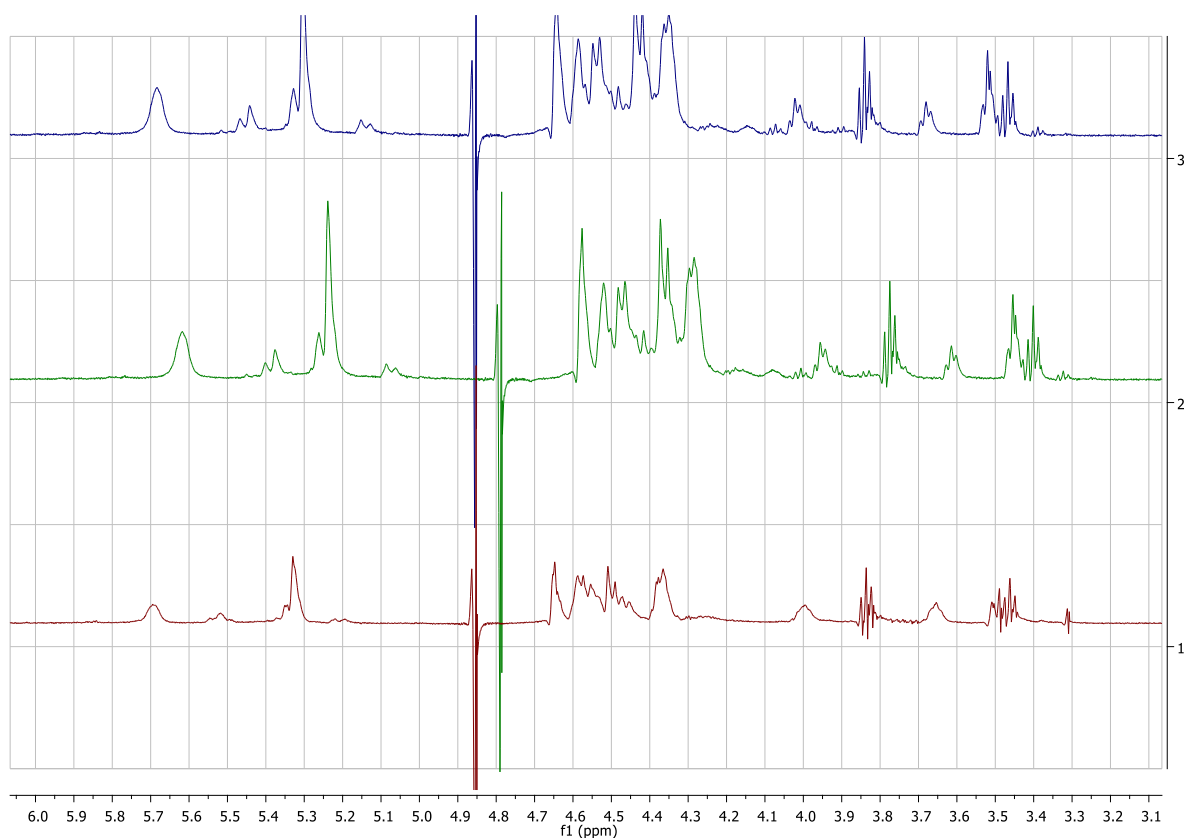
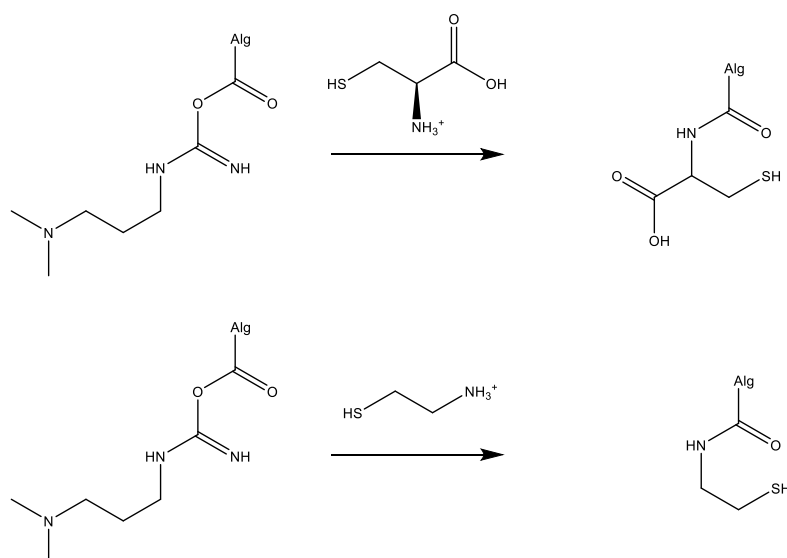


Figure 3.14. Stacked ¹H-NMR spectrum of thiol-substituted High-G alginates performed under pH 6.0 (top), pH 5.0 (middle) and pH 4.0 (bottom).

The reason for the difference in chemical shift values between the spectra was due to problems faced with the analytical software where peak referencing of overlay document was not possible.

The reaction pH was made more acidic following the addition of the thiol moiety as the initial amide formation was acid catalysed by protonating the amino terminal and facilitate the removal of the EDCI activating group (Scheme 3.6).



Scheme 3.6. Removal of EDCI activating group by acid-catalysed amide formation.

The adjustment of reaction pH before purification was necessary to promote the re-formation of the thiol moiety from its thio salt and to convert alginic acid into alginate, which facilitated the removal of unreacted materials. The pH adjustment also improved the structural integrity of the crude product which eased handling. Although it was believed that a higher thiolation degree may be obtained if left reacting for longer, it also raised concerns over the stability of the thiol functional groups over time as prolonged reaction time under acidic conditions leads to the formation of an amide salt which, given the zwitterionic nature of the thiol moiety itself, would be difficult to extract back out.

Figure 3.15 shows the significance of temperature on the thiolation experiments. Reactions performed at room temperature was considered unviable for further investigation despite the conditions posing less risk for the thiol moiety to degrade.¹⁵²

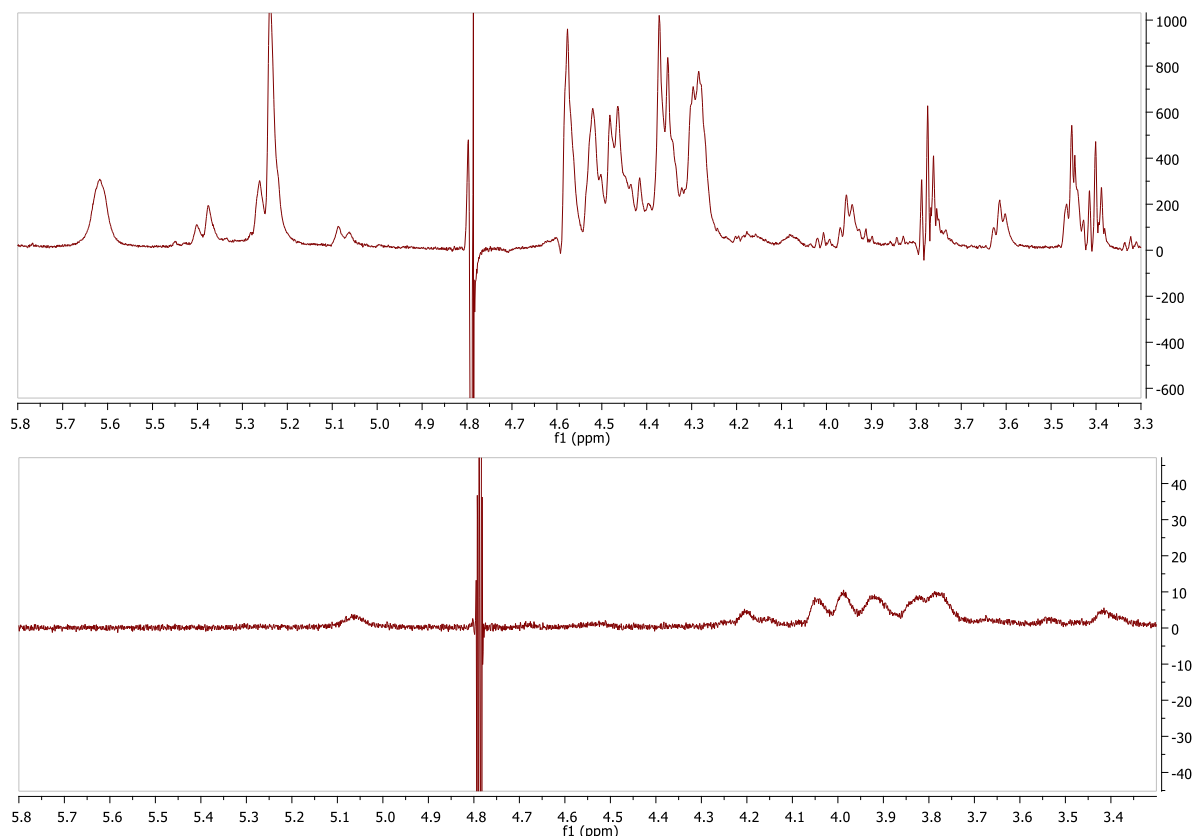


Figure 3.15. Stacked ^1H -NMR spectrum of thiolate-substituted High-G alginates performed under 40 $^{\circ}\text{C}$ (top) and at 25 $^{\circ}\text{C}$ (bottom).

The intensity of signals was significantly reduced for the reaction conducted at 25 $^{\circ}\text{C}$ relative to the reaction conducted at 40 $^{\circ}\text{C}$. The absence of characteristic polymeric signals (δ 4.2 to 5.65 ppm) suggested little-to-no substitution as the reaction proceeded too slowly for the thiol to be comparably noticeable in NMR spectra.

The time taken during the dialysis step was crucial and required heavy monitoring. Though every effort was made to minimise contact with light and air, the synthesised material would inevitably be exposed to air and light, albeit to a lesser extent, whilst undergoing purification by dialysis. This posed a big challenge as alginate having undergone higher degree of substitution had more thiol terminals susceptible to degrade and self-polymerise by formation of intra-polymeric disulphide linkages. The dialysis time was reduced from the original two days and ultimately resulting with a 16-hour dialysis period with four media changes with a net total of two day-long purification process.

3.4.3 Setbacks

Though the original reaction procedures were adapted to suit cysteamine hydrochloride, the replicate procedure when cysteine was used resulted in visible conglomeration of alginate to produce a soft slime-like consistency (Figure 3.16). It was hypothesised that, given the pKa value of cysteine carboxylic proton (1.71) the acidity from the cysteine induced a sharp pH change in the alginate, causing precipitation of insoluble alginic acid.⁷⁴ To test this hypothesis, the thiolation agent was dissolved in a basic media containing dilute sodium hydroxide and the pH-adjustment would be forgone to minimise the sharp pH change (Figure 3.17).



Figure 3.16. Thiolated alginate in solution after reacting against cysteine for 3 hrs in r.t. (25 °C). Gel aggregation is visible in solution (1 % w/w G-Alg in DI-H₂O).

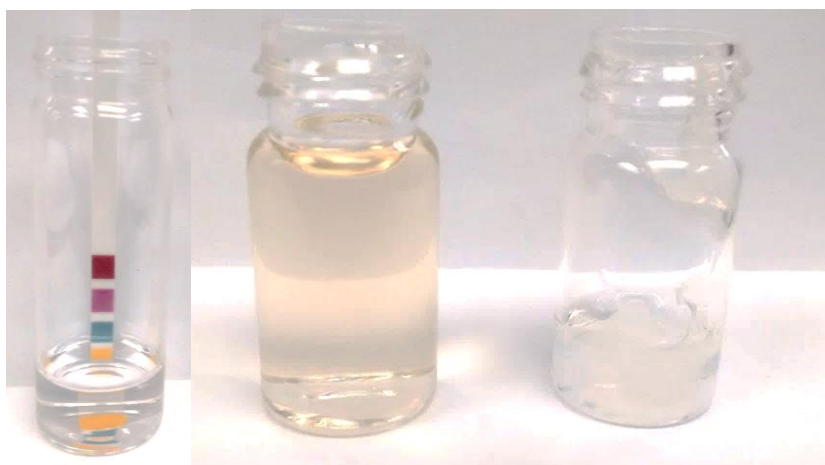


Figure 3.17. Left – Cysteine dissolved in aqueous alkaline media (Dil. NaOH; pH 8.0). Middle – pH-adjusted cysteine solution added to sodium alginate solution (1 % w/w G-alg in DI-H₂O). Right – Following addition of cysteine in powder form to sodium alginate solution (1 % w/w G-alg in DI-H₂O).

The gel aggregating effects were minimised but gel precipitates continued to form over the course of the reaction and purification step. The majority of alginate bulk gels was seen to have formed within the dialysis tubing during the purification step, as indicated by the visual appearance of the solution becoming more translucent (Figure 3.18).

This same phenomenon was observed when using both classifications of alginate, but the alginate gel differed in integral strength when handled with the high-M bulk gels being softer and more swollen, suggesting higher water retention, and the high-G counterpart being more stiff, fragile and brittle when handled.

The material was largely insoluble in water and other analytical co-solvent systems which prevented its analysis, which further suggested the possibility of thiol degradation to form disulphides during purification.



Figure 3.18. Left – High-G Thiolated alginate in solution following reaction and awaiting purification. A visible gel lump can be seen in solution. Right – Two samples of thiolated alginate (Left – M, Right- G) in solution after purification awaiting drying. Wisps of milky white can be seen in the alginate solution on the right.

3.4.4 Conclusion

The thiolation step, when reproduced, did not match the experimental results of that reported in the original publication from which this procedure was taken and adapted.¹⁴² The experimental results of analysed samples were consistent with data

from the same series of reactions and a yield upwards to 79 % can be afforded but poor degree of substitution was achieved, with a maximum DoS% of 12 % recorded. The stability of the thiol functional group in the synthesised material posed a big challenge on the purification step and post-synthesis handling. Further work is needed to further optimise the synthesis procedure and source an alternative method to purify the synthesised materials.

3.5 Alginate hydrogels: preparation, characterisation and tests

3.5.1 Preparation of alginate hydrogels

As part of the scientific investigation, modified alginate was used to form bulk gels by forming crosslinks via three different methods: ionotropic crosslink with calcium, crosslink with photoinitiator Irgacure 2959 and covalent crosslinks with an *in-situ* Michael-type addition reaction between acrylate and thiol moieties.

3.5.1.1 Preparation by ionotropic crosslinking

The ionotropic crosslinking of alginate strands to calcium ions occurred instantaneously in solution to afford the bulk gel. Attempts were made to exert higher control over the gelation mechanism by reducing the concentration of calcium solution used, but the rate of gelation remains the most difficult factor to monitor as the exterior wall of the alginate solution changes morphology instantaneously. Table 3.11 gives a simplified tabulated view on the conditions used for ionotropic gelation trials.

Table 3.11. Conditions used for ionotropic gelation trials.

Alginate specification	High-M	High-G
Conc. Alginate solution (% w/v)	3.5	
Conc. CaCl ₂ solution (M)	1	0.1

Ionotropic gelation trials were performed to investigate the alginate's ability to form gel and the gel stiffness as there was no access to a rheometer at the time of conducting the gelation trials. Trials with lower concentrations of calcium chloride used produced gels with lower internal mechanical integrity but an instantaneous formation of a soft gel exterior was observed. Attempts were made at monitoring the gelation process using a rheometer, but the gelation process occurred too rapidly for any useful data or knowledge to be obtained.

3.5.1.2 Preparation by photogelation crosslinking

Photogelation trials in the laboratory was conducted using Irgacure 2959 photoinitiator and resulted in a gelation process that was consistent both in time taken and the gel's mechanical properties (Table 3.12).

Table 3.12. Information of volumes used for photogelation trials.

Alginate conc.	Alginate vol.	Irgacure 2959 conc.	Irgacure 2959 vol.
2.5 % w/v	250 µL	1 % w/v	15 µL
3.5 % w/v	250 µL	1 % w/v	15 µL

Photogelation using Irgacure 2959 was successful and produced gels with high structural integrity, as shown by photographs (Figure 3.19). Gel curing was conducted in seven-minute windows with seven minute cooldown between

subsequent curing with clinical usages in mind in order to prevent harm to the patient and wound site. This method of gelation has shown benefits from a chemical perspective as it carried a low risk for thermal degradation. A tabulated view of reaction conditions can be found under Table 3.13.



Figure 3.19. Photographs of gels formed from photogelation. Left to right: 2.5 % w/v acrylated alginate with photoinitiator, 3.5 % w/v acrylated alginate with photoinitiator, covalent-crosslinked 3.5 % w/v alginate gel with photoinitiator, covalent-crosslinked 3.5 % w/v alginate gel with photoinitiator.

Table 3.13. Conditions used for photogelation experiments.

Alginate:QT volume ratio	5:1		
Irgacure 2959 incubation time (mins)	10	15	
Curing wavelength (nm)	257 – 276		
Curing time (mins)	7	14	21
Gelation vessels	Open-end syringe	Eppendorf tube	Centrifugation tube

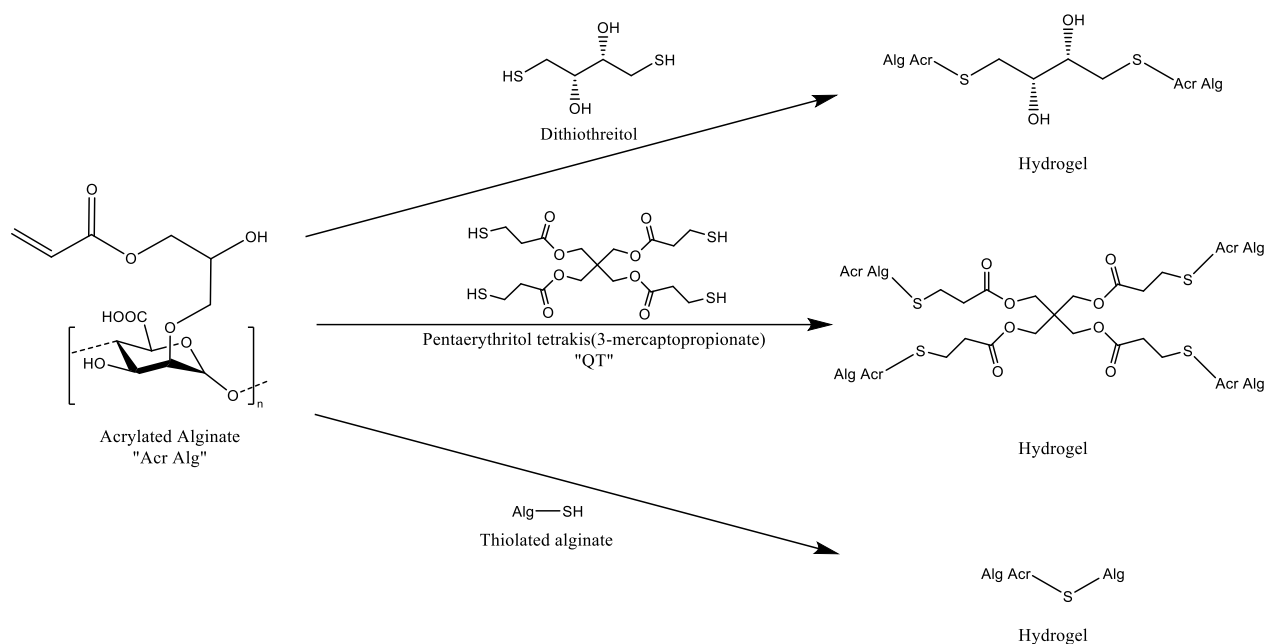
Gelation was performed using High-G substituted alginates with high degrees of substitution. The incubation time and curing times were trialled to investigate its significance of the gelation process. Three different reaction vessels were used for the gelation step which produces gel with different sizes and dimensions to further investigate the efficacy of the process should the alginate morphology changes to simulate different types of wound and wound sites receiving treatment.

Unexpectedly, the 2.5 % alginate solutions produced stiffer gels with higher malleability against the 3.5 % gels. The same alginate samples used in covalent crosslinking trials produced a similar trend. It was hypothesised that excess homogenisation of the alginates imposed adverse effects on the alginate's gelation behaviour. The effects of initial curing period were found to be negligible on the resultant gel's properties. All experiments produced a bulk gel during the first curing. Some 3.5 % w/v concentration solutions produced a bulk gel that was more malleable but became a robust gel following a second curing. The effects of prolonged curing time were studied as the gels undergo further curing to study the change in gel properties. The cured gels were more robust but was considered too stiff for the intended usage. However, concerns arose regarding the usage of UV- β light considering the end application. The usage of UV light for prolonged periods may cause adverse health effects such as cancer or skin blistering. It was decided to revisit photogelation as part of future work as a supplementary mode of crosslinking to strengthen the gel's properties. It should be noted that an increased initial curing period should be considered with actual application to factor in the increase in volumes handled.

3.5.1.3 Preparation by covalent crosslinking

3.5.1.3.1 Thiol moieties

The main experimental aim of this project was to create a polymeric network of acrylated-derivatised alginate using a variety of crosslinking methods, with an emphasis on Michael-type addition crosslinks using thiolated moieties to form hydrogel. Three thiol moieties were used in this work: Dithiothreitol (DTT), QT and thiol-modified alginates. A simplified schematic representation of covalent crosslink mechanism via Michael-type addition can be found under Scheme 3.7.



Scheme 3.7. Simplified depiction of crosslink mechanism between acrylated alginate and different thiol moieties to form hydrogel.

Initial gelation tests were conducted using QT due to its tetra-thiol functionality which possessed greater potential to form hydrogels with high polymeric density. DTT was also chosen for testing as its di-thiol functionality produces hydrogels with lower degree of crosslink which would be more malleable and would undergo degradation over time to allow easy dressing extraction, as reported by Emmakah *et al.*¹⁵³ In practice, the thiothreitol expressed very low stability above storage temperature and underwent a rapid oxidative process to form an intramolecular disulphide linkage under basic conditions which offered no capacity to form crosslinks (Figure 3.20).¹⁵⁴ This work used QT and thiolated alginates modified using cysteine and cysteamine as the thiol moieties needed for the *in-situ* Michael-type addition due to their stability under testing conditions and biocompatibility.

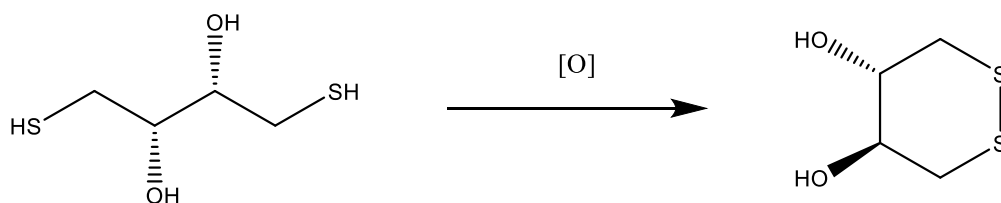


Figure 3.20. Oxidation of dithiothreitol into disulphide.¹⁵⁴

3.5.1.3.2 Preparation of alginate hydrogels

The covalent crosslinking of thiolated alginate posed several challenges which needed to be addressed. The primary obstacle was to deter potential further degradation of thiolated alginate during crosslinking. Secondly, a defined endpoint to the gelation process needed to be established, especially for gelation trials in the laboratory which were prepared without technical equipment to study the gelation mechanism. Alginate hydrogels were prepared in the laboratory in Eppendorf tubes and prepared *in-situ* in a rheometer whilst rheological measurements were taken. The endpoint of the two gelation methods were defined as:

- Laboratory gelation studies – The reaction vessel was gently inverted at designated time intervals. Once no free-flowing liquid was seen then the solution is said to have gelled. During this time, the gel is checked for its rigidity and size to establish whether it was a bulk gel or defined as gel particulates (Figure 3.21).
- Rheological gelation experiment – By monitoring the rheological test readings, the storage and loss moduli (G' and G'') figures were established. The point of gelation was defined as when the two moduli values crossover, indicating a change in intrinsic gel properties.



Figure 3.21. Photograph depicting no gelation (left), gel particulate formation (middle) and bulk gel formation (right).

From the laboratory gelation trials, samples were investigated for their ability to gel, the extent of gelation and the stiffness of the formed gel. A simplified view of gelation trials performed with different thiol moieties which include information such as

alginate specification, alginate DoS% denotation, concentration, volume ratio of alginate to crosslinking agent can be found under Tables 3.14 and 3.15.

Table 3.14. Simplified overview of laboratory gelation study conditions using acrylated alginate and thiolated alginate.

Acr-Alg specification	High-M, High-G		
DoS% denotation	Low	Med	High
Conc. Acr-Alg. solution (% w/v)	3.5	3.5	3.5
Thio-Alg specification	High-G		
DoS% denotation	Low	Med	High
Conc. Thio-Alg solution (% w/v)	3.5	3.5	3.5
Vol. ratio (Acr-Alg:Thio-Alg)	1:1		

Table 3.15. Simplified overview of laboratory gelation study conditions using acrylated alginate and QT crosslinker.

Acr-Alg specification	High-M, High-G		
DoS% denotation	Low	Med	High
Conc. Acr-Alg. solution (% w/v)	3.5	3.5	3.5
Conc. QT solution (% w/v; EA+TEA)	5, 10		
Vol. ratio (Acr-Alg:QT)	1:2.5	1:5	1:10

Reaction trials were conducted under mild basic conditions (pH 7.4, dil. NaOH) to catalyse the reactions. Results have shown that bulk gels were able to form but the time taken for gelation was long. Bulk gels formed for all trials using QT crosslinker

(columns 1-4) but trials which used thiolated alginate (columns 5-8) saw bulk gels form only with higher concentrations of thiol used (Figure 3.22).

Sets A, B and C contained acrylate-to-thiol concentration ratio of 1:5, 1:10 and 1:2.5, respectively. Set C, as expected, produced hydrogels with lower mechanical strength and the rate of gelation was slower. Sets A and B saw soft bulk gels form within 1 h and gradually strengthening over a period of 18 h whereas set C saw soft gels with similar stiffness form after 2 h and gradually strengthening over a period of 24 h. For thiolated alginate gelation trials, set A saw bulk gel began to form after 3 h. Sets B and C achieved partial gelation after 6 h and saw no difference over a period of 24 h.

Trials were conducted with both High-M and High-G alginates but similar results were obtained. Thiolated alginate-crosslinked gels were found to be significantly less robust compared to the QT-crosslinked counterpart even when the concentration ratio was kept consistent, suggesting a lower gelation efficacy due to steric effects from polymeric chains, potential degradation of the thiol functional group and lack of crosslink polymeric density.



Figure 3.22. Photograph of gelation study between acrylated alginate, thiolated alginate and QT crosslinker.

The effects of gelation medium were investigated as part of the gelation study, with some of the aqueous medium replaced by aprotic organic solvents. The resultant gel saw little difference in gel properties and can be assumed negligible for subsequent gelation trials. Unexpectedly, bulk gel was not formed when triethylamine, a known catalyst for Michael-type addition, was used but instead saw gel dissolution. The reasoning for this observation was unknown but can be hypothesised that the media

became too alkaline and subsequently caused a nucleophile-catalysed mechanism to occur.¹⁵⁵

3.5.2 Characterisation of prepared hydrogels

Numerous experiments were conducted on prepared gels to establish the gel properties, morphology and mechanical strengths. Tests such as release studies, SEM and rheological experiments were performed in order to establish the gelation profile, gel morphologies and mechanical properties. Gel tack tests and microbial suite experiments were not performed due to time constraints.

3.5.2.1 Release studies of alginate gels

Release studies were performed using a model drug to simulate the drug payload after dressing application. The model drug chosen was carmoisine for its solubility compatibility with the aqueous media handled as part of this project (Figure 3.23).

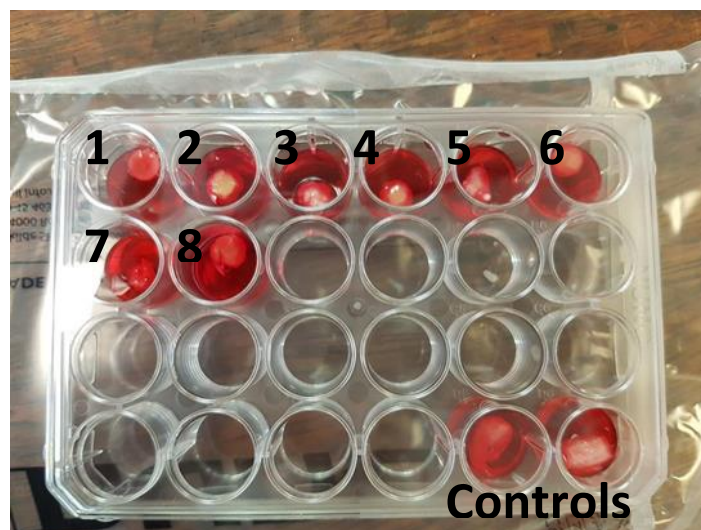


Figure 3.23. Prepared alginate gels being loaded with carmoisine solution.

In each set, experiment 1 contains hydrogels crosslinked via ionotropic gelation, experiment 2 contains hydrogels crosslinked via photo and ionotropic gelation, and

experiments 3 and 4 contain hydrogels crosslinked via covalent, photo and ionotropic gelation. Experiments 5 through 8 correspond in the same sequence as experiments 1 to 4. The standard calibration curve of carmoisine between 4.9×10^{-3} and $4.9 \times 10^{-1} \text{ mol dm}^{-3}$ was established at 412 nm (Figure 3.24). Please refer to Chapter 2 Section 2.2.2.4.1 for further information pertaining to experimental procedures.

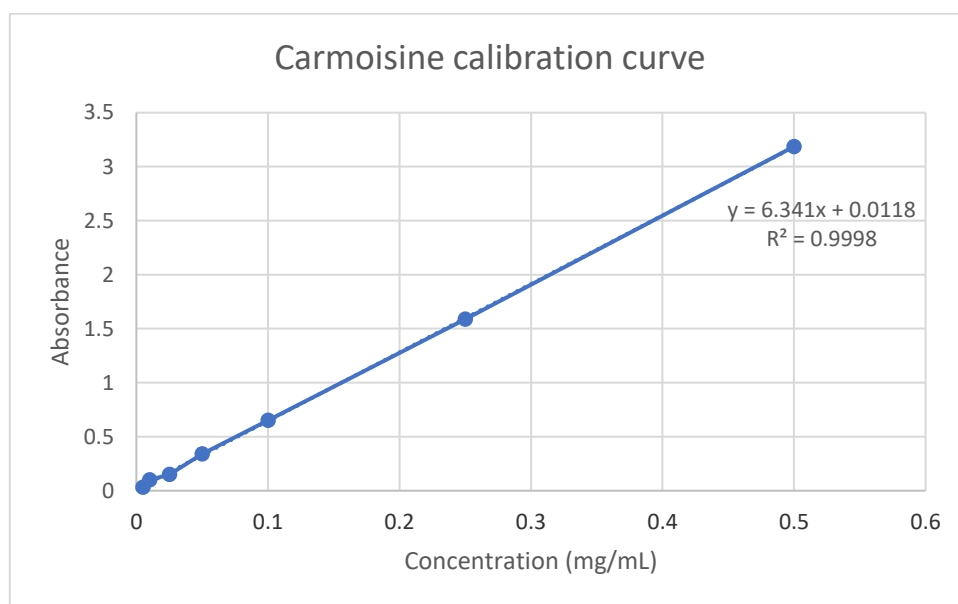


Figure 3.24. Carmoisine calibration curve in HPLC water at 412 nm.

UV-data showed the majority of carmoisine was released within the first 30 minutes and the release rate began to plateau after 60 minutes (Figure 3.25). The gels continued to retain traces of the drug even after 180 minutes and a full drug payload was not observed. The morphology of the gel was hypothesised to have negligible effect on the release profile due to its size but a more significant effect may be observed with a larger hydrogel. Moreover, the release profiles of the gels would differ when other drugs with different aqueous binding affinities and release behaviours were to be used.¹⁵⁶ The loading efficiency of the carmoisine was not determined as the mass of drug-loaded hydrogel was not recorded.

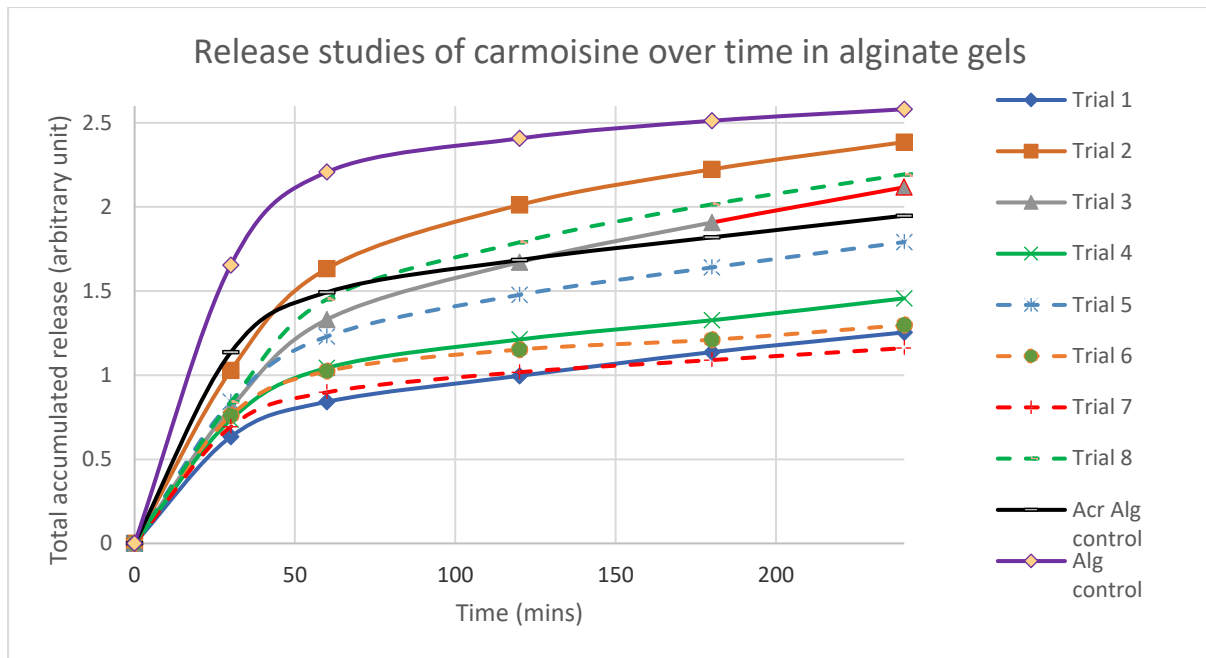


Figure 3.25. Graph showing release profiles of different alginate gels.

3.5.3 *In-situ hydrogel characterisation*

Oscillatory frequency and time tests were performed to establish the intrinsic gel properties and map the gelation timepoint. Frequency sweeps were conducted between 0.1 and 10.0 Hz frequency to mimic processes to which the hydrogel would be subjected whilst being pre, peri and post-usage of the wound dressing. Time tests were conducted at 5.0 Hz as a mid-point between the lower and upper values from the frequency sweeps. The sample was said to have gelled and the gelation timepoint established when G' crosses over with G'' . Lastly, the complex viscosity, G^* , offers an insight into the gel's stiffness.

3.5.3.1 *Rheological test data*

The usage of the cone geometry was rejected as any axial stress needed to be eliminated during testing. Cone geometries were also less desirable for the research output as it limited the gap between the Peltier plate and geometry. This work aimed

to establish the alginate's rheological profile through zero-shear velocity testing, which needed to be performed on a parallel plate system where only the sample's top layer was displaced with maximum shear at the sample's edge and zero-shear in the centre.

QT-crosslinked gels have been found to crosslink at $T = 2500$ s, or the equivalent of 42 minutes (Figure 3.26). The chemical nature of the Michael-type addition crosslink allows for a slow initial gelation but continues to strengthen over time.

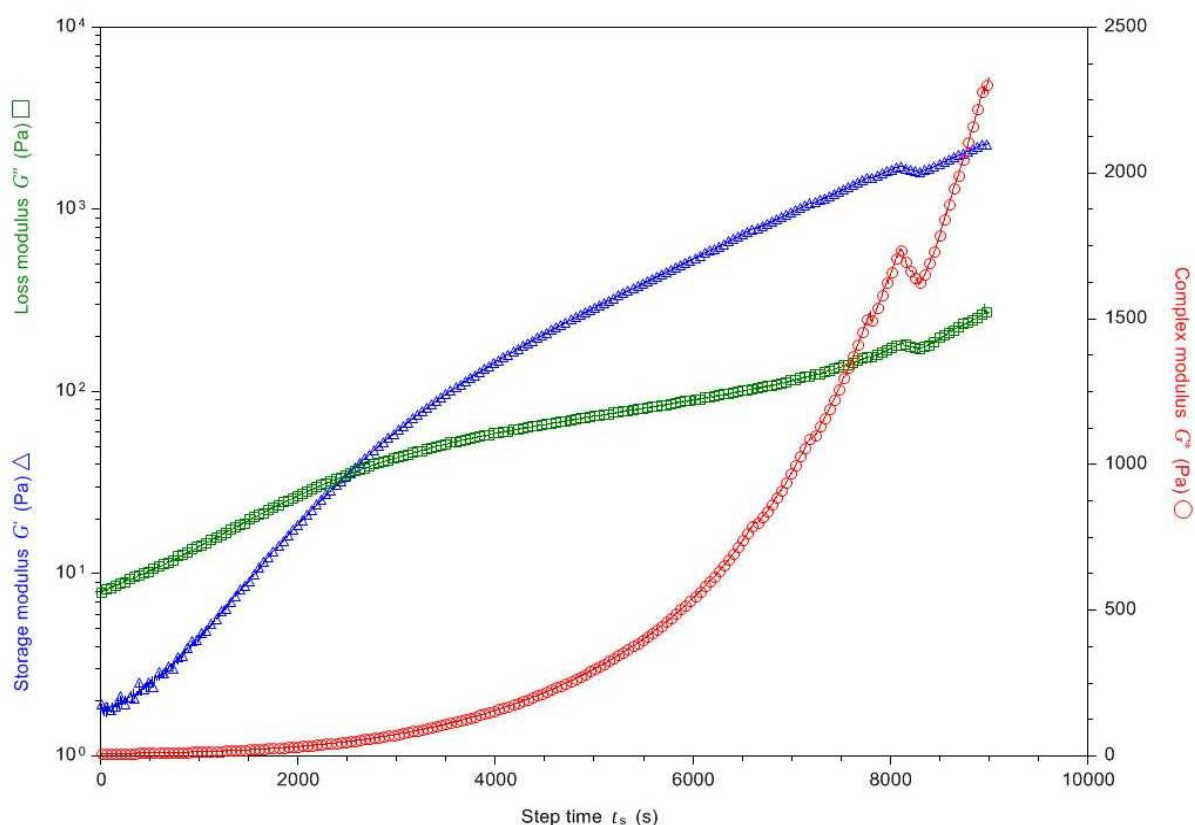


Figure 3.26. Rheological data from time test experiment using acrylated alginate with QT crosslinker.

The same experiments conducted using thiolate-modified alginate in lieu of crosslinker took 12000 s, equivalent to 200 minutes, before a crossover in moduli values was observed. The recorded gelation times were concordant with results obtained from initial gelation trials. (Section 3.5.1.3.2) A combination of thiolated alginate's low aqueous solubility and expressed low degrees of substitution contributed to the significant increase in gelation time. Sample dehydration was a common observation as a direct result of elevated testing temperatures and long

experiment time. To deter the hydration effect, a solvent trap was installed and a water reservoir was added. Dehydration effect of the alginate sample was observed at $T = 25000$ s and again at $T = 35000$ s (Figure 3.27). Photographs of alginate gels post-experiment can be found under Figure 3.28 where the alginate shrunk away from the edge of the geometry.

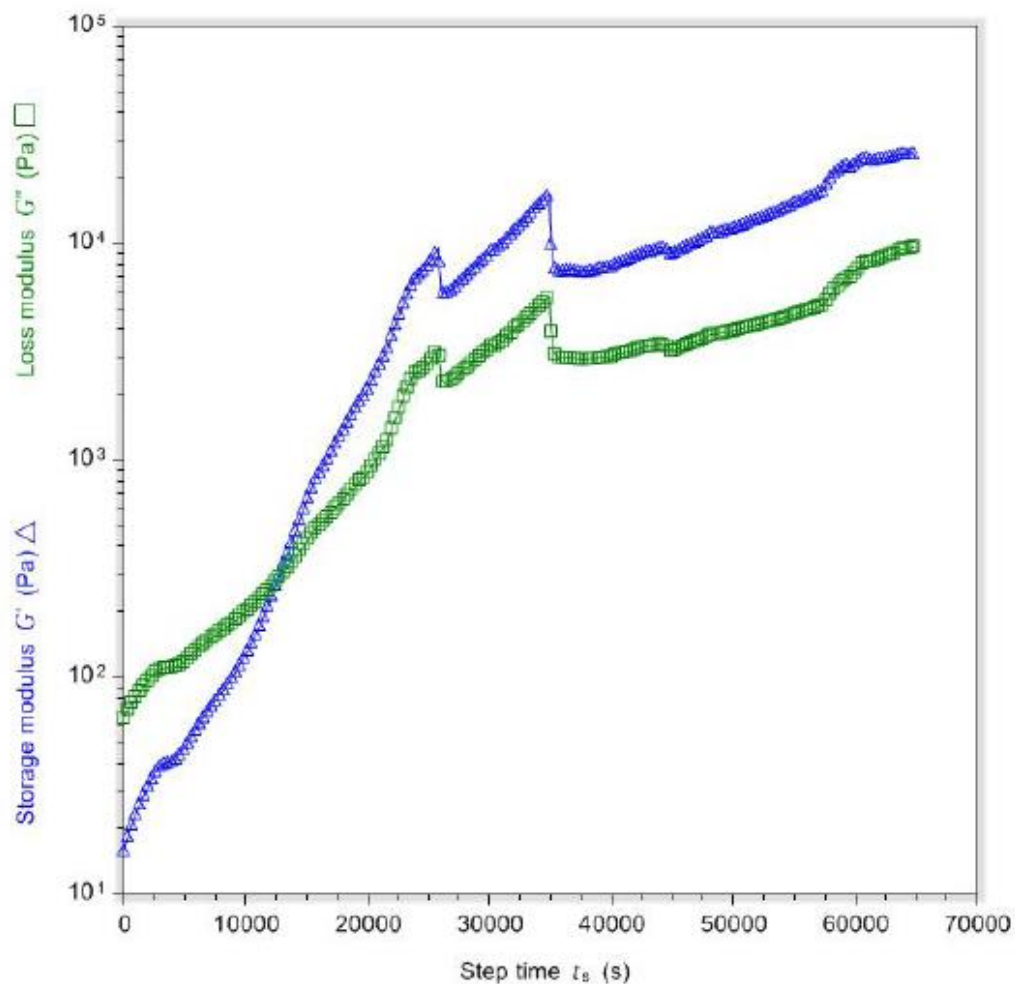


Figure 3.27. Rheological data from time test experiment using acrylated alginate with thiolated alginate. Sample dehydration is apparent from $T = 25000$ s.

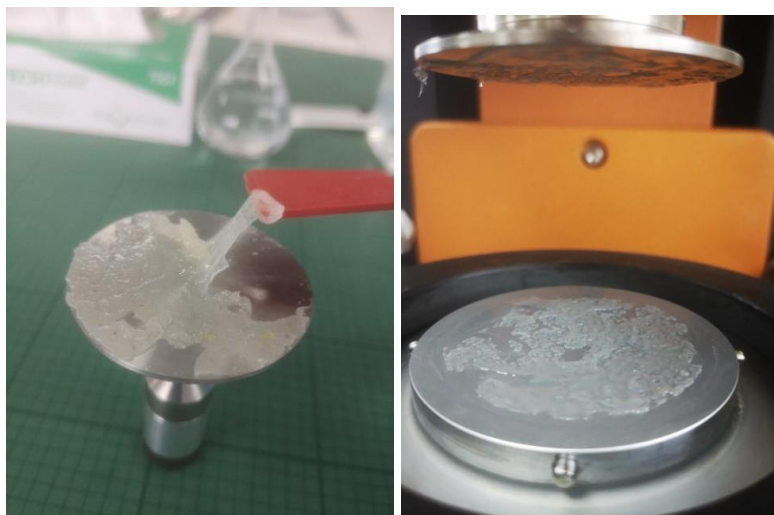


Figure 3.28. Photographs of hydrogels formed during rheological testing. Left – acrylated alginate with QT crosslinker. Right – acrylated alginate with thiolated alginate.

Oscillatory frequency sweep data was adjusted to sweep between 0.1 and 10.0 Hz frequencies as that alginate solutions was found to exhibit a shear thinning behaviour. The crossover of the moduli values and the decreased complex viscosity with increased shear frequency indicated this behaviour. (Figure 3.29)

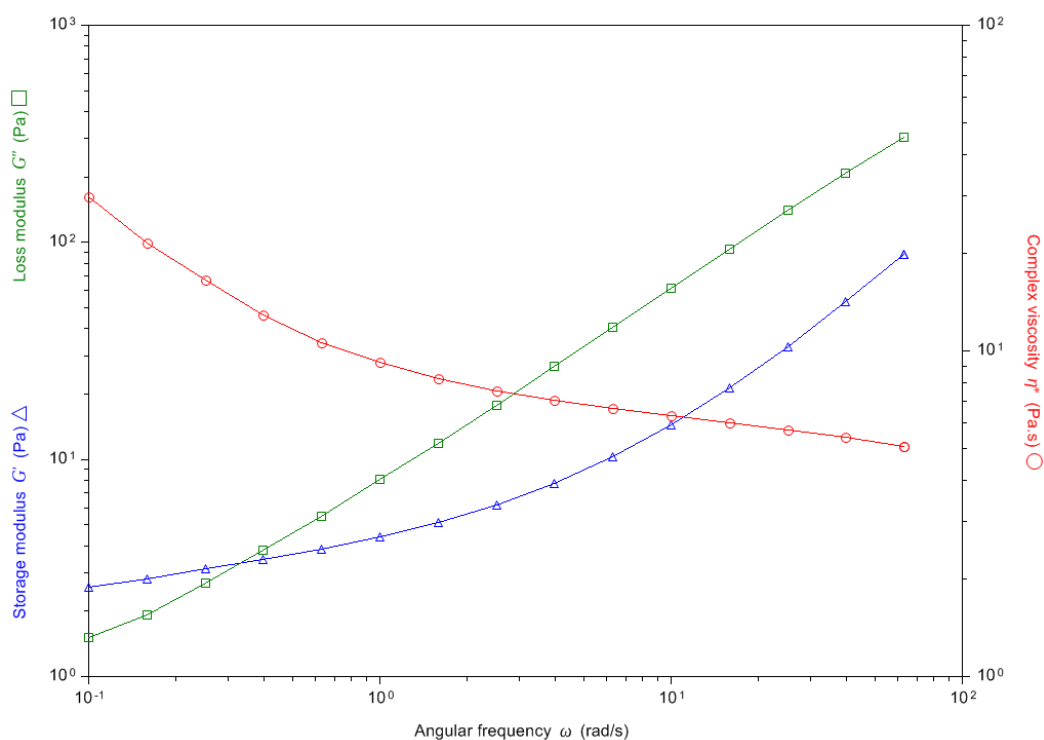


Figure 3.29. Rheological data of oscillatory frequency sweep between 0.1 and 100.0 Hz. A shear thinning behaviour was observed.

The 50 mm parallel plate produced unexpected results while testing (Figure 3.30). This was indicated by the random fluctuation in moduli values as this indicated a loss of contact between the Peltier plate and sampling material. This was a direct cause of the alginate solution being low in viscosity in addition to the wide geometry diameter inducing a larger shear stress on the edge of the sample as the plate oscillates which caused the sample to bulge and spill out the sides. The experiment protocol was modified to replace the 50 mm geometry parallel with the 20 mm parallel plate to lessen sample volume and shear stress to minimise risk of sample sagging or spillage. Although a sandblasted geometry was available for use, its larger diameter and absence of a water reservoir to prevent sample dehydration made it unsuitable for this study.

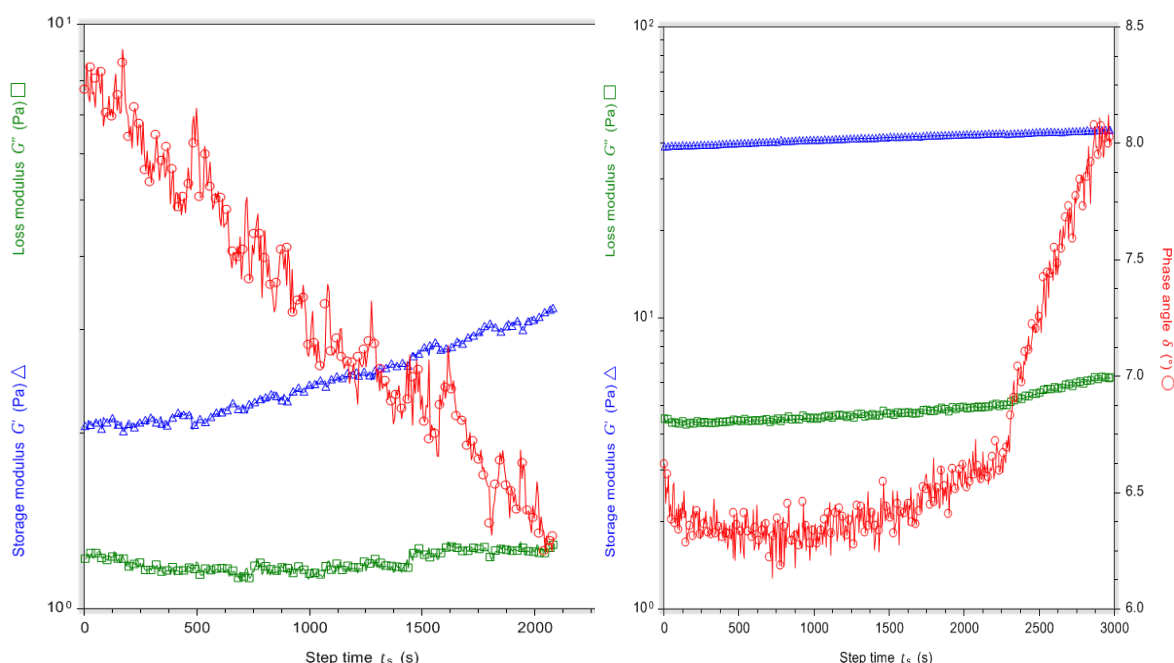


Figure 3.30. Data from time test rheological experiments. Left – 50 mm parallel plate. Right – 20 mm parallel plate.

The total injection volume was adjusted to 1.5 mL to account for the geometry diameter. The concentrations and volumes handled were adjusted accordingly to keep the acrylate and thiol content consistent to allow direct comparison across experimental data sets with different materials conducted at the same concentrations. Tables 3.16 and 3.17 show the respective solid content for the experiments conducted.

Table 3.16. Tabulated view of volumes handled for rheological experiments using acrylate-modified alginate and QT crosslinker.

DoS% denotation	Acr-Alg conc. (% w/v)	Acr-Alg volume (mL)	QT conc. (% w/v)	QT volume (mL)	Solid content (mg)
High	5.8	1.4	10	0.1	81.2
Medium	2.8	1.45	10	0.05	40.6
Low	1.4	1.48	10	0.03	20.5

Table 3.17. Tabulated view of volumes handled for rheological experiments using acrylate-modified alginate and thiolate-modified alginate.

DoS% denotation	Acr-Alg conc. (% w/v)	Acr-Alg volume (mL)	Thio-Alg conc. (%) w/v)	Thio-Alg volume (mL)	Solid content (mg)
High	5.8	0.75	5.03	0.75	81.2
Medium	2.8	0.75	2.61	0.75	40.6
Low	1.4	0.75	1.34	0.75	20.5

The alginate solution concentration and its degree of substitution played a significant role in the stiffness of the gel, where a combination of high DoS% and high alginate solution concentration produced hydrogels with higher storage moduli values (Figures 3.31 and 3.32). It was observed that alginates with fewer acrylate or thiolate groups were lower in viscosity compared to their highly substituted counterparts when dissolved in solution. The same phenomenon was observed for alginates with High-G and High-M alginate classifications.

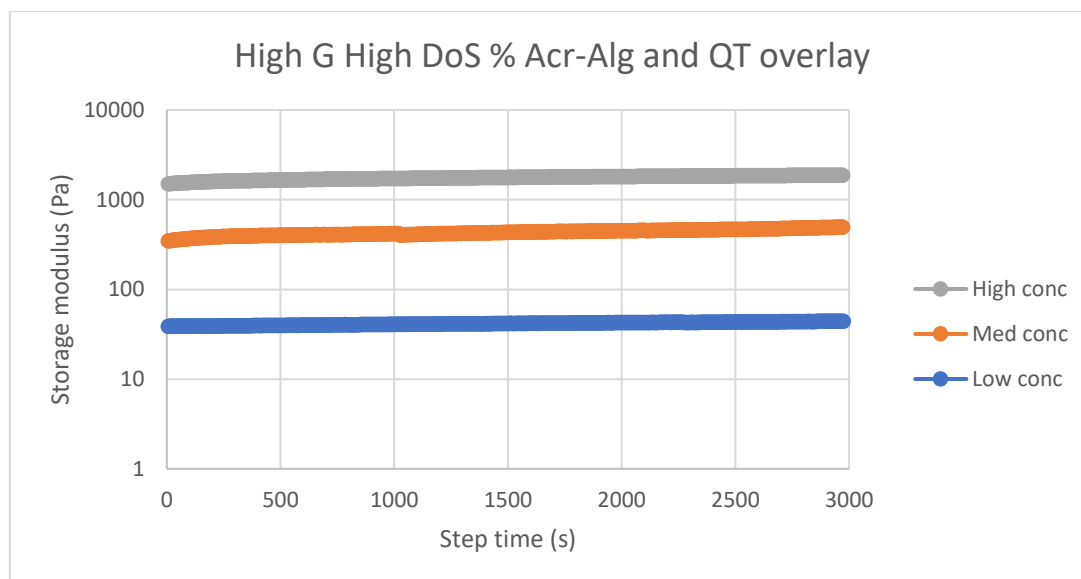


Figure 3.31. Overlay of storage modulus values obtained from rheological experiment. Alginate samples were High-G and all exhibited DoS% between 25-30 % with varying concentration in solution. Loss moduli and phase angle values omitted for simplicity.

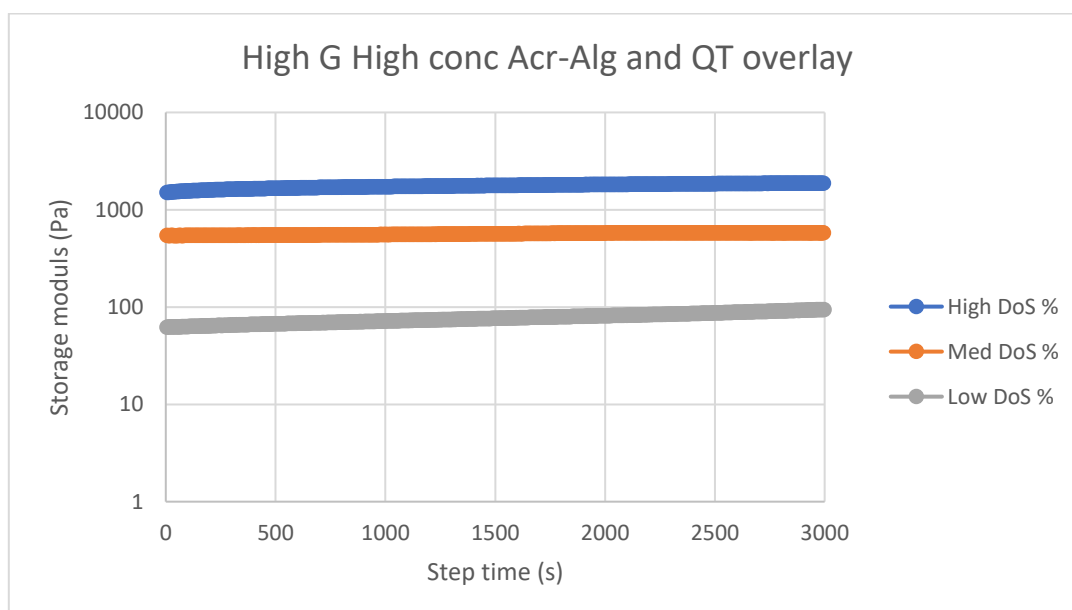


Figure 3.32. Overlay of storage modulus values obtained from rheological experiment. Alginate samples were High-G, dissolved at 5.8 % w/v and exhibited varying DoS%. Loss moduli and phase angle values omitted for simplicity.

It was discovered that rheological experiments which used alginate solutions dissolved at lower concentrations was too low in viscosity for the geometry used.

(Figures 3.33 and 3.34) This hypothesis was strengthened by sampling negative or fluctuating data points and absence of data points between $T = 1000$ and 12000 s, indicating a loss of contact between the Peltier plate and sample. The fluctuations of recorded phase angle values indicated a loss in traction between the sample and geometry with every oscillation. It was hypothesised that the alginate solution was displaced by and moved with the geometry, but structurally recovered due to its fluid behaviour which then caused the body of solution to displace in position.

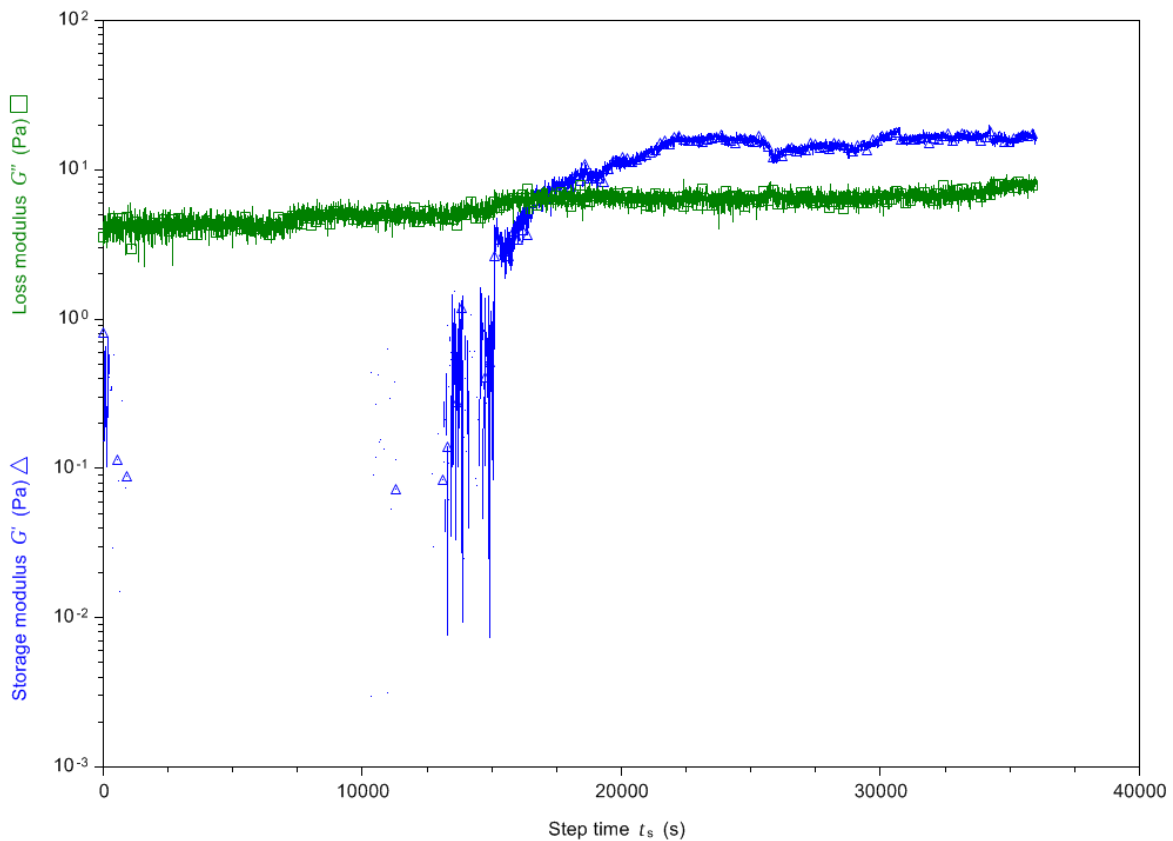


Figure 3.33. Rheological data from oscillatory time test on a High-M alginate sample, low DoS%, dissolved at low concentration.

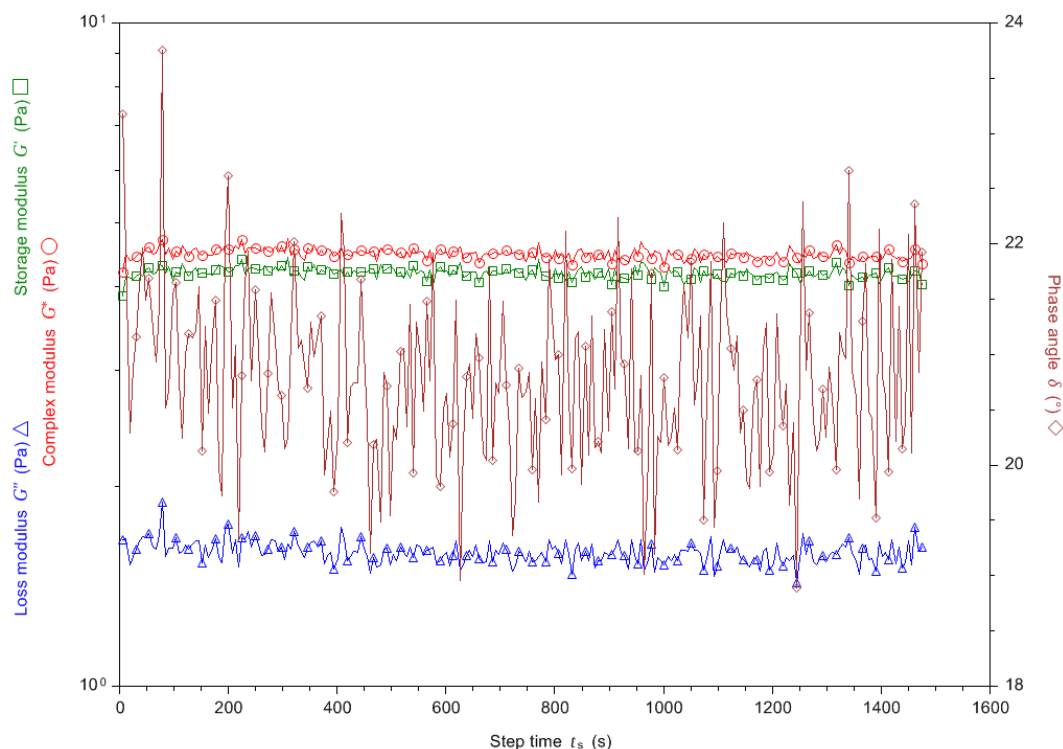


Figure 3.34. Rheological data from oscillatory time test on a High-G alginate sample, low DoS%, dissolved at medium concentration.

Formed alginate hydrogels saw storage moduli values in the region between 10^2 and 10^3 Pa and was classed as a soft viscoelastic solid.¹⁵⁷ Despite the low integral mechanical strength, this was to be expected for gels formed via Michael-type addition

Preliminary creep tests were performed on formed gels to establish the material's linear viscoelastic region (LVE region), to investigate the maximum shear strain the hydrogel can withstand without breaking, and study the hydrogel's ability to structurally recover over time between shear cycles. Creep test data shows the material experienced shear thinning, as indicated by the convergence of the loss and storage moduli values, as the structure experienced increased shear strain but was able to structurally recover consistently with negligible difference in rheological behaviour in subsequential creep test cycles. The upper limit at which the creep test was conducted takes into account the maximum strain the material would experience during use (Figure 3.35).¹³⁴

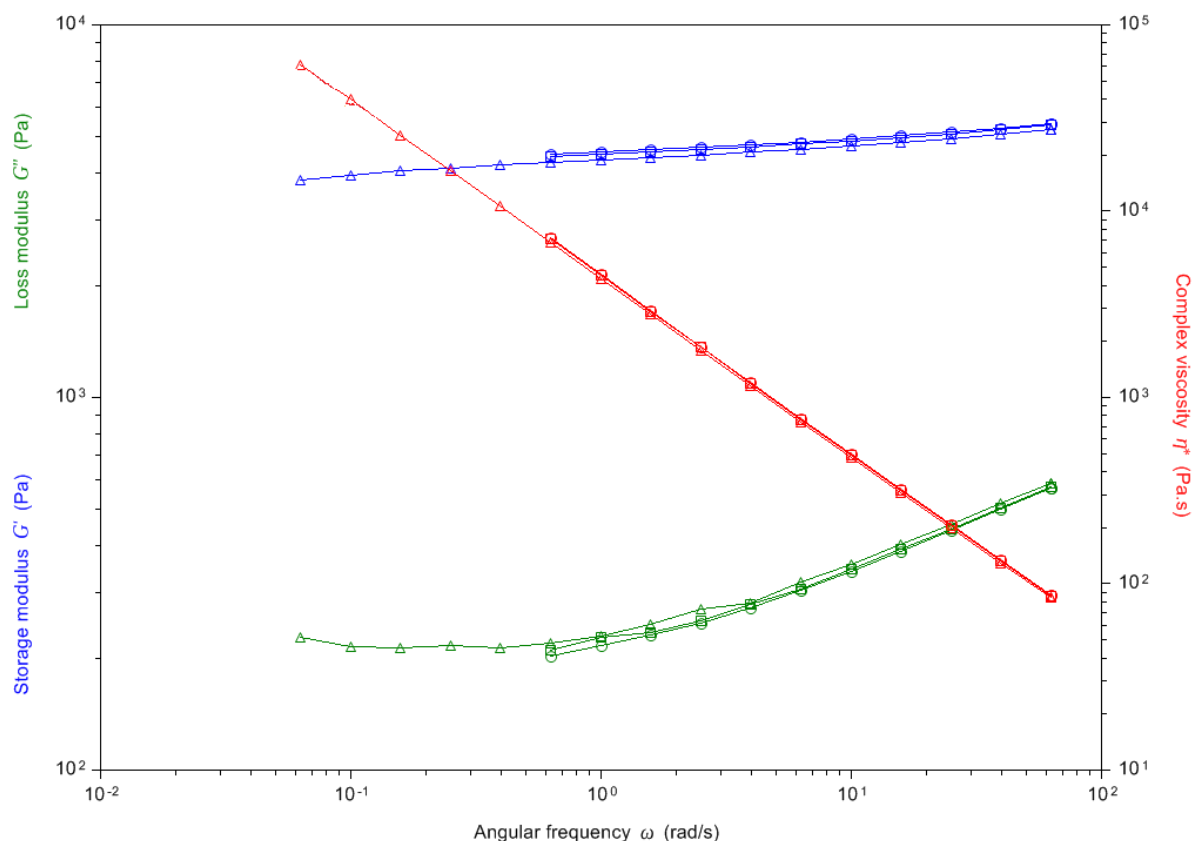


Figure 3.35. Creep test data of formed alginate gel.

3.5.3.2 Microscopy tests

Scanning electron microscopy (SEM) allows better visualisation of materials, both before and after gelation to better understand its surface morphology and porosity. Digital confocal microscopy was used with wet samples as Environmental SEM (ESEM) was unable to be performed.

Distinct alginic strand fibres can be seen in SEM images of both the acrylate and thiolated alginates before taken for gelation (Figure 3.36). This visualisation suggests that these strands function as channels in the polymeric network during water uptake and facilitates moisture retention. Thiolated alginate's more amorphous structure can be attributed to its drying process.

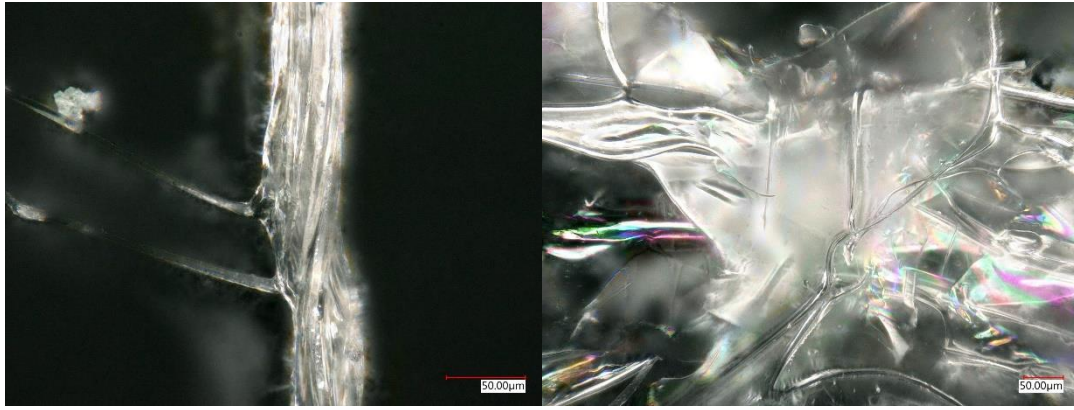


Figure 3.36. SEM images of acrylated (left) and thiolated (right) alginate.

These alginate strands were no longer visible upon gelation. Confocal microscopy images suggest the alginic strands were hydrated and consumed to form gel but poor resolution of the microscopic imaging due to the testing conditions may prevent stray alginic strands from being visualised. (Figure 3.37)

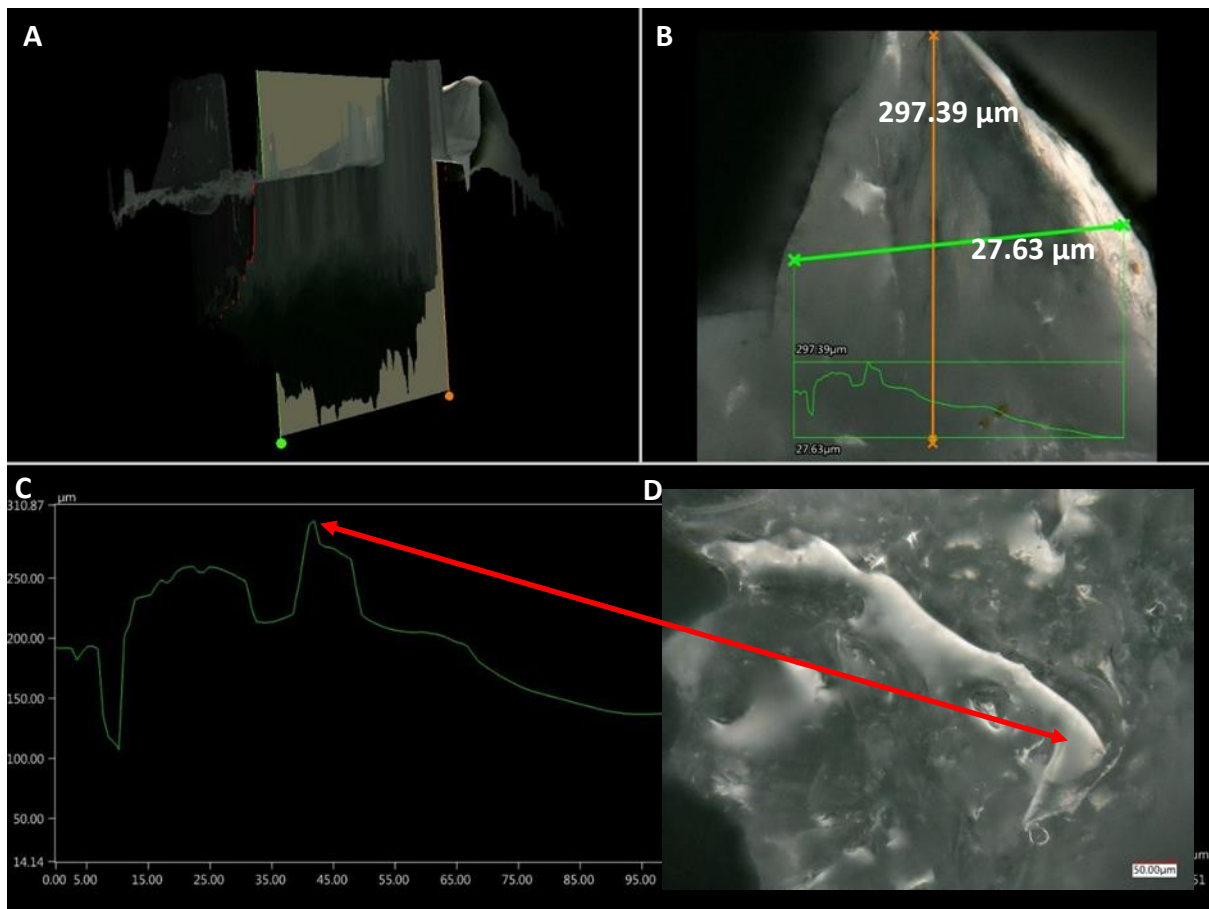


Figure 3.37. Confocal image of alginate hydrogel. A: Focal plane image of hydrogel. B: Dimension measurement from its highest point. C: Visualisation of the cross section. D: Microscopic image.

Microscopic imaging showed that the gel's surface morphology was porous and concave in certain areas, likely to be as a result of handling. It was hypothesised that with prolonged gelation the covalently crosslinked hydrogel would stiffen and the risk of structural deformation would diminish.

Dome droplets of QT solution were seen embedded within the gel in images of gels crosslinked with QT. This suggested that the gelation proceeds at a slower but constant rate with some QT still unspent. (Figure 3.38)



Figure 3.38. Microscopic image of an alginate gel. Droplets of QT crosslinker can be seen embedded under the gel surface.

3.5.4 Conclusion

Gelation of synthesised alginates was achieved by ionotropic, covalent and photo-crosslinking. The rate of gelation for ionotropic processes occurs instantaneously despite lower concentrations were used and was very difficult to control.

Photogelation saw gels form very consistently both in time taken and stiffness. However, prolonged exposure to UV- β light raised concerns for adverse health effects. Crosslinking via Michael-type addition reactions produced mixed results. The classification, DoS% and solution concentration all had a significant impact on the gelation rate and gel properties.

The gelation times determined from laboratory and *in-situ* rheological testing were concordant. However, the viscosity and dehydration of materials during testing posed a big obstacle to overcome as both induces a sizeable error margin.

Time test on alginate hydrogels showed good structural recovery and resistance to breakage under shear stress but can undergo shear thinning at higher frequencies. Scanning electron microscopy showed the alginic network consisting of channels made of polymeric fibres, which saw the fibres hydrate to form a gel network. Some QT-crosslinked hydrogels saw traces of unspent crosslinker embedded under the surface of the gel.

High-resolution microscopic images of prepared hydrogels using SEM were unobtained due to its moisture content, which resulted in the use of confocal microscopy as a substitute method. ESEM tests should be performed for future microscopic work to improve imaging quality.

Future work on this work should include refining the covalent crosslinking step to produce bulk gels more consistently using thiolated alginate. Considering the end application, the gelation model should also be revisited to incorporate more rapid gelation mechanisms to reflect the clinical need. Hydrogels with hybrid crosslinks may be studied to produce a hard gel exterior rapidly which allows the Michael-type addition process to occur over time. Further rheological tests should be conducted with a sandblasted plate with smaller geometry diameter to increase grip and contact with the gel solution whilst minimising shear stress on the solution surface. Formed gels should be taken for tack test and microbial tests to establish its resistance to tearing and resistance to biofilm formation.

Chapter 4: Conclusions, project direction and future work

4.1 Introduction

Presented in this chapter are general conclusions and a summary of the research work conducted as part of this project. Herein, the author's concluding remarks and insights for future research direction for successive researchers of this project area are included.

4.2 General discussion

In this project, novel alginate hydrogels were successfully prepared and its gelation timepoint monitored using *in-situ* analytical techniques. The acrylation precursor was synthesised with high degrees of purity and good yield. Overall, this material possesses great potential as a wound therapeutic given its natural properties. Its chemical versatility and the resultant material's ability to become a drug delivery vehicle further boosts its promise in the treatment of chronic wounds.

The usage of glycidyl acrylate as the acrylation agent and the gelation via Michael-type addition for diabetic foot healing applications marks the material's novelty. The prepared hydrogels expressed high moisture retention capabilities, low cytotoxicity, ability to be loaded with a drug and its biocompatibility makes the hydrogel a good potential candidate as a wound therapeutic. However, there were areas in this project which require further refinement to improve the gelation efficiency in addition to the gel's mechanical and tensile properties.

It is with regret to report that full characterisations of the synthesised materials were not performed due to technical difficulties faced during the research period. Future work should endeavour to fully characterise prepared materials to allow better scientific conclusions to be drawn.

4.3 Future work

In this research, two samples of sodium alginate used which are rich in mannuronate and guluronate residues, respectively. A large difference in the alginate specimens' molecular weight (Mp 106 kDa and 418kDa, respectively) translated to a drastic difference in its chemical and mechanical behaviour. Future research work should aim to employ other specifications of sodium alginate with similar molecular weight distribution.

The acrylation and thiolation of sodium alginate produced yields which were unexpected and less than desirable for large-scale synthesis given the magnitude of unreacted materials remaining at the end of the reaction. It would be possible to perform a life cycle analysis on the synthesis steps and gauge whether if it would be more cost-effective and energy-efficient to include a step to chemically salvage unreacted starting materials. To make the modification processes attractive and viable for industrial-scale synthesis there would need to be more work dedicated to altering the synthesis procedures to improve the substitutive yield of reactions performed. Another aspect that needs further investigation is the method for alginate drying used. A potential future project is to investigate the effects different drying methods has on alginate morphology and its efficacy when taken for gelation tests.

A major hurdle faced in the synthesis part of this research period is the stability of the thiolate functional group. A large proportion of synthesised material auto polymerised in solution during synthesis which contributes to the low degree of thiolation yielded. This problem would need to be resolved to further advance the project in the direction originally intended. It is extremely difficult to prevent thiol degradation during the dialysis step as the crude product is repeatedly exposed to air for prolonged periods but yet it is not possible to fully forego this step without a heavy compromise in the material's purity. The author therefore suggests the inclusion of a disulphide reduction step prior to gelation to regenerate thiol functional groups needed for crosslink.

The results herein suggest that the acrylation reagent should be substituted for one with improved stability and less susceptible to autopolymerisation, such as poly(ethylene glycol) diacrylate (PEGDA). The diacrylate-functionality allows better chain elongation and PEG offers better stability in storage and especially during

gelation, where the material may be exposed to stimuli considering the end-application. PEGMEMA also expresses lower cytotoxicity compared to glycidyl acrylate, further increasing its attractiveness as a potential substitute.

Analytical characterisation for synthesised materials was performed in partial due to technical faults. As a result, many of the result conclusions were drawn based on empirical evidence and estimations based on early research work or work presented by other researchers. NMR analyses of acrylated alginate should be performed at higher temperature to improve visibility of the alginic backbone region, and thiolated alginate NMR experiments should be performed with increased scans to increase overall resolution. In addition, GPC and IR experiments need to be performed on synthesised hydrogel precursors to prove the success of substitution, and to aid the determination of degree of substitution.

The gelation timepoint was successfully mapped via *in-situ* rheological experiments, and the hydrogels' resistance to shear forces and its ability to structurally recover were monitored. Future work should include comprehensive rheological test to establish the hydrogels' full rheological profile. The hydrogels would undergo tack testing to simulate dressing stretching and removal, as well as determine the elastic tensile strength of the material. Scanning electron microscopy of alginate hydrogels could not be performed with good resolution as the model could not support ESEM functionality, which resulted in the use of confocal microscopy as a compromise. Lastly, microbial suite experimentation of hydrogels may be performed to test for its bioavailability and cytotoxicity over the concerns of the toxicological risks of certain reagents used in this work.

Although the Michael-type addition gelation of alginate was achieved, the time taken for gelation (ca. 60 minutes) was unrealistic when considering real-world applications. Although the material would undergo crosslink over time to form a more robust gel there was no scientific data to determine the terminal gel stiffness. Attempts at rheological mapping often resulted in sample dehydration. The author suggests a revisit to the original project aims to incorporate other crosslink pathways to prepare hybrid-crosslinked hydrogels to produce soft capped hydrogels in a shorter timeframe which translates to quicker visits at the dressing clinics and improving patients' mobility post dressing application.

- 1 I. D. F. D. Atlas, *International Diabetes Federation*, 2019, vol. 266.
- 2 World Health Organization, *Int. Diabetes Fed.*, 2021, 6.
- 3 L. Guariguata, D. R. Whiting, I. Hambleton, J. Beagley, U. Linnenkamp and J. E. Shaw, *Diabetes Res. Clin. Pract.*, 2014, **103**, 137–149.
- 4 K. Ogurtsova, J. D. da Rocha Fernandes, Y. Huang, U. Linnenkamp, L. Guariguata, N. H. Cho, D. Cavan, J. E. Shaw and L. E. Makaroff, *Diabetes Res. Clin. Pract.*, 2017, **128**, 40–50.
- 5 M. S. Udler, J. Kim, M. von Grotthuss, S. Bonàs-Guarch, J. B. Cole, J. Chiou, C. D. Anderson, M. Boehnke, M. Laakso, G. Atzmon, B. Glaser, J. M. Mercader, K. Gaulton, J. Flannick, G. Getz and J. C. Florez, *PLOS Med.*, 2018, **15**, e1002654.
- 6 World Health Organization, *Classification of diabetes mellitus*, 2019, vol. 21.
- 7 V. Vijayakumar, S. K. Samal, S. Mohanty and S. K. Nayak, *Int. J. Biol. Macromol.*, 2019, **122**, 137–148.
- 8 B. B. Seo, M. R. Park and S. C. Song, *ACS Appl. Mater. Interfaces*, 2019, **11**, 15201–15211.
- 9 A. D. Association, *Classification and Diagnosis of Diabetes : Standards of Medical Care in Diabetes - 2018*, 2018, vol. 41.
- 10 H. Wu, S. Yang, Z. Huang, J. He and X. Wang, *Informatics Med. Unlocked*, 2018, **10**, 100–107.
- 11 W. Xu, C. Qiu, M. Gatz, N. L. Pedersen, B. Johansson and L. Fratiglioni, *Diabetes*, 2009, **58**, 71–77.
- 12 R. M. Anjana, V. Baskar, A. Thakarakkattil, N. Nair, S. Jebarani, M. K. Siddiqui, R. Pradeepa, R. Unnikrishnan, C. Palmer, E. Pearson and V. Mohan, *BMJ Open Diabetes Res., Care*, 2020, **8**, e001506.
- 13 C. Sims-robinson, B. Kim, A. Rosko and E. L. Feldman, *Nat. Rev. Neurol.*, 2010, **6**, 551–559.
- 14 A. Lapolla and M. G. Dalfrà, *Front. Diabetes*, 2015, **24**, 11–22.

- 15 C. Kim, K. M. Newton and R. H. Knopp, *Diabetes Care*, 2002, **25**, 1862–1868.
- 16 N. G. Clark, K. M. Fox and S. Grandy, *Diabetes Care*, 2007, **30**, 2868–2873.
- 17 A. E. Kitabchi and B. M. Wall, *Med. Clin. North Am.*, 1995, **79**, 9–37.
- 18 D. M. Maahs, J. M. Hermann, N. Holman, N. C. Foster, T. M. Kapellen, J. Allgrove, D. A. Schatz, S. E. Hofer, F. Campbell, C. Steigleder-Schweiger, R. W. Beck, J. T. Warner and R. W. Holl, *Diabetes Care*, 2015, **38**, 1876–1882.
- 19 J. J. Duby, R. K. Campbell, S. M. Setter, J. R. White and K. A. Rasmussen, *Am. J. Heal. Pharm.*, 2004, **61**, 160–173.
- 20 K. Juster-Switlyk and A. G. Smith, *F1000Research*, 2016, **5**, 738.
- 21 A. T. Hirsch, M. H. Criqui, D. Treat-jacobson, J. G. Regensteiner, M. A. Creager, J. W. Olin, S. H. Krook, M. E. Walsh, M. M. Mcdermott and W. R. Hiatt, *J. Am. Med. Assoc.*, 2001, **286**, 1317–1324.
- 22 M. H. Criqui and V. Aboyans, *Circ. Res.*, 2015, **116**, 1509–1526.
- 23 S. A. Shah, M. Sohail, M. Usman, S. Khan, M. De Matas and V. Sikstone, *Int. J. Biol. Macromol.*, 2019, **139**, 975–993.
- 24 P. Chadwick, M. Edmonds, J. MsCardle, D. Armstrong, J. Apelqvist, M. Botros, G. Clerici, J. Cundell, S. Ehrler, M. Hummel, B. A. Lipsky, J. L. L. Martinez, R. Thomas and S. Tulley, *Wounds Int.*, 2014, **5**, 27.
- 25 L. A. Lavery, D. G. Armstrong and L. B. Harkless, *J. Foot Ankle Surg.*, 1996, **35**, 528–531.
- 26 B. A. Lipsky, A. R. Berendt, H. G. Deery, J. M. Embil, W. S. Joseph, A. W. Karchmer, J. L. Lefrock, D. P. Lew, J. T. Mader, C. Norden and J. S. Tan, *Guidel. Diabet. Foot Infect.*, 2004, **39**, 885–910.
- 27 T. B. Santema, E. A. Lenselink, R. Balm and D. T. Ubbink, *Int. Wound J.*, 2016, **13**, 1137–1141.
- 28 F. W. Wagner, *Foot Ankle Int.*, 1981, **2**, 64–122.
- 29 A. Ndip and E. B. Jude, *Int. J. Low. Extrem. Wounds*, 2009, **8**, 82–84.
- 30 D. M. Mehraj, *Int. J. Orthop. Sci.*, 2018, **4**, 933–935.

- 31 M. E. Edmonds and A. V. M. Foster, *Br. Med. J.*, 2006, **332**, 407–410.
- 32 S. Young, *Diabet. Foot J.*, 2014, **17**, 29–33.
- 33 R. R. Yotsu, N. M. Pham, M. Oe, T. Nagase, H. Sanada, H. Hara, S. Fukuda, J. Fujitani, R. Yamamoto-Honda, H. Kajio, M. Noda and T. Tamaki, *J. Diabetes Complications*, 2014, **28**, 528–535.
- 34 J. S. Tan, *Baillière's Clin. Rheumatol.*, 1999, **13**, 149–161.
- 35 L. L. Humphrey, P. J. Palumbo, M. A. Butters, J. W. Hallett, C. Chu, W. M. O. Fallon and D. J. Ballard, *Arch. Intern. Med.*, 1994, **154**, 885–892.
- 36 A. J. Rosenbaum, S. Banerjee, K. M. Rezak and R. L. Uhl, *J. Am. Acad. Orthop. Surg.*, 2018, **26**, 833–843.
- 37 M. S. Granick, A. Sood and N. L. Tomaselli, *Adv. Wound Care*, 2014, **3**, 511–529.
- 38 S. Gist, I. Tio-Matos, S. Falzgraf, S. Cameron and M. Beebe, *Clin. Interv. Aging*, 2009, **4**, 269–287.
- 39 C. Ligresti and F. Bo, *Int. Wound J.*, 2007, **4**, 21–29.
- 40 D. J. Leaper, G. Schultz, K. Carville, J. Fletcher, T. Swanson and R. Drake, *Int. Wound J.*, 2012, **9**, 1–19.
- 41 G. Guarro, F. Cozzani, M. Rossini, E. Bonati and P. Del Rio, *Acta Biomed.*, 2021, **92**, e2021226.
- 42 G. S. Schultz, D. J. Barillo, D. W. Mazingo, G. A. Chin, E. Ayello, C. Dowsett, V. Falanga, K. Harding, M. Romanelli, G. Sibbald, M. Stacey, L. Teot and W. Vanscheidt, *Int. Wound J.*, 2004, **1**, 19–32.
- 43 J. R. Hilton, D. T. Williams, B. Beuker, D. R. Miller and K. G. Harding, *Clin. Infect. Dis.*, 2004, **39**, S100-3.
- 44 L. I. F. Moura, A. M. A. Dias, E. Carvalho and H. C. de Sousa, *Acta Biomater.*, 2013, **9**, 7093–7114.
- 45 A. Toulon, L. Breton, K. R. Taylor, M. Tenenhaus, D. Bhavsar, C. Lanigan, R. Rudolph, J. Jameson and W. L. Havran, *J. Exp. Med.*, 2009, **206**, 743–750.

- 46 J. C. Dumville, M. O. Soares, S. O'Meara and N. Cullum, *Diabetologia*, 2012, **55**, 1902–1910.
- 47 S. Dhivya, V. V. Padma and E. Santhini, *Biomedicine*, 2015, **5**, 24–28.
- 48 M. A. Fonder, G. S. Lazarus, D. A. Cowan, B. Aronson-Cook, A. R. Kohli and A. J. Mamelak, *J. Am. Acad. Dermatol.*, 2008, **58**, 185–206.
- 49 A. Ghadban, L. Albertin, M. Rinaudo and A. Heyraud, *Biomacromolecules*, 2012, **13**, 3108–3119.
- 50 J. C. Dumville, S. O'Meara, S. Deshpande and K. Speak, *Cochrane Database Syst. Rev.*, 2013, **2017**, 1–54.
- 51 J. F. Guest, G. W. Fuller and P. Vowden, *Int. Wound J.*, 2018, **15**, 43–52.
- 52 D. Upton, K. Solowiej, C. Hender and K. Y. Woo, *J. Wound Care*, 2012, **21**, 53–61.
- 53 V. Basic-Kes, I. Zavoreo, K. Rotim, N. Bornstein, T. Rundek and V. Demarin, *Acta Clin Croat*, 2011, **50**, 289–302.
- 54 R. Gobi, P. Ravichandiran, R. S. Babu and D. J. Yoo, *Polymers*, 2021, **13**, 1962.
- 55 Z. Hussain, H. E. Thu, A. N. Shuid, H. Katas and F. Hussain, *Curr. Drug Targets*, 2017, **19**, 527–550.
- 56 M. Mir, M. Najabat Ali, A. Barakullah, A. Gulzar, M. Arshad, S. Fatima and M. Asad, *Prog. Biomater.*, 2018, **7**, 1–21.
- 57 J. M. Anderson, A. Rodriguez and D. T. Chang, *Semin. Immunol.*, 2009, **20**, 86–100.
- 58 P. B. Malafaya, G. A. Silva and R. L. Reis, *Adv. Drug Deliv. Rev.*, 2007, **59**, 207–233.
- 59 I. Kim, S. Seo, H. Moon, M. Yoo, I. Park, B. Kim and C. Cho, *Biotechnol. Adv.*, 2008, **26**, 1–21.
- 60 A. Sannino, C. Demitri and M. Madaghiele, *Materials*, 2009, 353–373.
- 61 J. F. Mano, G. A. Silva, H. S. Azevedo, P. B. Malafaya, R. A. Sousa, S. S.

- Silva, L. F. Boesel, J. M. Oliveira, T. C. Santos, A. P. Marques, N. M. Neves and R. I. Reis, *J. R. Soc. interface*, 2007, **4**, 999–1030.
- 62 P. Y. Lee, E. Cobain, J. Huard and L. Huang, *Mol. Ther.*, 2007, **15**, 1189–1194.
- 63 S. Liu, T. Jiang, R. Guo, C. Li, C. Lu, G. Yang, J. Nie, F. Wang, X. Yang and Z. Chen, *ACS Appl. Bio Mater.*, 2021, **4**, 2769–2780.
- 64 J. O. Kim, J. Y. Choi, J. K. Park, J. H. Kim, S. G. Jin, S. W. Chang, D. X. Li, M.-R. Hwang, J. S. Woo, J.-A. Kim, W. S. Lyoo, C. S. Yong and H.-G. Choi, *Biol. Pharm. Bull.*, 2008, **31**, 2277–2282.
- 65 E. J. Paul and B. Padmapriya, *Mater. Today Proc.*, 2019, **23**, 91–99.
- 66 B. V. Slaughter, S. S. Khurshid, O. Z. Fisher, A. Khademhosseini and N. A. Peppas, *Adv. Mater.*, 2009, **21**, 3307–3329.
- 67 S. A. Sell, P. S. Wolfe, K. Garg, J. M. McCool, I. A. Rodriguez and G. L. Bowlin, *Polymers*, 2010, **2**, 522–553.
- 68 V. Arul, R. Kartha and R. Jayakumar, *Life Sci.*, 2007, **80**, 275–284.
- 69 N. H. Service, Drug Tariff 2015, <https://www.drugtariff.nhsbsa.nhs.uk>, (accessed 21 October 2021).
- 70 C. Valenta and B. G. Auner, *Eur. J. Pharm. Biopharm.*, 2004, **58**, 279–289.
- 71 I. Manjubala, *ACS Omega*, 2018, **3**, 12622–12632.
- 72 L. Vinklárková, R. Masteiková, G. Foltýnová, J. Muselík, D. Vetchý, S. Pavloková and J. Bernatoniien, *J. Appl. Med.*, 2017, **15**, 313–320.
- 73 V. Kanikireddy, K. Varaprasad, T. Jayaramudu, C. Karthikeyan and R. Sadiku, *Int. J. Biol. Macromol.*, 2020, **164**, 963–975.
- 74 B. H. A. Rehm, *Alginates: Biology and Applications*, Springer, Berlin, 1st edn., 2009.
- 75 Y. Zhao, Z. Li, Q. Li, L. Yang, H. Liu, R. Yan, L. Xiao, H. Liu, J. Wang, B. Yang and Q. Lin, *Macromol. Rapid Commun.*, 2020, **41**, e2000441.
- 76 G. T. Grant, E. R. Morris and D. A. Rees, *FEBS Lett.*, 1973, **32**, 195–198.

- 77 T. Andersen, B. L. Strand, K. Formo, E. Alsberg and B. E. Christensen, *Carbohydr. Chem.*, 2021, **37**, 227–258.
- 78 T. T. Khong, O. A. Aarstad, G. Skjåk-Bræk, K. I. Draget and K. M. Vårum, *Biomacromolecules*, 2013, **14**, 2765–2771.
- 79 F. A. Johnson, D. Q. M. Craig and A. D. Mercer, *J. Pharm. Pharmacol.*, 1997, **49**, 639–643.
- 80 H. Grasdalen, *Carbohydr. Res.*, 1983, **118**, 255–260.
- 81 A. Penman and G. R. Sanderson, *Carbohydr. Res.*, 1972, **25**, 273–282.
- 82 H. Grasdalen, B. Larsen and O. Smidsrod, *Carbohydr. Res.*, 1979, **68**, 23–31.
- 83 E. M. Vilén, M. Klinger and C. Sandström, *Magn. Reson. Chem.*, 2011, **49**, 584–591.
- 84 T. Salomonsen, H. M. Jensen, D. Stenbæk and S. B. Engelsen, *Carbohydr. Polym.*, 2008, **72**, 730–739.
- 85 B. Renoust, G. Melançon and M.-L. Viaud, in *Social Network Analysis - Community Detection and Evolution*, eds. R. Missaoui and I. Sarr, Springer International Publishing, Cham, 2014, pp. 89–117.
- 86 S. G. Keswani, A. B. Katz, F. Lim and P. Zoltick, *Wound Repair Regen.*, 2004, **12**, 497–504.
- 87 A. T. Badillo, S. Chung, L. Zhang, P. Zoltick and K. W. Liechty, *J. Surg. Res.*, 2007, **143**, 35–42.
- 88 A. Ahmed, G. Getti and J. Boateng, *Drug Deliv. Transl. Res.*, 2018, **8**, 1751–1768.
- 89 D. R. Zhou, H. Y. Deng, L. L. Pu, S. L. Lin, R. Gou and F. L. Wang, *Medicine*, 2021, **100**, e23984.
- 90 A. Ahmed, G. Getti and J. Boateng, *Int. J. Pharm.*, 2021, **606**, 120903.
- 91 A. M. Stephen, G. O. Phillips and P. A. Williams, *Food Polysaccharides and Their Applications: Second Edition*, 2016.
- 92 A. Haug and B. Larsen, *Acta Chem. Scand.*, 1963, **17**, 1653–1662.

- 93 E. M. Ahmed, *J. Adv. Res.*, 2015, **6**, 105–121.
- 94 V. Javvaji, A. G. Baradwaj, G. F. Payne and S. R. Raghavan, *Langmuir*, 2011, **27**, 12591–12596.
- 95 K. Maji, S. Dasgupta, R. Bhaskar and M. K. Gupta, *Biomed. Mater.*, 2020, **15**, 055019.
- 96 D. Mondragon, MPhil thesis, Bangor University, 2019.
- 97 J. Guo, H. Zhang, C. Li, L. Zang and J. Luo, *J. Nanomater.*, 2011, **2012**, 1–8.
- 98 F. Araiza-Verduzco, E. Rodríguez-Velázquez, H. Cruz, I. A. Rivero, D. R. Acosta-Martínez, G. Pina-Luis and M. Alatorre-Meda, *Materials*, 2020, **13**, 1–14.
- 99 P. Matricardi, M. Pontoriero, T. Coviello, M. A. Casadei and F. Alhaique, *Biomacromolecules*, 2008, **9**, 2014–2020.
- 100 I. Rubio-Elizalde, J. Bernáldez-Sarabia, A. Moreno-Ulloa, C. Vilanova, P. Juárez, A. Licea-Navarro and A. B. Castro-Ceseña, *Carbohydr. Polym.*, 2019, **206**, 455–467.
- 101 X. Wang, T. Hao, J. Qu, C. Wang and H. Chen, *J. Nanomater.*, 2015, **2015**, 1–8.
- 102 A. Pourjavadi, H. Ghasemzadeh and R. Soleyman, *J. Appl. Polym. Sci.*, 2007, **105**, 2631–2639.
- 103 I. Popescu, M. Turtoi, D. M. Suflet, M. V. Dinu, R. N. Darie-Nita, M. Anghelache, M. Calin and M. Constantin, *Int. J. Biol. Macromol.*, 2021, **180**, 418–431.
- 104 S. Summonte, G. F. Racaniello, A. Lopedota, N. Denora and A. Bernkop-Schnürch, *J. Control. Release*, 2021, **330**, 470–482.
- 105 G. Xu, L. Cheng, Q. Zhang, Y. Sun, C. Chen, H. Xu, Y. Chai and M. Lang, *J. Biomater. Appl.*, 2016, **31**, 721–729.
- 106 H. W. Ooi, C. Mota, A. Tessa Ten Cate, A. Calore, L. Moroni and M. B. Baker, *Biomacromolecules*, 2018, **19**, 3390–3400.

- 107 K. Veerubhotla, Y. Lee and C. H. Lee, *Pharm. Res.*, 2021, **38**, 885–900.
- 108 Y. Deng, A. Shavandi, O. V. Okoro and L. Nie, *Carbohydr. Polym.*, 2021, **270**, 118360.
- 109 H. Zhang, A. Qadeer and W. Chen, *Biomacromolecules*, 2011, **12**, 1428–1437.
- 110 European Chemicals Agency, European Chemicals Agency (ECHA) database, <https://echa.europa.eu/information-on-chemicals/cl-inventory-database/-/discli/details/49316>, (accessed 28 October 2021).
- 111 A. Tochwin, PhD thesis, Bangor University, 2016.
- 112 N. Ohura, S. Ichioka, T. Nakatsuka and M. Shibata, *J. Wound Care*, 2005, **14**, 401–404.
- 113 I. I. Rabi, J. R. Zacharias, S. Millman and P. Kusch, *Phys. Rev.*, 1938, **53**, 318.
- 114 H. Friebolin and J. K. Beconsall, *Basic one-and two-dimensional NMR spectroscopy*, Wiley-VCH, Weinheim, 5th edn., 2005.
- 115 R. K. Harris, E. D. Becker, S. M. Carbral de Menezes, R. Goodfellow and P. Granger, *Pure Appl. Chem.*, 2001, **73**, 1795–1818.
- 116 D. Gruyter, *Pure Appl. Chem.*, 2008, **29**, 625–628.
- 117 S. K. Bharti and R. Roy, *Trends Anal. Chem.*, 2012, **35**, 5–26.
- 118 M. Davidovich-Pinhas and H. Bianco-Peled, *Acta Biomater.*, 2011, **7**, 625–633.
- 119 H. Yao, J. Wang, J. Yin, S. Nie and M. Xie, *Food Res. Int.*, 2021, **143**, 110290.
- 120 V. Balevicius and K. Aidas, *Appl. Magn. Reson.*, 2007, **32**, 363–376.
- 121 H. E. Gottlieb, V. Kotlyar and A. Nudelman, *J. Org. Chem.*, 1997, **62**, 7512–7515.
- 122 N. M. Hasim, MSc report, Bangor University, 2016.
- 123 D. A. Skoog, F. J. Holler and S. R. Crouch, *Principles of Instrumental Analysis*, Thomson Brooks/Cole, Belmont, 7th edn., 2018.
- 124 D. F. Swinehart, *J. Chem. Educ.*, 1962, **39**, 333–335.
- 125 J. C. Moore, *J. Polym. Sci. Part A Gen. Pap.*, 1964, **2**, 835–843.

- 126 K. N. Ramsackal, K. Ward and J. V Smith, in *Caribbean Science and Innovation Meeting 2019*, eds. K. N. Ramsackal, K. Ward and J. V Smith, Caribbean Science and Innovation Meeting 2019, Le Gosier, 2019, pp. 1–4.
- 127 T. G. Scholte, N. L. J. Meijerink, H. M. Schoffeleers and A. M. G. Brands, *J. Appl.*, 1984, **29**, 3763–3782.
- 128 A. A. Askadskii, *Physical properties of Polymers - Prediction and Control*, Gordon and Breach, Moscow, 2nd edn., 1996.
- 129 L. H. Judovits, R. C. Bopp, U. Gaur and B. Wunderlich, *J. Polym. Sci.*, 1986, **24**, 2725–2741.
- 130 G. Gellerstedt, in *Methods in Lignin Chemistry*, eds. S. Y. Lin and C. W. Dence, Springer Berlin Heidelberg, Berlin, Heidelberg, 1992, pp. 487–497.
- 131 W. R. Schowalter, *Mechanics of non-Newtonian Fluids*, Pergamon Press, Oxford, 1st edn., 1978.
- 132 E. C. Bingham and L. Sarver, *J. Am. Chem. Soc.*, 1920, **42**, 2011–2022.
- 133 W. Malvern International, *A basic introduction into rheology*, 2016.
- 134 T. G. Mezger, *Applied rheology: With Joe Flow on Rheology Road*, Anton Paar GmbH, Graz, 8th edn., 2018.
- 135 A. Björn, P. Segura de La Monja, A. Karlsson, J. Ejlertsson and B. H. Svensson, in *Biogas*, ed. S. Kumar, InTech, Rijeka, 1st edn., 2012, pp. 64–76.
- 136 Basics of rheology, International Bureau of Weights and Measures., 2006, **1**, 180.
- 137 P. Lehericey, P. Snabre, A. Delots, N. Holten-andersen and T. Divoux, *J. Rheol.*, 2021, **65**, 427–436.
- 138 D. McMullan, *Scanning*, 1995, **17**, 175–185.
- 139 D. Semwogerere and E. R. Weeks, in *Encyclopedia of Biomaterials and Biomedical Engineering*, eds. G. Wnek and G. Bowlin, Taylor & Francis, Boca Raton, 2nd edn., 2005, pp. 1–10.
- 140 A. Nwaneshiudu, C. Kuschal, F. H. Sakamoto, R. R. Anderson, K.

- Schwarzenberger and R. C. Young, *J. Invest. Dermatol.*, 2012, **132**, 1–5.
- 141 Q. Zhang, A. Anastasaki, G. Z. Li, A. J. Haddleton, P. Wilson and D. M. Haddleton, *Polym. Chem.*, 2014, **5**, 3876–3883.
- 142 A. Bernkop-Schnürch, C. E. Kast and M. F. Richter, *J. Control. Release*, 2001, **71**, 277–285.
- 143 A. Tochwin, A. El-betany, H. Tai, K. Y. Chan, C. Blackburn and W. Wang, *Polymers*, 2017, **9**, 1–15.
- 144 G. L. Ellman, *Arch. Biochem. Biophys.*, 1959, **82**, 70–77.
- 145 G. F. Pauli, S. N. Chen, C. Simmler, D. C. Lankin, T. Gödecke, B. U. Jaki, J. B. Friesen, J. B. McAlpine and J. G. Napolitano, *J. Med. Chem.*, 2015, **58**, 9061.
- 146 E. J. Lee, H. J. Park, S. M. Kim and K. Y. Lee, *Macromol. Res.*, 2018, **26**, 322–331.
- 147 M. Gonzalez-perez, *Int. J. Sci. Adv. Technol.*, 2015, **5**, 1–5.
- 148 S. A. Bencherif, A. Srinivasan, F. Horkay, J. O. Hollinger, K. Matyjaszewski and N. R. Washburn, *Biomaterials*, 2008, **29**, 1739–1749.
- 149 Q. Zhang, A. Anastasaki, G.-Z. Li, A. J. Haddleton, P. Wilson and D. M. Haddleton, *Polym. Chem.*, 2014, **5**, 3876.
- 150 A. Tiwari, J. J. Grailer, S. Pilla, D. A. Steeber and S. Gong, *Acta Biomater.*, 2009, **5**, 3441–3452.
- 151 G. L. Ellman, *Arch. Biochem. Biophys.*, 1958, **74**, 443–450.
- 152 M. Lo Conte and K. S. Carroll, in *The chemistry of thiol oxidation and detection*, eds. U. Jakob and D. Reichmann, Springer, Dordrecht, 1st edn., 2013, pp. 1–51.
- 153 A. Emmakah, H. Arman, J. Bragg, T. Greene, M. Alvarez, P. Childress, W. Goebel, M. Kacena, C. Lin and T. Chu, *Biomed. Mater.*, 2017, **12**, 025011.
- 154 W. Konigsberg, *Methods Enzymol.*, 1972, **25**, 185–188.
- 155 L. J. Van Den Bos, J. Dinkelaar, H. S. Overkleeft and G. A. Van Der Marel, *J. Am. Chem. Soc.*, 2006, **128**, 13066–13067.

- 156 C. U. Nielsen, R. Andersen, B. Brodin, S. Frokjaer and B. Steffansen, *J. Control. Release*, 2001, **73**, 21–30.
- 157 D. T. N. Chen, Q. Wen and P. A. Janmey, *Annu. Rev. Condens. Matter Phys.*, 2010, **1**, 301–322.

Appendix

A.1 GPC data

Calibration Used: 5/9/2018 4:35:06 PM

Calibration Type: Narrow Standard Curve Fit Used: 1 K: 14.1000 Alpha: 0.7000

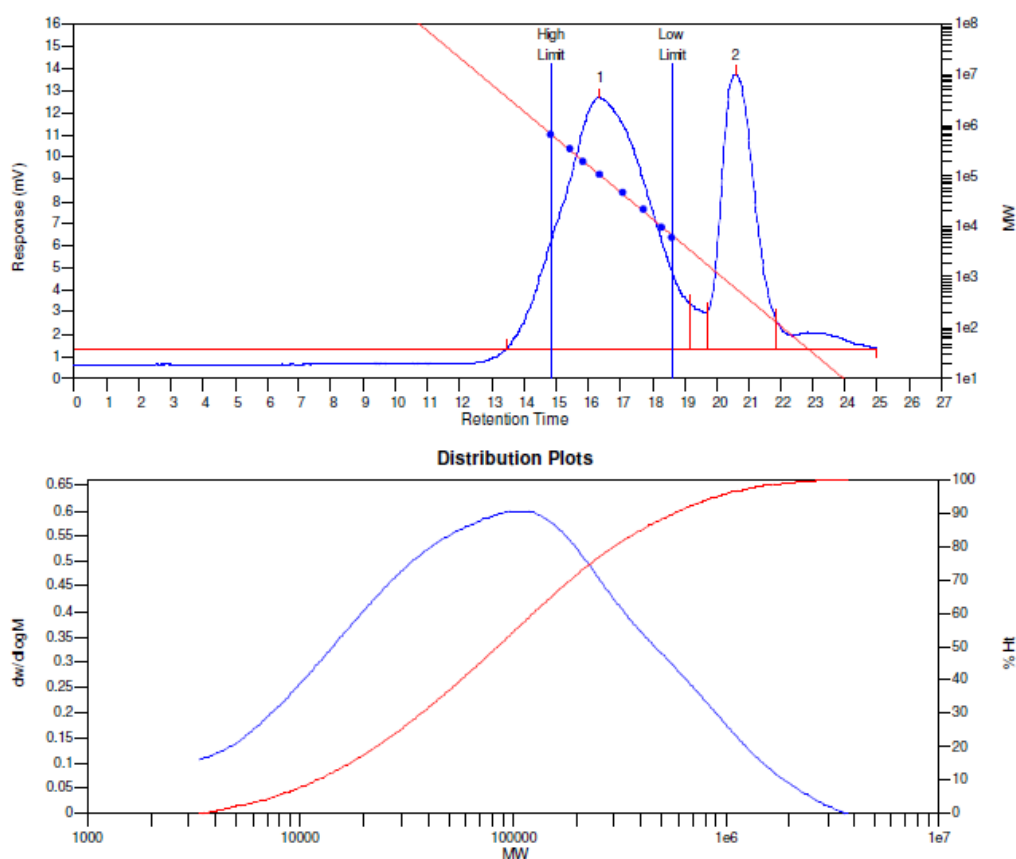
Calibration Curve: $y = 13.704178 - 0.530606x^1$

High Limit MW RT: 14.83 mins

Low Limit MW RT: 18.63 mins

Flow Marker RT: 0.00 mins FRCF: 1.0000

FRM Name:



MW Averages

Peak No	Mp	Mn	Mw	Mz	Mz+1	Mv	PD
1	106848	32233	212578	786677	1429566	164239	6.59504
2	618	451	605	775	939	581	1.34146

Processed Peaks

Peak No	Name	Start RT (mins)	Max RT (mins)	End RT (mins)	Pk Height (mV)	% Height	Area (mV.secs)	% Area
1		13.45	16.35	19.18	11.353	47.7579	2139.49	70.6527
2		19.72	20.57	21.82	12.419	52.2421	888.688	29.3473

Figure A.1. GPC trace of High-M alginate.

Calibration Used: 5/9/2018 4:35:06 PM

Calibration Type: Narrow Standard Curve Fit Used: 1

K: 14.1000 Alpha: 0.7000

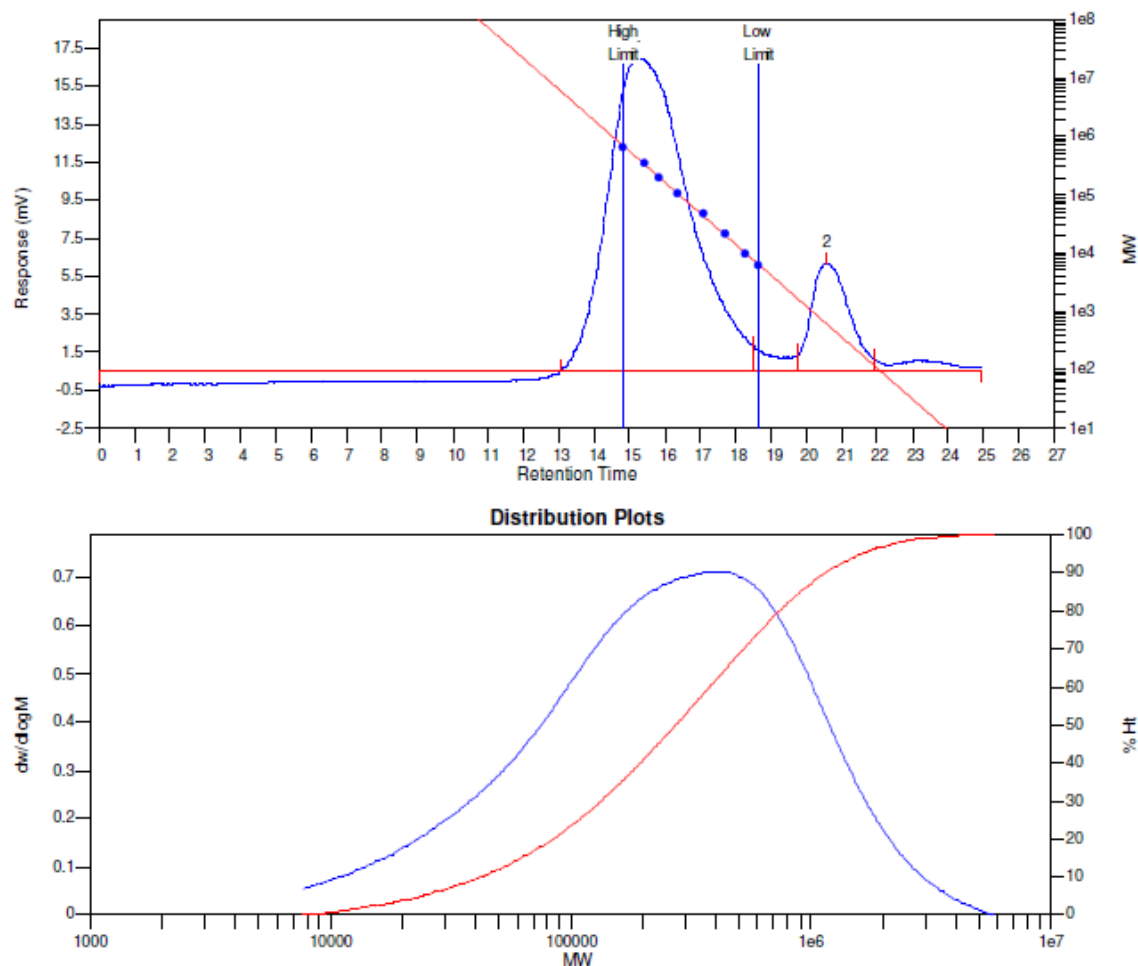
Calibration Curve: $y = 13.704178 - 0.530606x^{1.1}$

High Limit MW RT: 14.83 mins

Low Limit MW RT: 18.63 mins

Flow Marker RT: 0.00 mins FRCF: 1.0000

FRM Name:



MW Averages

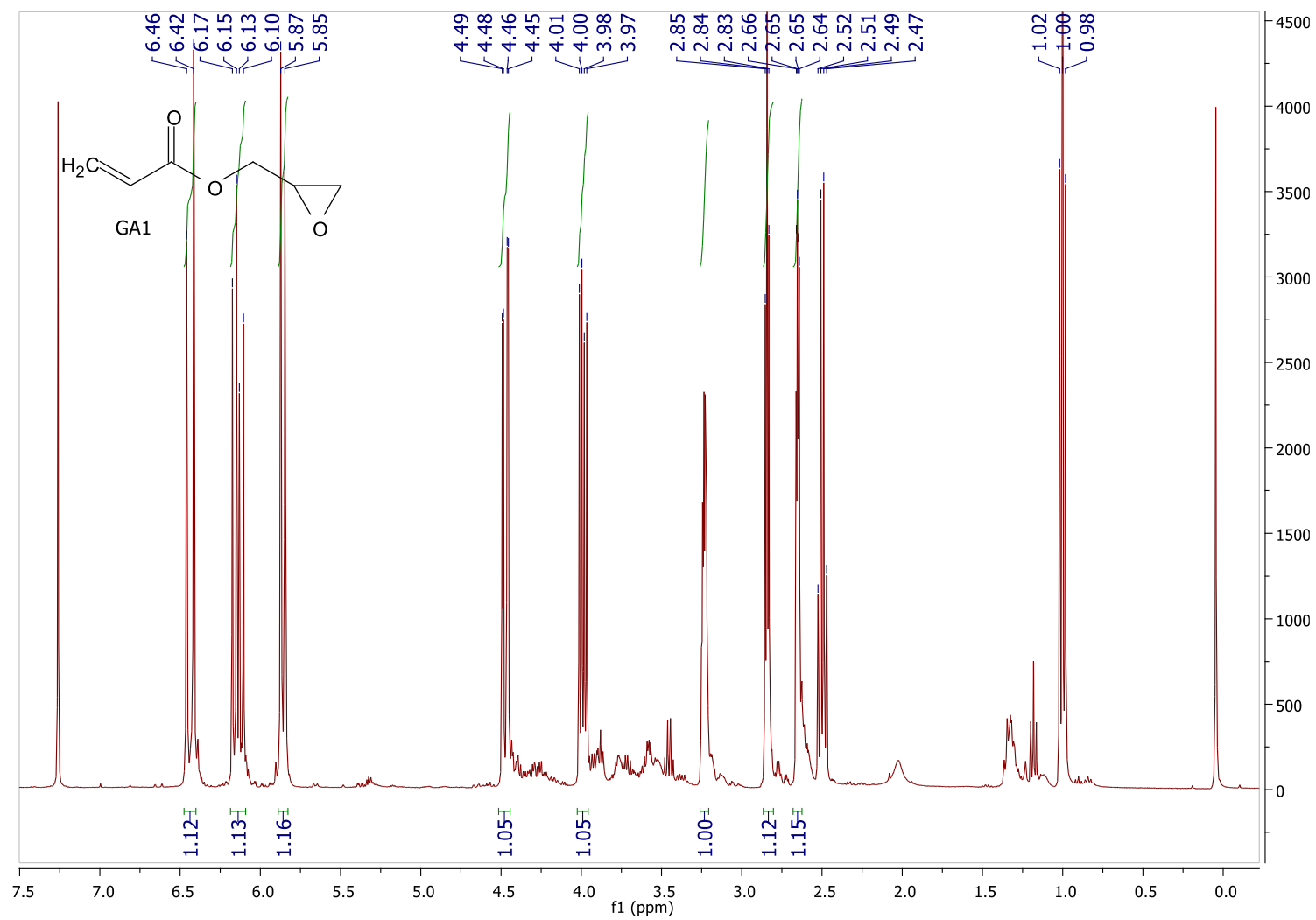
Peak No	Mp	Mn	Mw	Mz	Mz+1	Mv	PD
1	418099	103825	473576	1185331	2008441	397996	4.56129
2	631	434	592	761	917	567	1.36406

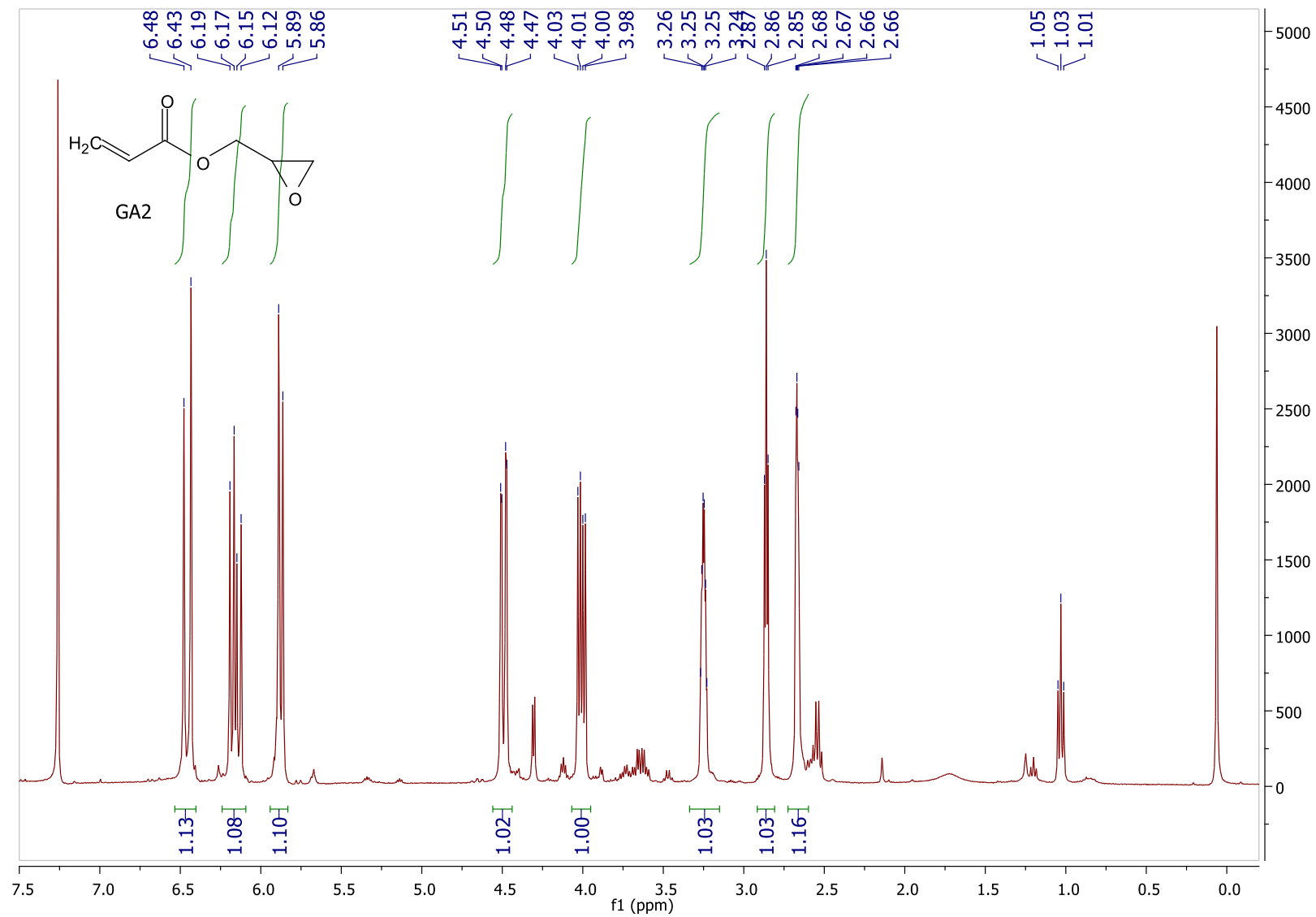
Processed Peaks

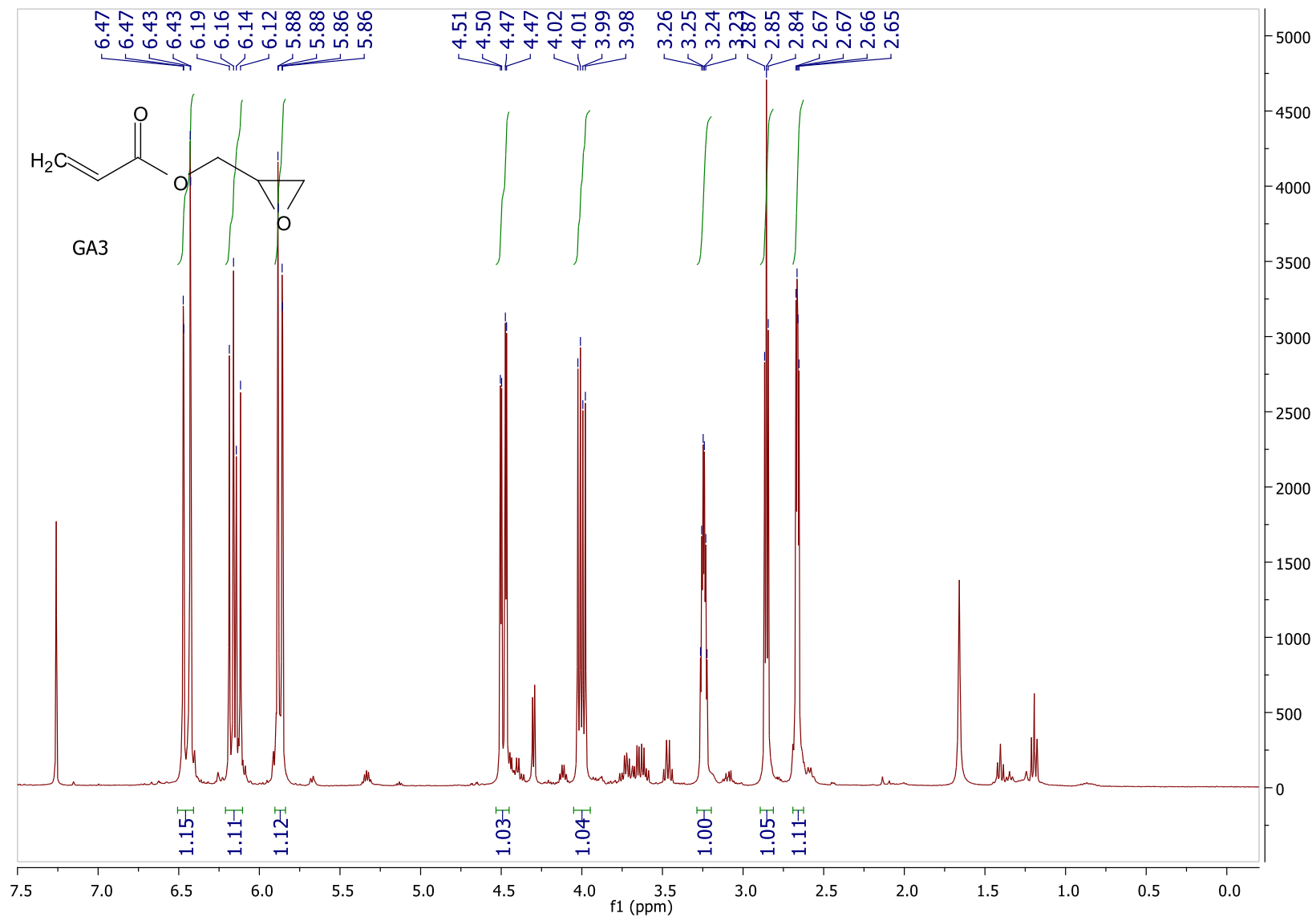
Peak No	Name	Start RT (mins)	Max RT (mins)	End RT (mins)	Pk Height (mV)	% Height	Area (mV.secs)	% Area
1		13.08	15.23	18.50	16.4149	74.5272	2601.38	86.3252
2		19.75	20.55	21.90	5.6105	25.4728	412.085	13.6748

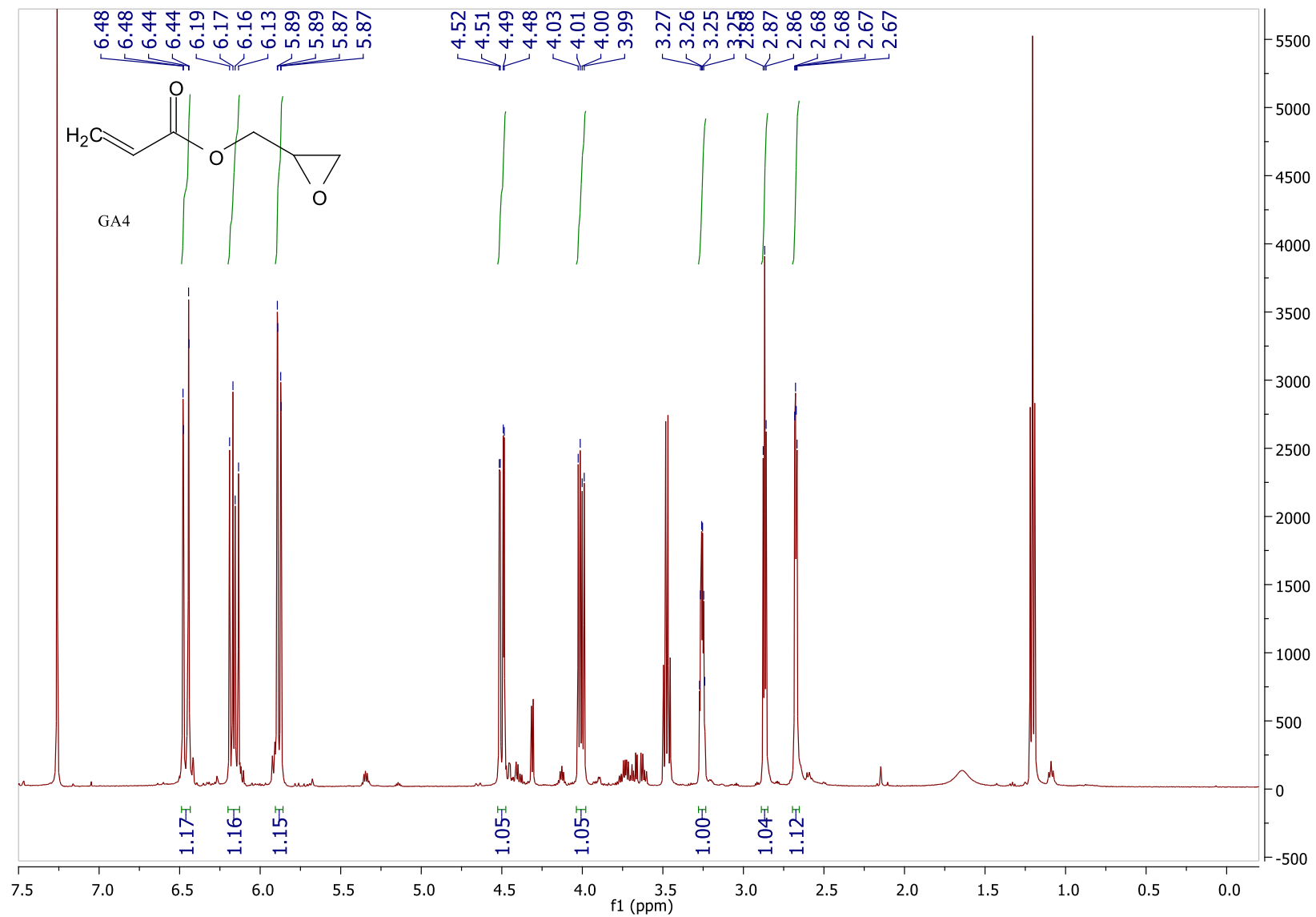
Figure A.2. GPC trace of High-G alginate.

A.2 NMR data

Figure A.3. ^1H NMR spectrum of GA1.

Figure A.4. ^1H NMR spectrum of GA2.

Figure A.5. ^1H NMR spectrum of GA3.

Figure A.6. ^1H NMR spectrum of GA4.

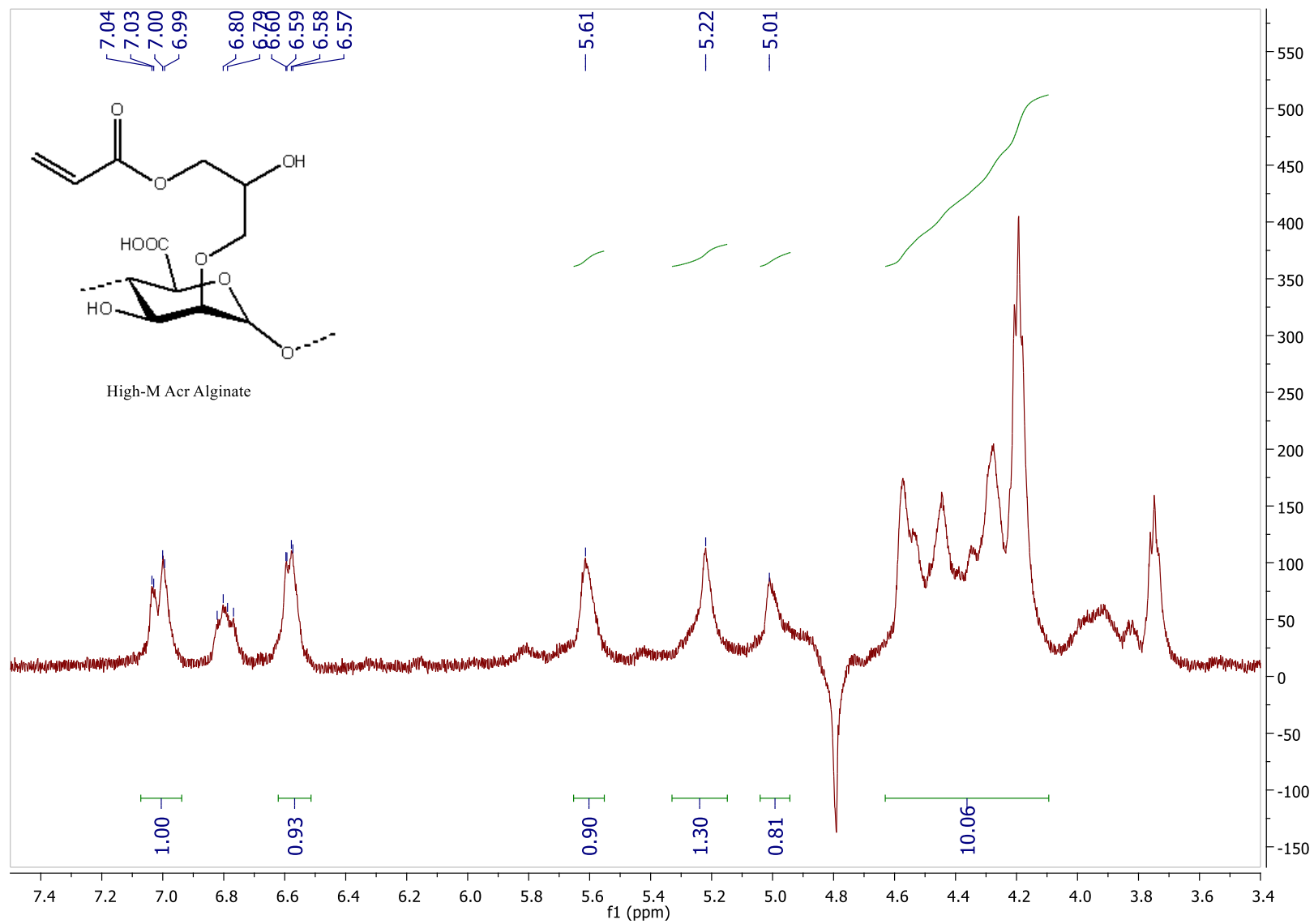


Figure A.7. ^1H NMR spectrum of High-M acrylated alginate.

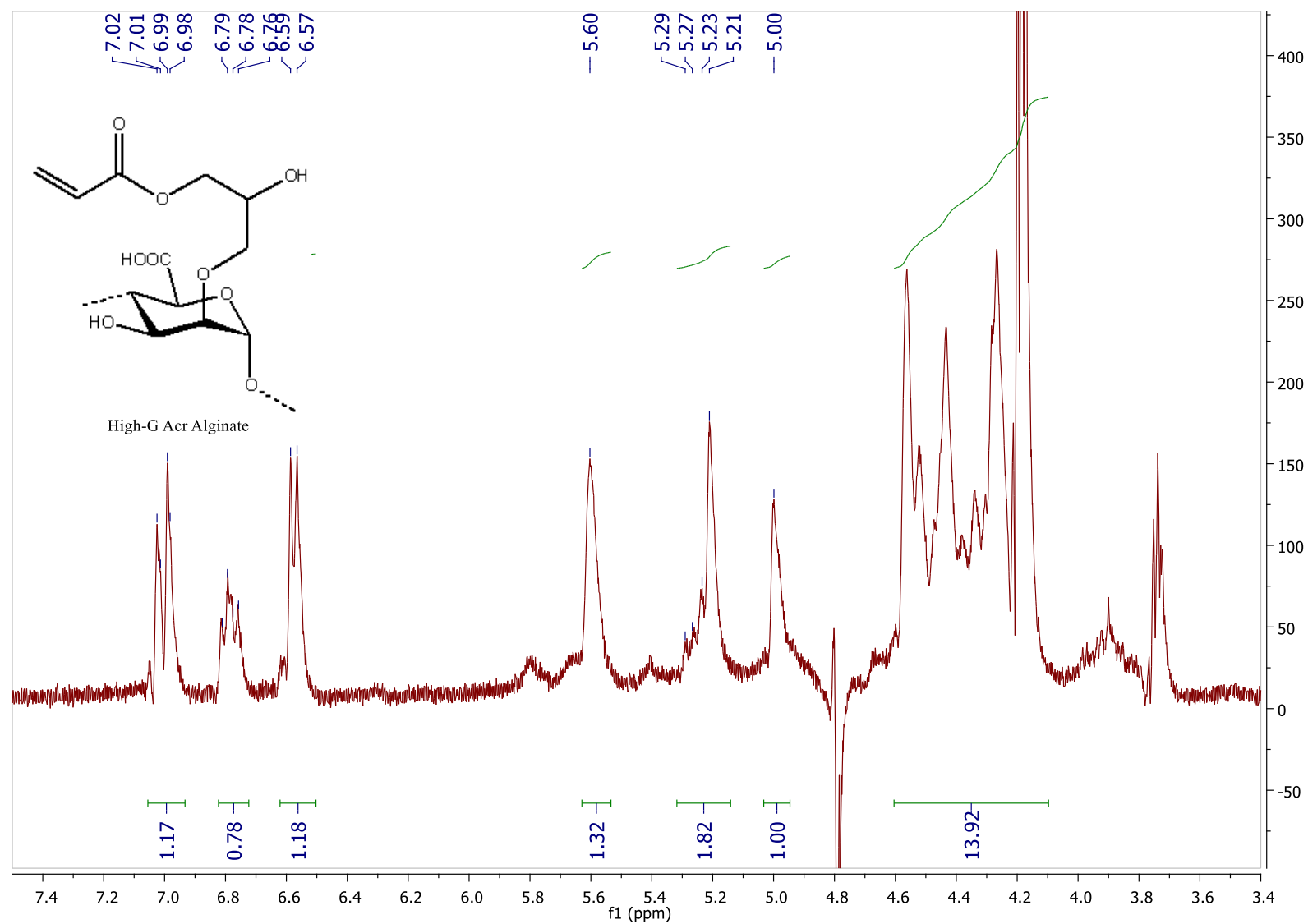


Figure A.8. ^1H NMR spectrum of High-G acrylated alginate.

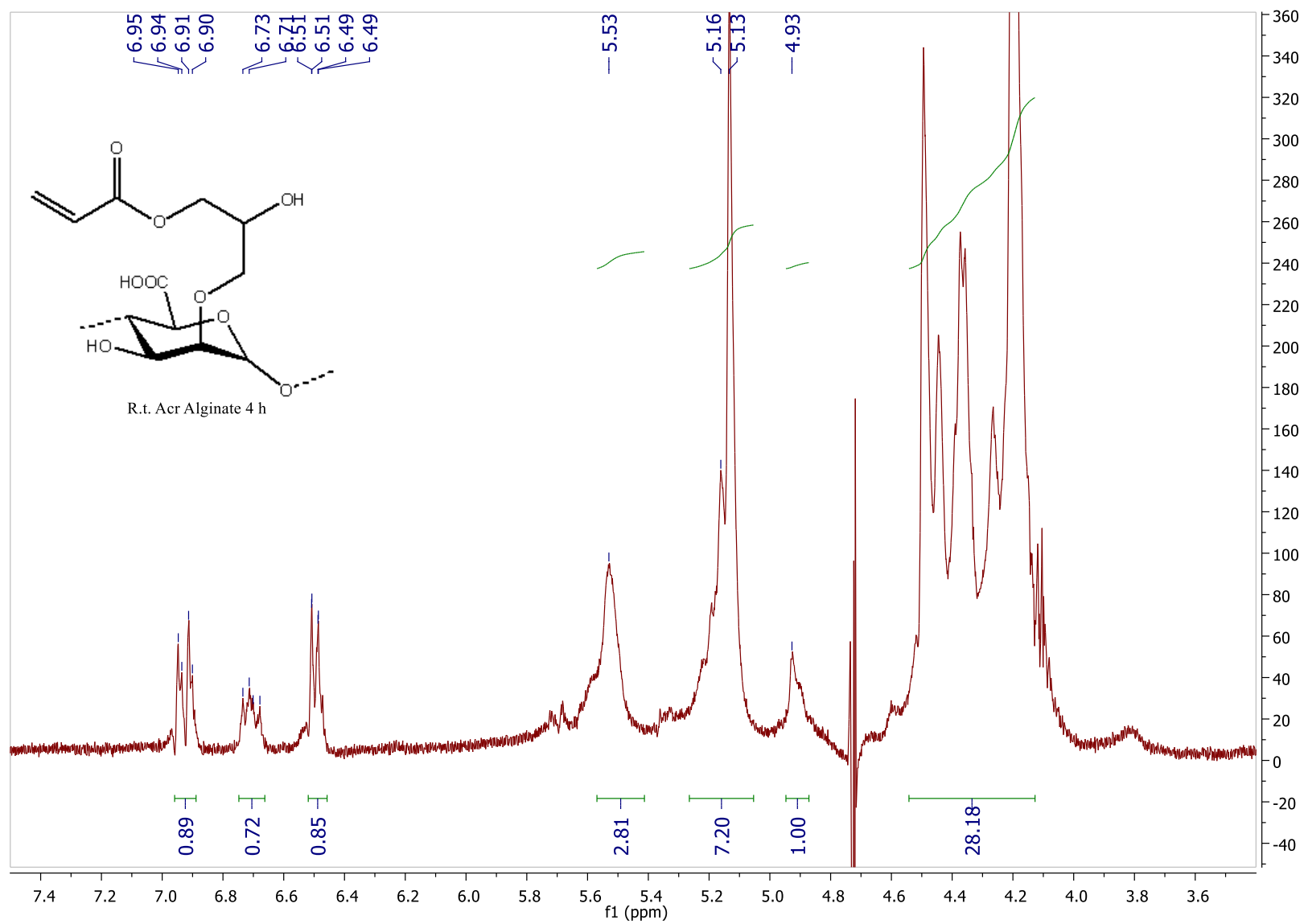


Figure A.9. ^1H NMR spectrum of acrylated alginate reaction conducted at room temperature for 4 hours.

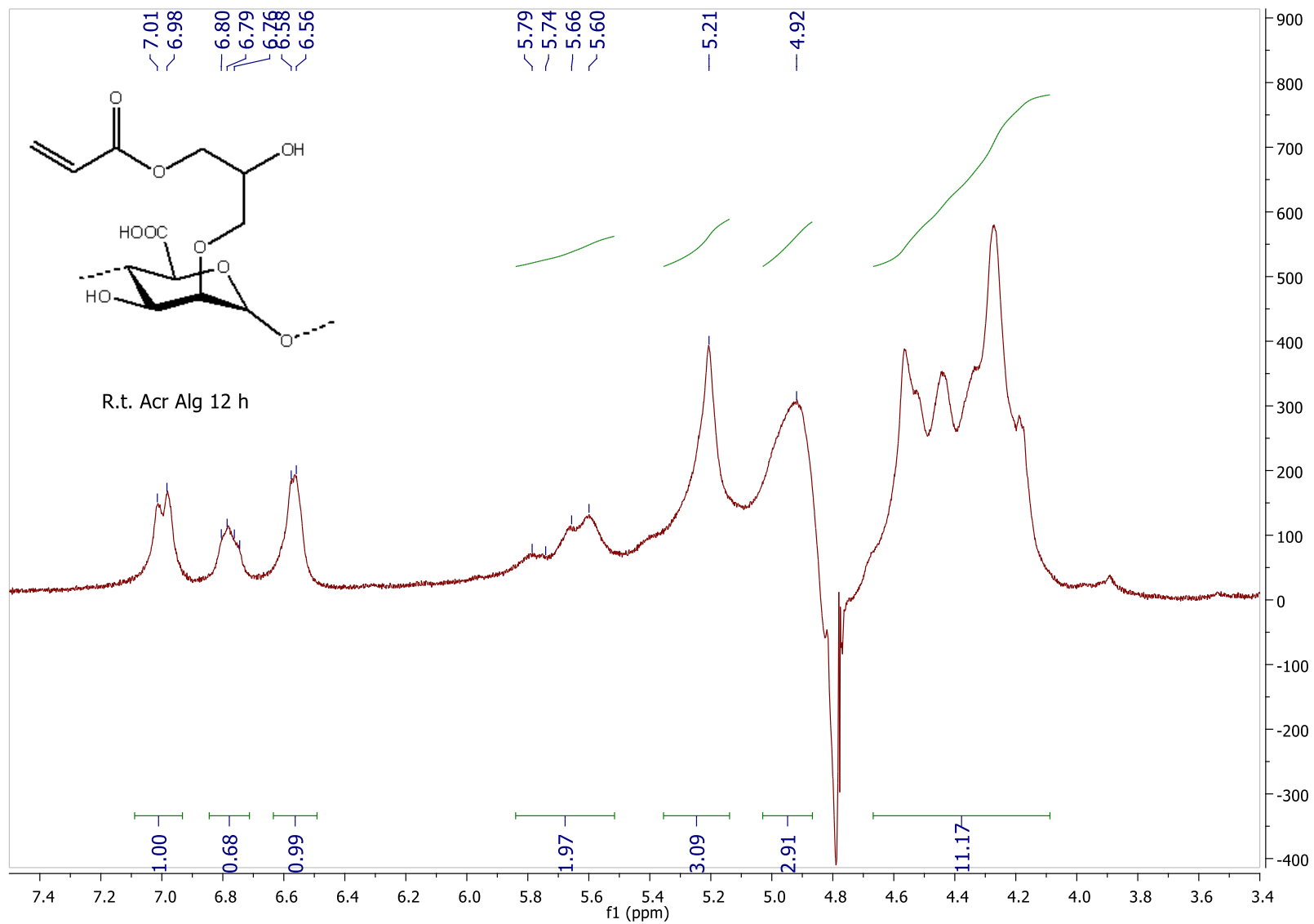


Figure A.10. ¹H NMR spectrum of acrylated alginate reaction conducted at room temperature for 12 hours.

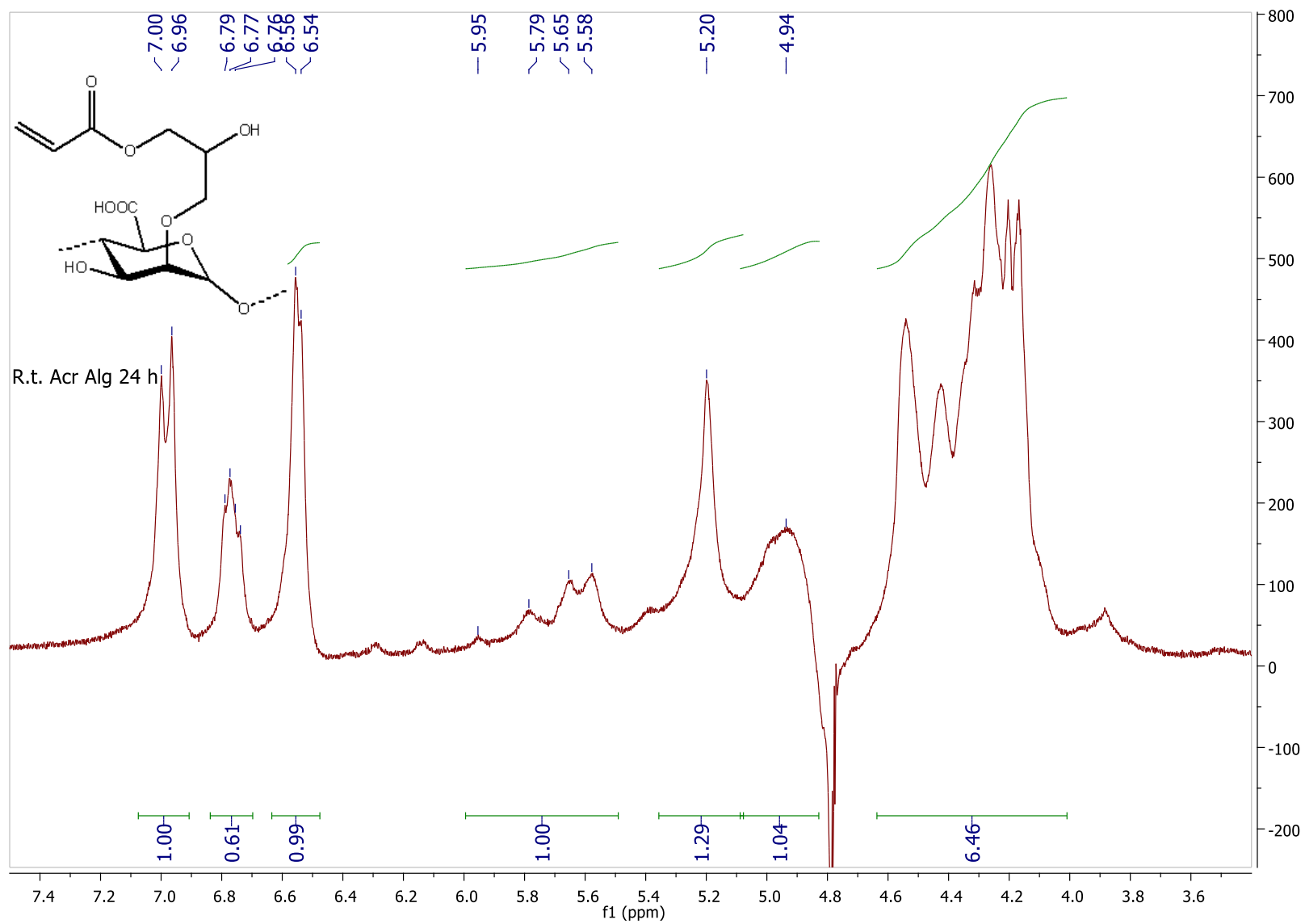
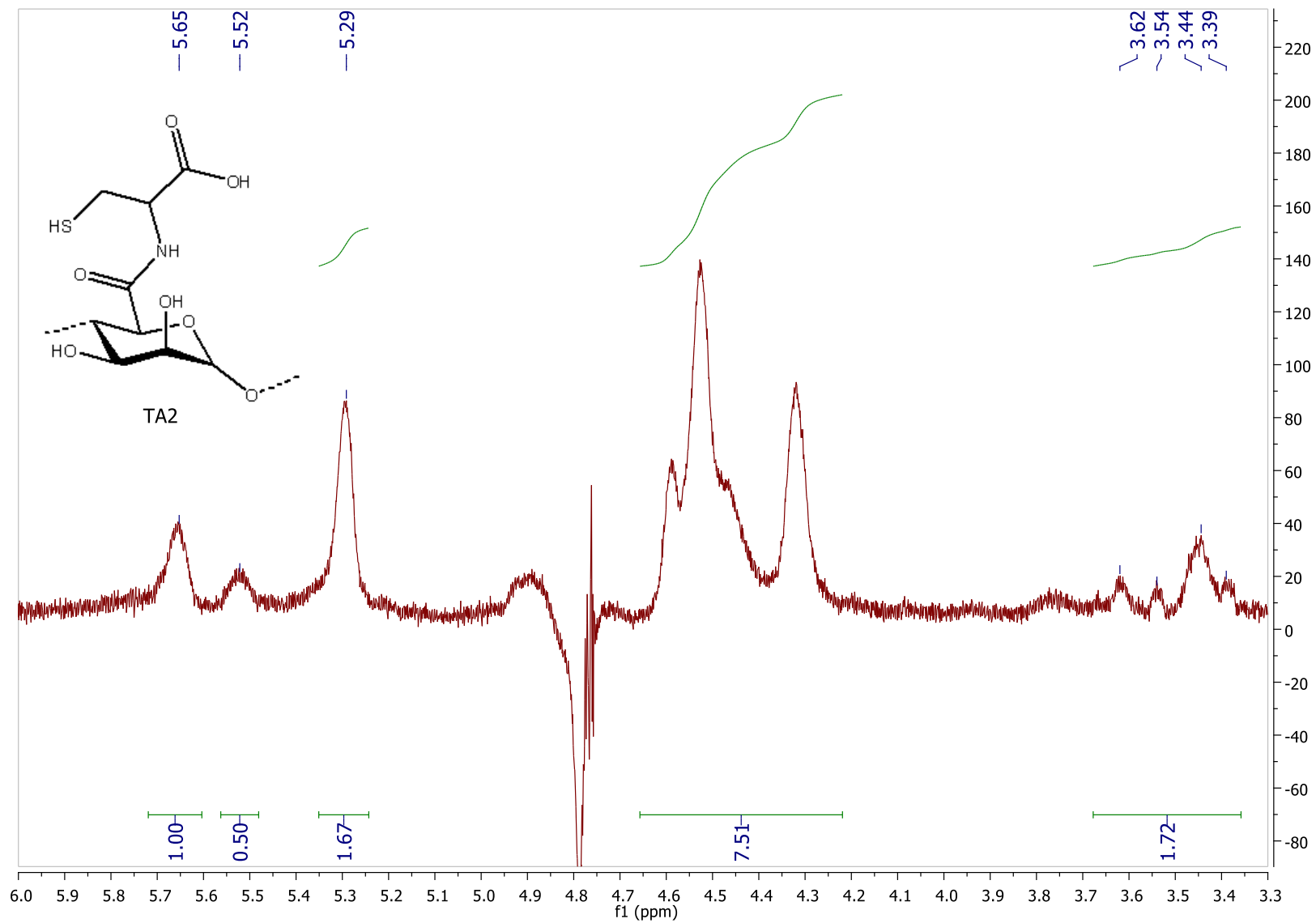
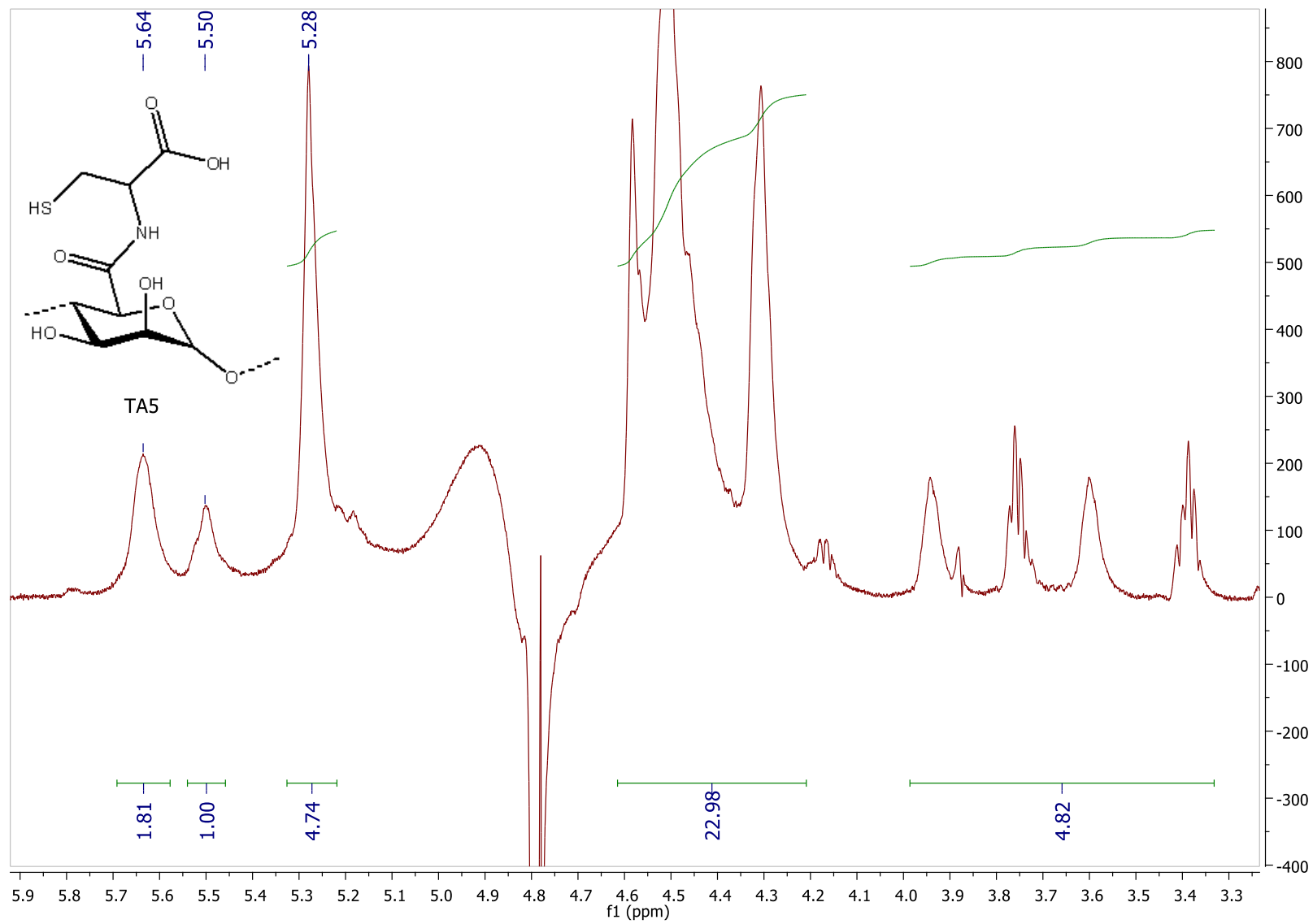
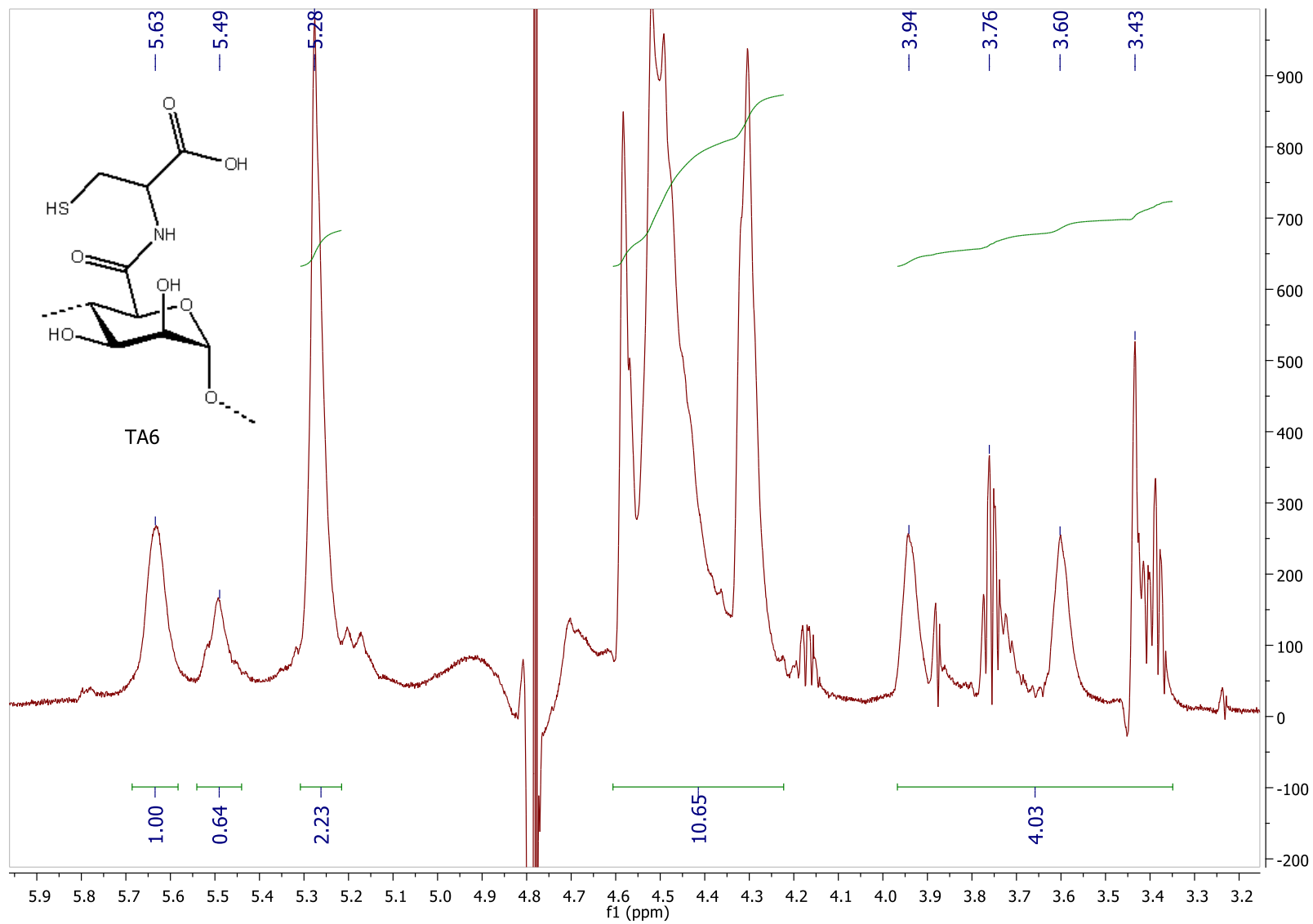
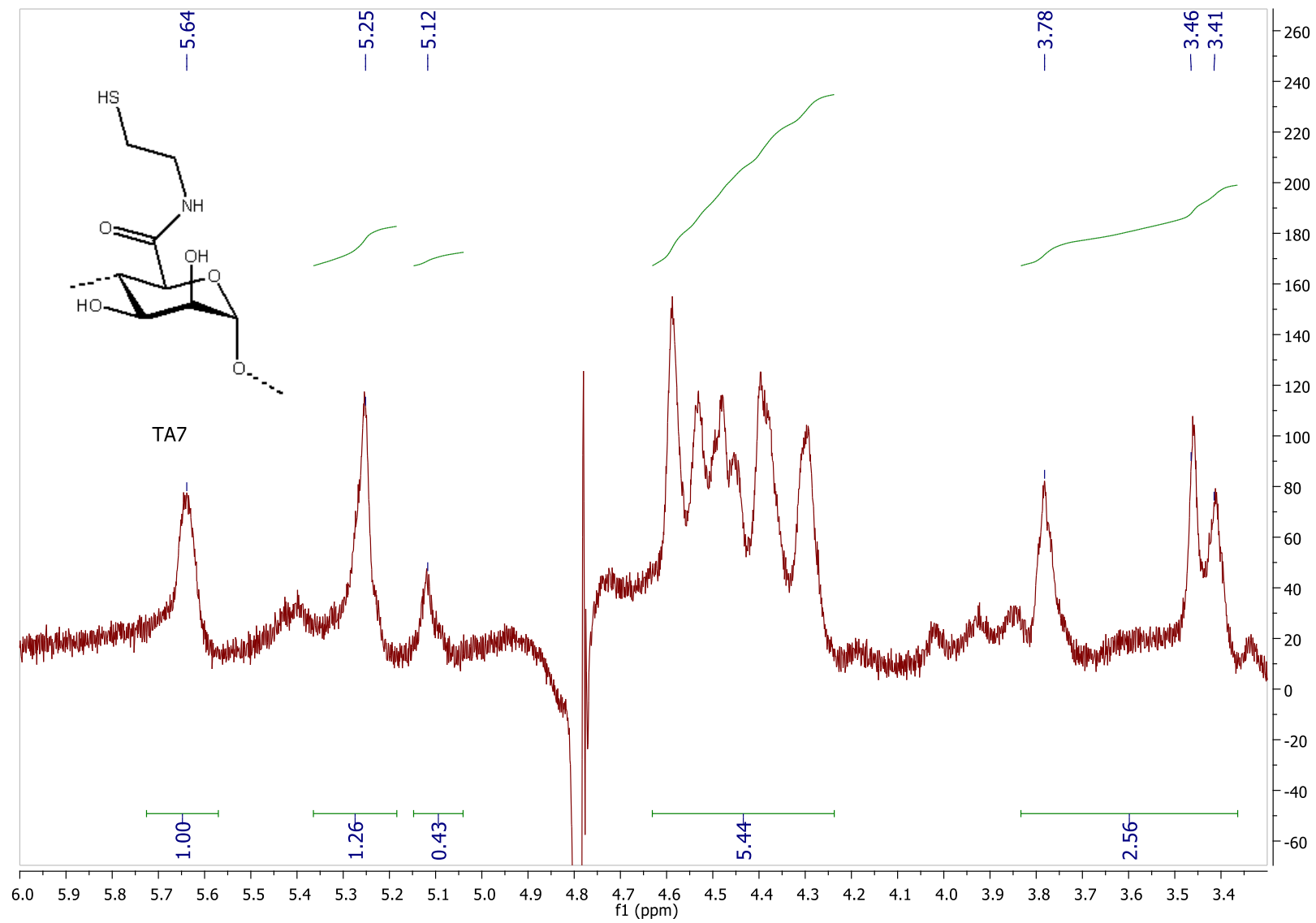


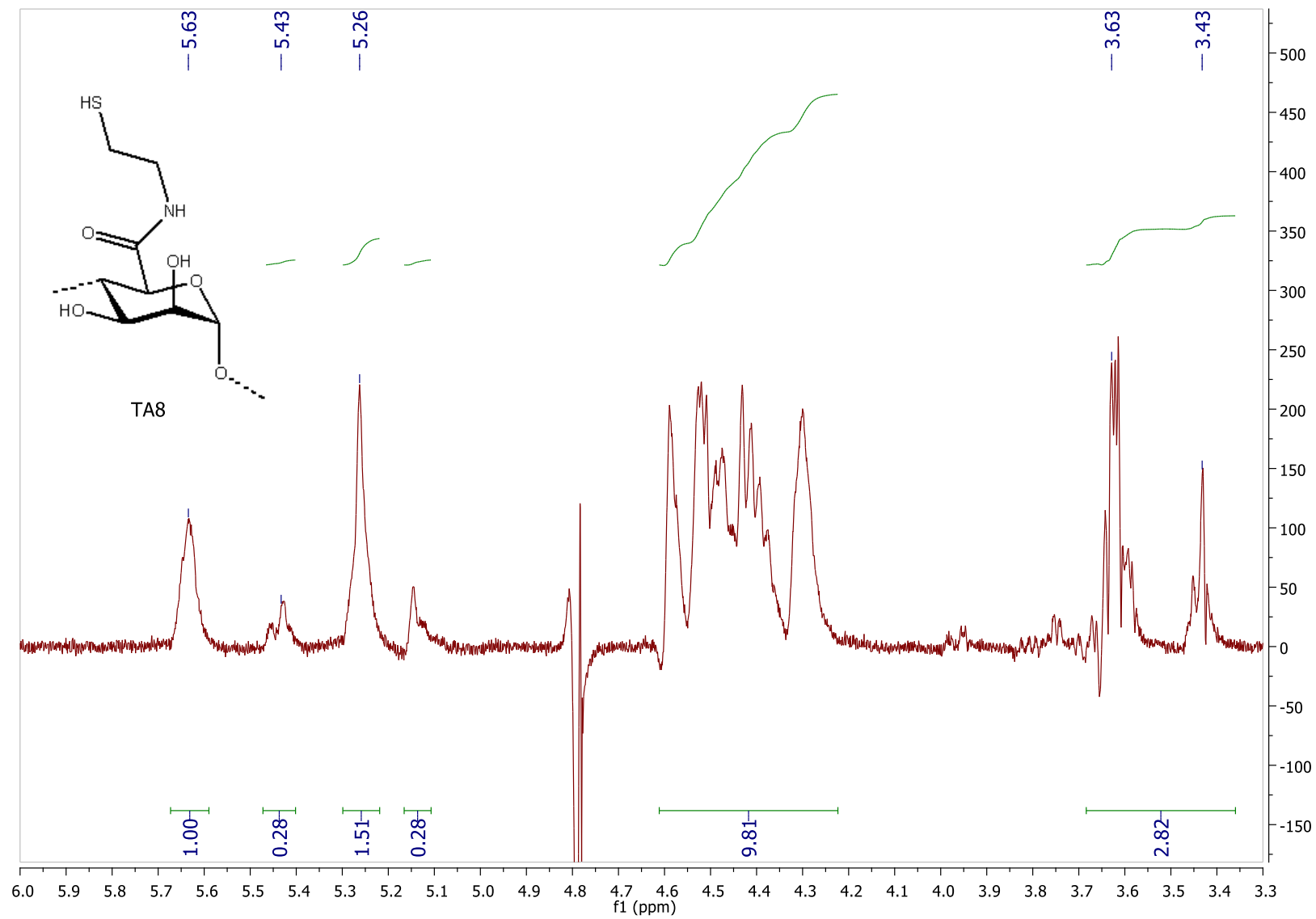
Figure A.11. ^1H NMR spectrum of acrylated alginate reaction conducted at room temperature for 24 hours.

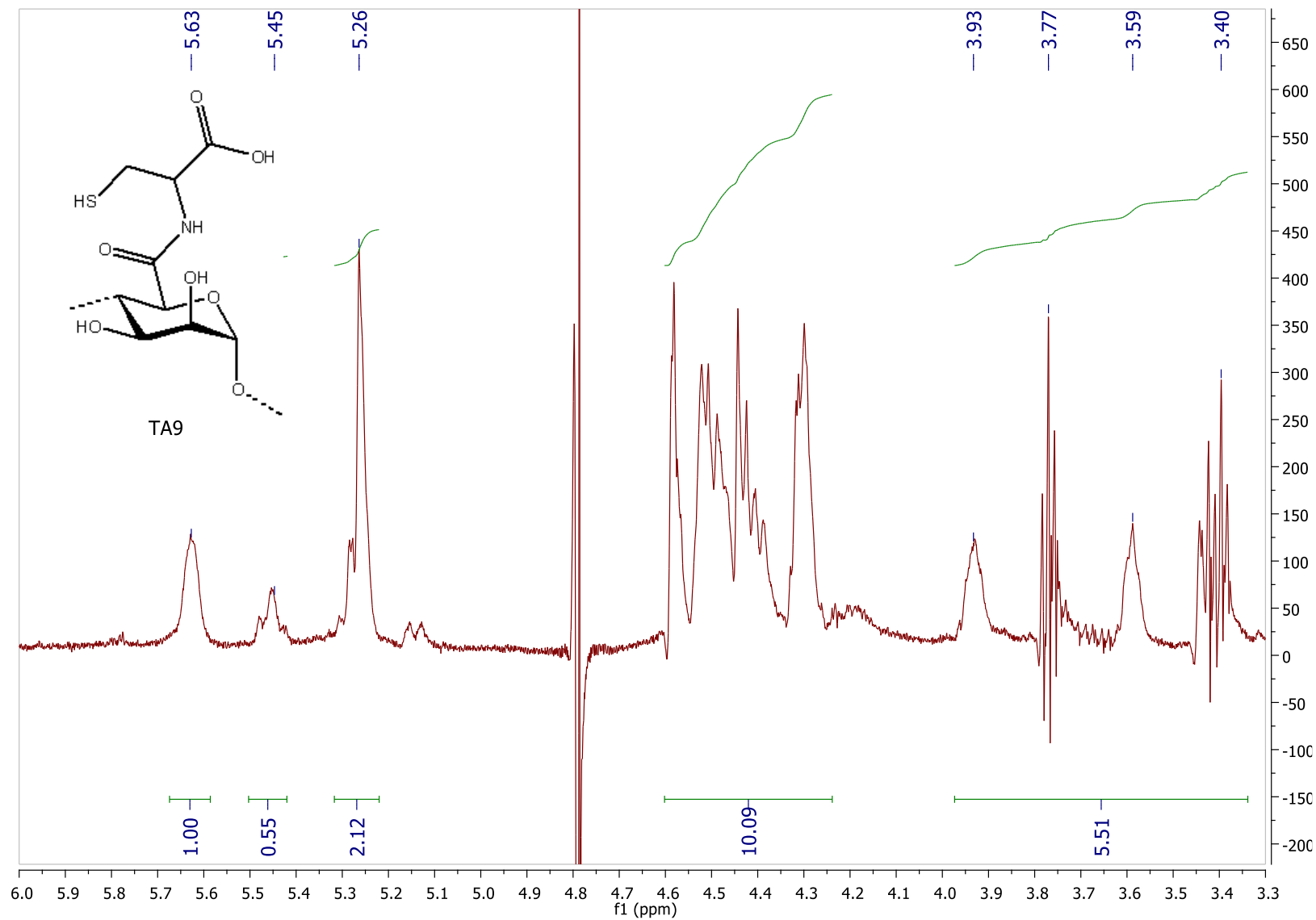
Figure A.12. ^1H NMR spectrum of TA2.

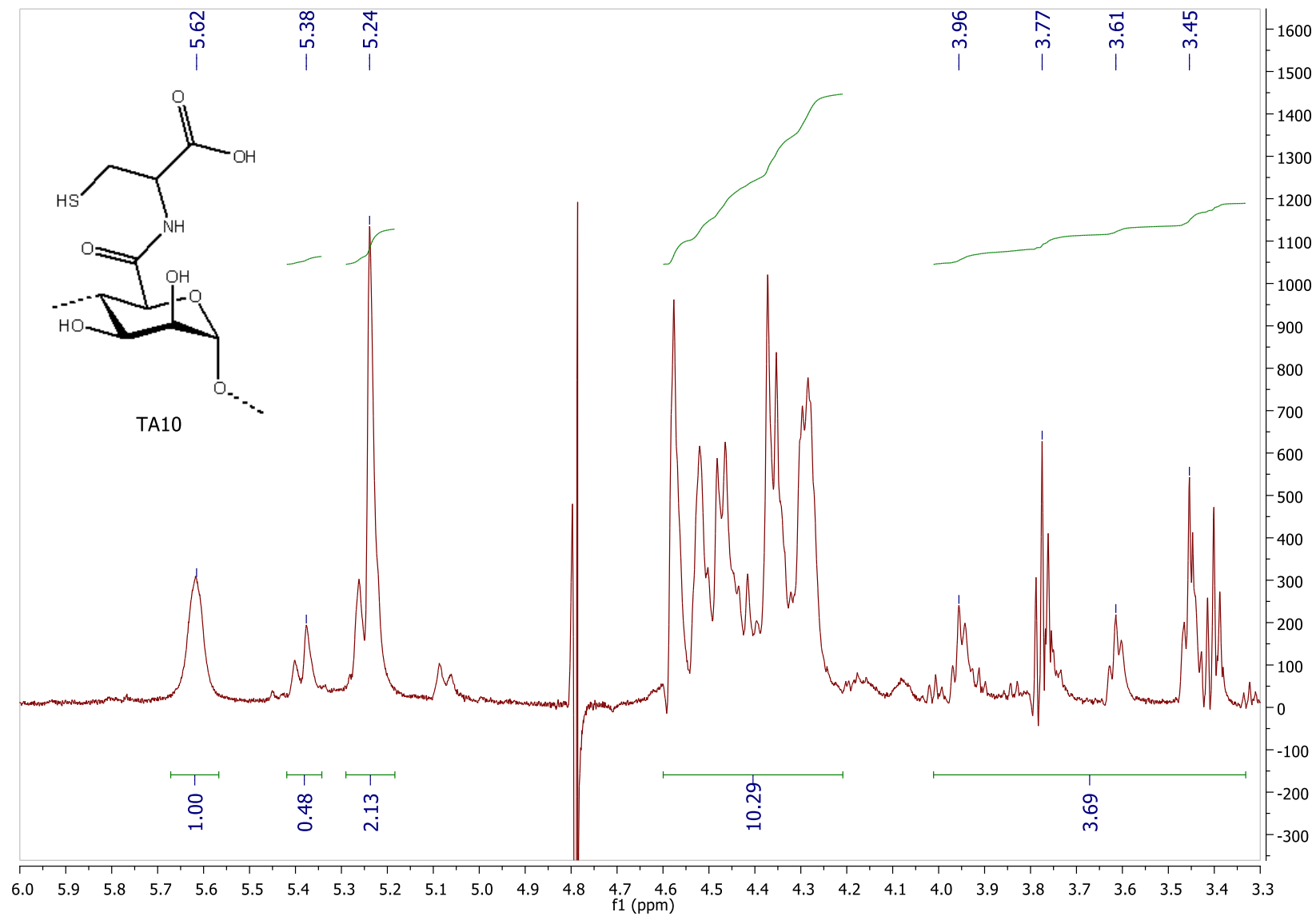
Figure A.13. ^1H NMR spectrum of TA5.

Figure A.14. ^1H NMR spectrum of TA6.

Figure A.15. ^1H NMR spectrum of TA7.

Figure A.16. ^1H NMR spectrum of TA8.

Figure A.17. ^1H NMR spectrum of TA9.

**Figure A.18.** ^1H NMR spectrum of TA10.